

***Atomic Force Microscopy:
A novel tool for the analysis of the mechanism of action
of antimicrobial peptides on target membranes***

by

Dale Holroyd

Hons. (Biochemistry)

Thesis presented in partial fulfilment of the requirements for the

degree

Masters of Science (Biochemistry)

in the

Faculty of Science

at the

University of Stellenbosch

Supervisor: Dr. M. Rautenbach

Department of Biochemistry

University of Stellenbosch

April 2003

Declaration

I, the undersigned, hereby declare that the work contained in this thesis is my own original work and that I have not previously in its entirety or in part submitted it at any university for a degree.

Dale L. Holroyd

Summary

Nanoscale visualisation of live cells and cellular components under physiological conditions has long been a goal in microscopy. The objective of this study was to validate the use of Atomic Force Microscopy (AFM) as a new tool in unravelling the mysteries of antimicrobial peptide mechanism of action. Using the simplest AFM imaging technique, we were able to analyse the influence of haemolytic melittin and anti-bacterial magainin 2 on different target membranes at nanometer resolution, without using fixing agents.

First, magainin 2 was synthesised and purified by gel permeation chromatography and high performance liquid chromatography (HPLC). The purity of magainin 2 and melittin, isolated from bee venom (Sigma-Aldrich), was verified with electrospray ionisation mass spectrometry (ESI-MS). Second, dose-response experiments were used to determine the optimum peptide/target cell ratio that would allow interaction with the membrane without causing lysis. Third, peptide/target-cell samples were placed on silica plates and visualised using contact mode AFM. Images obtained of the cells before and after peptide treatment, showed distinct changes in cell membrane surface topology. We observed grooves, lesions, membrane collapse and vesiculation depending on the concentration, type of peptide and target-cell used, allowing us to make conclusions regarding the mechanism of action of melittin and magainin 2.

In comparison with model membrane studies, our AFM results show that a peptide can function by more than one mechanism of action depending on the structural composition of the membrane, which appears to have specific segregated lateral organisation. Magainin 2 (non-toxic) selectively targets cell membranes using different mechanisms of action. In this way it can lyse bacterial membranes (anti-bacterial agent) using one mechanism, while using another mechanism to interact with mammalian cells at physiological concentrations, without destroying them. In contrast, melittin (toxic) is non-selective, and uses the same mechanism of interaction with bacterial and mammalian cells.

In conclusion, we propose a new holistic model for the mechanism of action of antimicrobial peptides.

Opsomming

Nanoskaal visualisering van lewende selle en sellulêre komponente onder fisiologiese toestande is al 'n geruime tyd 'n mikpunt in mikroskopie. Die doel van hierdie studie was om antimikrobiële peptiede se meganisme van werking op teikenselle op nanoskaalvlak met AFM te visualiseer. Sonder om fikseermiddels by te voeg, het ons die eenvoudigste AFM tegniek gebruik om die effek van hemolitiese melittien en anti-bakteriële magainin 2 op verskillende teikenselle, in nanometer resolusie, waar te neem.

Eerstens is Magainin 2 gesintetiseer en gesuiwer met behulp van gelpermeasie chromatografie en hoë doeltreffendheid vloeistof chromatografie (HPLC). Die suiwerheid van magainin 2 en kommersiële bye gif melittien, is bevestig met behulp van elektrospoei-ionisasie massaspektrometrie (ESI-MS). Tweedens, is dosis-respons eksperimente gebruik om die optimale peptied/teikensel verhouding te bepaal voordat membraanliese plaasvind. Derdens, is peptied/teikensel monsters op silika plate gevisualiseer met gebruik van kontak AFM. Die beelde van die selle, voor en na peptied behandeling, het duidelike veranderinge in seltopologie getoon. Ons het groewe, letsels, membraaninstorting en vesikulasie, afhangende van die konsentrasie peptied en teikensel gebruik, waargeneem. Dit het ons toegelaat om tot gevolgtrekkings te kom aangaande die meganisme van werking van melittien en magainin 2.

In ooreenstemming met model membraan studies, het ons AFM resultate gewys dat 'n peptied veelvoudige meganismes van werking kan hê, afhangende van die strukturele samestelling van die membraan, wat klaarblyklik laterale segregasie toon. Magainin 2 (nie-giftig) is selektief ten opsigte van teikenselle omdat dit gebruik maak van verskillende meganismes van werking op bakteriële en soogdier selle. In teenstelling is melittien (giftig) nie-selektief, en gebruik dieselfde meganisme van werking op bakteriële en soogdierselle.

Tenslotte, stel ons 'n nuwe model vir die meganisme van werking voor.



Life is a journey of souls. I say thanks to all those participating in mine.



Acknowledgements

I would like to express my thanks and gratitude to the following persons:

- Dr. M. Rautenbach, my supervisor and friend, for her critical evaluation and constant support. Thanks Marina, you have taught me so much.
- Mrs. Gertrude Gerstner, for her peptide synthesis training, the RBC assay and proofreading.
- Marè Vlok for his training and assistance with the bacterial assays.
- Navin Naidoo, for proofreading. Thanks for so many insightful discussions about Life, the Universe and Everything.
- Viveka Vadyvaloo for proofreading.
- Dr. Tinus van der Merwe, a truly good person. Thanks for the electrospray mass spectrometry work.
- Sue Marais for AFM technical assistance.
- All the technical staff at the department of Biochemistry. Without you the wheels would stop turning.
- And last but not least my good friends, Doug, Dyl, Et, Lionel and Rob. Thank-you for your unconditional friendship over the years.

Table of Contents

LIST OF ABBREVIATIONS AND ACRONYMS	ix
PREFACE.....	xiii
CHAPTER 1 VISUALISING THE INFLUENCE OF ANTIMICROBIAL PEPTIDES ON TARGET CELL MEMBRANES	
1.1 INTRODUCTION.....	1.1
1.1.1 <i>Types of antimicrobial peptides</i>	1.1
1.1.2 <i>Influence of membrane structure on the mechanism of action of antimicrobial peptides</i>	1.6
1.1.3 <i>Mechanism of action</i>	1.9
1.2 VISUALISATION OF ANTIMICROBIAL ACTIVITY.....	1.20
1.2.1 <i>Microscopy</i>	1.22
1.2.2 <i>Atomic Force Microscopy</i>	1.24
1.3 REFERENCES.....	1.26
CHAPTER 2 SYNTHESIS AND PURIFICATION OF MAGAININ 2	
2.1 INTRODUCTION.....	2.1
2.2 MATERIALS.....	2.6
2.2.1 <i>General reagents and solvents</i>	2.6
2.2.2 <i>Derivatives, catalysts and resins for peptide synthesis</i>	2.6
2.2.3 <i>Reagents and solvents for chromatography</i>	2.6
2.2.4 <i>Drying and storage of reagents and products</i>	2.7
2.3 METHODS.....	2.7
2.3.1 <i>Preparation of solvents</i>	2.8
2.3.2 <i>Preparation and quality control of the amino acid derivative</i>	2.9
2.3.3 <i>Synthesis of the peptides</i>	2.11
2.3.4 <i>Purification of the peptides</i>	2.13
2.3.5 <i>Analysis of purified peptides</i>	2.14
2.4 RESULTS AND DISCUSSION.....	2.16
2.4.1 <i>Synthesis 1 of Magainin 2</i>	2.16
2.4.2 <i>Synthesis 2 of Magainin 2</i>	2.20
2.4.3 <i>Synthesis 3 of Magainin 2</i>	2.27
2.5 CONCLUSIONS.....	2.31
2.6 REFERENCES.....	2.32

CHAPTER 3 IMAGING THE ACTION OF MEMBRANE-ACTIVE PEPTIDES ON DIFFERENT TARGET CELLS USING ATOMIC FORCE MICROSCOPY

3.1 INTRODUCTION.....	3.1
3.2 MATERIALS.....	3.5
3.3 METHODS.....	3.6
3.3.1 Preparation of erythrocytes.....	3.6
3.3.2 Haemolysis dose response assays.....	3.6
3.3.3 Preparation of erythrocytes for AFM.....	3.7
3.3.4 Preparation of bacterial cells.....	3.7
3.3.5 Antibacterial activity dose response assays.....	3.8
3.3.6 Preparation of <i>E.coli</i> for AFM.....	3.8
3.3.7 AFM imaging.....	3.9
3.4 RESULTS.....	3.9
3.4.1 Dose response parameters.....	3.9
3.4.2 Atomic Force Microscopy.....	3.11
3.5 DISCUSSION.....	3.30
3.6 CONCLUSIONS.....	3.35
3.7 REFERENCES.....	3.35

CHAPTER 4 GENERAL DISCUSSION

4.1 PEPTIDE SYNTHESIS.....	4.1
4.2 AFM VISUALISATION.....	4.2
4.3 THE “PHASE-TRANSITION” MODEL.....	4.4
4.4 REFERENCES.....	4.7

List of Abbreviations and Acronyms

α	alpha
β	beta
3D	three-dimensional
μm	micrometer
A	Alanine
AFM	Atomic Force Microscopy
Aib	α -amino-isobutyric acid
Ala	Alanine
Am	Amide
Arg	Arginine
Asn	Asparagine
Asp	Aspartic acid
C	Cysteine
Ca^{2+}	calcium ion
<i>C. albicans</i>	<i>Candida albicans</i>
CFU	colony forming units
CL	cardiolipin
Cys	Cysteine
D	Aspartic acid
DCC	dicyclohexylcarbodiimide
DCM	dichloromethane
DIPEA	N, N'-diisopropylethyl amine
DLPC	1,2-dilauroyl- <i>sn</i> -glycero-3-phosphocholine
DMF	N, N'-dimethylformamide
DMPC	1,2-dimyristoyl- <i>sn</i> -glycero-3-phosphocholine
DOPC	dioleoylphosphatidylcholine
DPhPC	1,2-diphytanoyl- <i>sn</i> -glycero-3-phosphocholine
DPPC	dipalmitoyl-L- α -phosphatidylcholine
E	Glutamic acid
<i>E. coli</i>	<i>Escherichia coli</i>
ESI-MS	electrospray ionization mass spectrometry

F	Phenylalanine
FDNB	1-fluoro-2,4-dinitrobenzene
Fmoc	N ⁹ -fluorenylmethyloxycarbonyl
G	Glycine
Gln	Glutamine
Glu	Glutamic acid
Gly	Glycine
H _{ii}	inverse hexagonal
H	Histidine
His	Histidine
HF	hydrofluoric acid
HOBt	1-hydroxybenzotriazol
HPLC	high performance liquid chromatography
I	Isoleucine
Ile	Isoleucine
L _α	lamellar
L	Leucine
Leu	Leucine
LTA	lipoteichoic acid
LPS	lipopolysaccharides
Lys	Lysine
K	Lysine
M ₂₃	magainin 2
[M ₂₃]	magainin 2 molecular ion
M	Methionine
M	molar
mbh	4, 4'-dimethoxybenzhydryl
Met	Methionine
Mg ²⁺	magnesium ion
MHC	minimum haemolytic concentration
MIC	minimum inhibitory concentration
MS	mass spectrometry
<i>m/z</i>	mass over charge ratio
N	Asparagine

nm	nanometer
NMP	<i>N</i> -methylpyrrolidone
OD	optical density
P/L	peptide to lipid ratio
P	Proline
PBS	phosphate buffered saline
PA	phosphatidic acid
PC	phosphatidylcholine
PE	phosphatidylethanolamine
PG	phosphatidylglycerol
PI	phosphatidylinositol
Pfp	pentafluorophenyl
Phe	Phenylalanine
Pro	Proline
PS	phosphatidylserine
POPC	1-palmitoyl-2-oleoyl- <i>sn</i> -glycero-3-phosphocholine
PyBOP [®]	benzotriazol-1-yl-oxy-tris-pyrrolidinophosphonium hexafluorophosphate
Q	Glutamine
R	Arginine
S	Serine
SDS	sodium dodecyl sulphate
Ser	Serine
SM	sphingomyelin
SPPS	solid phase peptide synthesis
STM	scanning tunneling microscopy
T _H	transition temperature
T	Threonine
tBoc	N ^α - <i>t</i> -butyloxycarbonyl
tBu	<i>t</i> -butyl ester
TFA	trifluoroacetic acid
THF	tetrahydrofuran
Thr	Threonine
Trp	Tryptophan
Tyr	Tyrosine

V	Valine
Val	Valine
W	Tryptophan
Y	Tyrosine

Preface

Model membrane studies have provided brilliant groundwork towards a better understanding of antimicrobial peptides and their mechanism of action. However, they fail to capture many biological features found in natural membranes, which in turn, influence the interaction with antimicrobial peptides. In order to take our understanding to the next level, alternative techniques are required for studying biological membranes. This thesis describes atomic force microscopy (AFM) as alternative technique for the analysis of the mechanism of action of antimicrobial peptides.

Chapter 1 provides a general overview of the influence that both antimicrobial peptides and lipid composition have on the mechanism of action. It also details the shortcomings of model membrane studies and the alternatives found in techniques such as AFM. Chapter 2 details the synthesis and purification of magainin 2. In Chapter 3 I discuss the optimisation of the AFM technique and the results achieved for melittin and magainin 2 on erythrocytes and *E.coli*. A revised version of this chapter is in preparation for publication. In Chapter 4 an integrated overview of the work is given together with a new holistic model leading into the future prospects of this study.

Chapter 1

Visualising the influence of antimicrobial peptides on target cell membranes

1.1 Introduction

During the course of evolution, organisms have increased their ability to defend themselves against pathogens by producing specialised substances that protect them against microbial invasion. Consequently, bacterial resistance to conventional antibiotics has become a major problem worldwide, with certain strains of bacteria already resistant to all available drugs [1-2]. Clearly, the development of a new family of antibiotics is a pressing issue. Antimicrobial peptides are considered strong candidates, because their proposed mode of action is different from conventional antibiotics. The major problem facing scientists is that most antimicrobial peptides are not only toxic to microorganisms, but also to mammalian cells. Therefore, research is currently focused on improving the potency and specificity of these peptides so that they only target microbes. In order to achieve this goal, it is important to understand the mechanism of action of these agents and the reasons for their selectivity against microbes.

1.1.1 Types of antimicrobial peptides

There is no doubt that the overwhelming structural diversity of antimicrobial peptides has obscured a clear understanding of their mechanism of action. Although this complicates the design of improved synthetic agents, it does shed a positive light on the broad range of opportunities available for future development.

We can categorise antimicrobial peptides (Table 1.1), some of which fall into more than one category, according to the following structural properties: (i) linear peptides (most of which have α -helix secondary structures); (ii) linear repeat-motif peptides (with a high frequency of one or more amino acids); (iii) peptides with a single loop structural motif which could be N

Table 1.1 Antimicrobial peptide categories

PEPTIDE	SEQUENCE
Linear	
Magainin 2 (amphibian)	GIGKFLHSAKKFGKAFVGEIMNS
Melittin (bee venom)	GIGAVLKVLTTGLPALISWIKRKRQQ-Am
Alamethicin (fungus)	Ac-UPUAUAQUVUGLUPVUUEQF
Linear repeat-motif	
Bactenecin (bovine neutrophils)	RL C RIVVIRV C R*
Indolicin (bovine neutrophils)	ILPWKWPWWPWRR-Am
Single-loop	
Brevinin IE (amphibian)	FLPL LAGL AANF LPKIF CKIT R KC
Multiple-loop	
α -defensin HNP-1 (human)	A CY C RIPA C IAGERRYGTC IYQGRLWAF CC
β -defensin BNBD-12 (bovine)	GLPS CGRNGGV CIPIR CPVPMRQIGT C FGRPVKC C RSW
Tachyplesin 1 (crab)	KW C FRV C YRGI C YRR C R-Am
Protegrin 1 (porcine leukocytes)	RGGRL C Y C RRRF C VC VGR
Nisin (gram-positive bacteria)	IbAIaLA α PGA K α GALMGANM K α A α A HASIHVaK

Am = Amide; * = also falls in single loop category;

solid line = disulphide bonds; **S**= thio-ether bonds; **a**= 2,3-didehydroalanine;

b= 2,3-didehydrobutyrine; α = α -aminobutyrate

to C, disulphide or thio-ether bonded; (iv) peptides with multiple loops due to disulphide or thio-ether bonds (most of which have predominately β -sheet secondary structures).

1.1.1.1 Linear peptides

Most linear antimicrobial peptides have α -helical structures, are cationic, and show an amphipathic character. Some well known examples include PGS and the 23-residue non-haemolytic magainins, both found on amphibian skin [3]. Magainin and several analogues have shown a wide range of activity against gram-positive and gram-negative bacteria [4,5], and fungi [5]. They also show activity against malarial parasites [6], protozoa [5], and a variety of human and murine tumor cells [7-9]. Magainin has been shown to form toroidal anion selective pores in membranes [10,11]. Two other well-known examples include haemolytic 26-residue bee-venom melittin [12], and non-toxic 37-residue giant silk moth cecropin A [13]. These two peptides are structurally similar and are active against gram-positive and gram-negative bacteria, and show lytic activity against target cells. It has also recently been shown that they inhibit HIV transcription [14]. Melittin has also been shown to have antiviral activity by direct lysis and inhibition of replication. [15,16].

There are also α -helical peptides that are hydrophobic or sometimes even slightly anionic. Alamethicin, produced by the fungus *Trichoderma viride* is a well-studied example and forms part of a group known as the peptaibols, which are characterized by having a high proportion of α -amino-isobutyric acid (Aib) residues [17]. In addition, these peptides are lipopeptides, which are acylated at the N-terminal. The name of this group is derived from the fact that they have an 1,2-amino alcohol at the C-terminal [17]. Alamethicin has been shown to form α -helical clusters that traverse the bilayer and surround an aqueous pore that can transport ions [18]. Another peptide that is hydrophobic and forms a helical transmembrane structure is gramicidin A [19]. In membranes it forms a cation-selective right-handed β -helix that traverses the membrane as a single-stranded head-to-head dimer [20]. Both alamethicin and gramicidin A show minimal selectivity between microbes and mammalian cells, limiting their pharmacological applications.

1.1.1.2 Linear repeat-motif peptides

Certain peptides have an amino acid composition that is rich in one or more specific amino acids. For example, histatins are produced in human saliva and form part of a histidine-rich family active against oral cavity pathogens and the common human fungal pathogen *Candida albicans* [21,22]. Peptides rich in arginine or proline are produced by mammal neutrophils from cathelin-associated propeptides (cathelicidin family). Examples include bovine bactenecin [23,24] that influences transport and energy mechanisms, and porcine prophenin and PR-39, which have shown to inhibit DNA as well as protein synthesis [25,26]. Tritrpticin [27] and indolicidin [28] are 13-residue peptides that also form part of the cathelicidin family and are examples of antimicrobial peptides that are rich in tryptophan. Indolicidin appears to permeabilise bacteria without lysing them [28] and can form conductance channels. The formation of conductance channels suggests that indolicidin can self-associate and that the haemolytic activity of this peptide is associated with the concentration required for its self-association. Indolicidin is also active against human immunodeficiency virus 1 (HIV-1).

1.1.1.3 Single loop peptides

A large number of antimicrobial peptides isolated from the *Rana* frog species are characterised by a large linear segment followed by a C-terminal cationic loop linked by a disulphide bridge containing 7 amino acids. Examples include brevenins [29], gaegurins [30], esculentin and ranalexin [31]. The C-terminal loop of brevenin IE has an amino acid composition similar to polymyxin B and has been presumed to play an important role in its antimicrobial activity [29]. Experiments on ranalexin analogues confirm the above assumption [31]. Bactenecin from bovine neutrophils [23] also fall into this category together with the class IIa or “pediocin-like” bacteriocins, which are produced by lactic acid bacteria (LAB) [32]. The latter fall into this category because they contain two cysteines that can possibly form a single disulphide bond. They are only active against gram-positive bacteria with high specificity for *Listeria* strains [32]. Another interesting group of peptides from the *Rubiaceae* plant family was recently discovered to possess antimicrobial activity and consists of four macrocyclic end-to-end 30 amino acid residue cyclic peptides [33]. These peptides (kalata, circulin A and B, and cyclopsychotride) also have a cysteine knot motif. The knotted motif is the result of one disulfide bond being threaded through the other two. This structural motif is also found in protease inhibitors and toxins and together with the cyclic backbone,

confers high rigidity to the structure. Circulin A and B have been shown to have anti-viral activity and may play a future role as anti-HIV drugs [34].

1.1.1.4 Multiple loop peptides

The multiple loop motif is found in the largest group of peptides and includes insect, plant and mammalian defensins, as well as tachyplesins, protegrins, and lantibiotics.

Mammalian defensins are β -sheet peptides with between 29 and about 40 amino acid residues and three intramolecular cysteine-disulphide bonds [35,36]. The α - and β -defensins differ with respect to the placement and connectivity of their 6 cysteine residues, the structures of their precursors and their patterns of expression [37,38]. The α -defensins have a broad spectrum of activity compared to the β -defensins, which have activity limited towards gram-negative bacteria [37,38]. Comparatively, insect defensins contain three disulphide bonds, but there are distinct differences in sequence and secondary structure, with antimicrobial activity limited to gram-positive bacteria [39]. Plant defensins contain three or four disulphide bonds and their activity varies widely from being antibacterial to being highly active against plant pathogenic fungi [40].

Other peptides include tachyplesins from the horse-shoe crab, which are all 17-residue peptide amides consisting of two antiparallel β -sheets separated by a β -turn and stabilised by two disulphide bonds. They permeabilise both bacterial and artificial lipid membranes and translocate across lipid bilayers, which has been coupled to transient pore-formation [41]. Tachyplesin analogues are active against HIV with low cytotoxicity [42].

Protegrins are defensins that are structurally similar to tachyplesins and share their broad spectrum of activity against bacteria, fungi, and viruses [43]. Unlike some of the larger defensins [35], protegrins retain activity in physiological concentrations of sodium chloride. Truncated protegrins with 12 residues manifest potent antibacterial activity, whereas the four additional residues are required for optimal candidacidal activity [44,35].

The lantibiotics are class II bacteriocins produced by strains of *Lactococcus* and other gram-positive bacteria. They are divided into two structural groups, namely group A, consisting of linear cationic peptides with multiple loop structures (nisin, epiderma, subtilin, PEP5, and lactocin S) and group B, consisting of small circular neutral peptides (cinnamycin, duramycin,

and ancovenin) with mersacidin and actagardine sharing properties of both groups [32,45]. Besides lanthionine and its analogue 3-methylanthionine, all lantibiotics contain didehydroalanine and/or didehydrobutyrine. The most well studied lantibiotic is 34-residue nisin, which is produced by several strains of *L. lactis*, and characteristic of most lantibiotics, is very active against a wide range of gram-positive bacteria [45]. It has also been used for over forty years as an antimicrobial agent for food preservation [46].

1.1.2 Influence of membrane structure on the mechanism of action of antimicrobial peptides

It is generally accepted that most antimicrobial peptides, regardless of sequence, size, charge, diastereomerism, L- or D-amino acid composition, and secondary or tertiary structure, use a mode of action on target membranes that is not receptor-specific [47]. The strongest support comes from studies showing that enantiomers (consisting solely of D-amino acids) of lytic melittin, cecropin, magainin and androctonin show activity indistinguishable from their parent molecules [48-51]. Nisin Z, however, is an exception that uses membrane anchored cell wall precursor lipid II as a receptor [52]. Nevertheless, target-membrane selectivity of cationic peptides has largely been attributed to prokaryote cell membranes being negatively charged, compared with eukaryotes, which are predominantly zwitterionic. The outer surface of gram-negative and gram-positive bacteria contains lipopolysaccharides and teichoic/lipoteichoic acids respectively, giving both surfaces a negative charge [53]. In addition, the phospholipids of the inner membrane of gram-negative and the single membrane of gram-positive bacteria are also negatively charged. In contrast, the outer section of normal mammalian cells is predominantly zwitterionic [54]. Selectivity studies on cecropins [55], magainins [56], dermaseptins [57] and others [49,58-61] have all demonstrated a lower affinity to zwitterionic phospholipid membranes compared to acidic phospholipid membranes. However, the selectivity is not solely based on charge and can be influenced by the structural properties of the specific lipid components of the target-membrane. For example, cynamycin appears to show specificity for phosphatidylethanolamine (PE) [62] and sapecin exhibits a specific affinity for cardiolipin (CL) [63]. Magainin has shown to permeabilise membranes composed of phosphatidylglycerol (PG) at lower concentrations (peptide to lipid ratio (P/L) of 1:100) than membranes composed of other negatively charged lipids such as phosphatidylserine (PS), phosphatidic acid (PA), and cardiolipin (CL) (P/L ratios of 1:50 to 1:20) [64,65].

These examples highlight the importance that this aspect of selectivity can have on the mechanism of action of antimicrobial peptides when compared to the variation that occurs among target-membranes (see Table 1.2).

Table 1.2. Phospholipid composition (w%) of the cytoplasmic membrane of gram-positive and gram-negative bacteria [66,67] and human erythrocytes [68].

Species	% PG	% PE	% CL	% Other
Gram-positive bacteria:				
<i>S. aureus</i>	57	0	43	0
<i>Staphylococcus epidermis</i>	90	0	1	9
<i>Bacillus megaterium</i>	40	40	5	15
<i>Bacillus subtilis</i>	29	10	47	14
Gram-negative bacteria:				
<i>Escherichia coli</i>	6	82	12	0
<i>Salmonella typhimurium</i>	33	60	7	0
<i>Pseudomonas cepacia</i>	18	82	0	0
Human erythrocytes	0	28.4	0	70.9*

*31% phosphatidylcholine (PC), 23.5% sphingomyelin, 13% PS, 2.2% PA and 1.2% phosphatidylinositol (PI)

A structural analysis of lipid components shows that they are predominantly arranged in a bilayer with the polar head groups facing outwards and the non-polar acyl chain tails pointing inward. However, alternative non-lamellar phases also exist (Fig. 1.1) because the structural properties can be either positive-curvature inducing or negative-curvature inducing [69]. Lipids with small head groups (e.g. PE and PS) promote negative curvature strain because there is a comparatively larger cross-sectional area available for the acyl chain tails and a smaller area is required for the head groups (Fig. 1.1). If the bilayer stress reaches a critical point, it can result in inverted phases where the polar head groups face inwards and the non-polar tails face outwards [69]. Alternatively, large head groups (e.g. PG and CL) promote positive curvature strain because there is a comparatively larger cross-sectional area required for the polar head groups and a smaller area available for the lipid acyl chain tails (Fig. 1.1). If the bilayer stress reaches a critical point, it can result in micelles [69]. The bilayer stress of

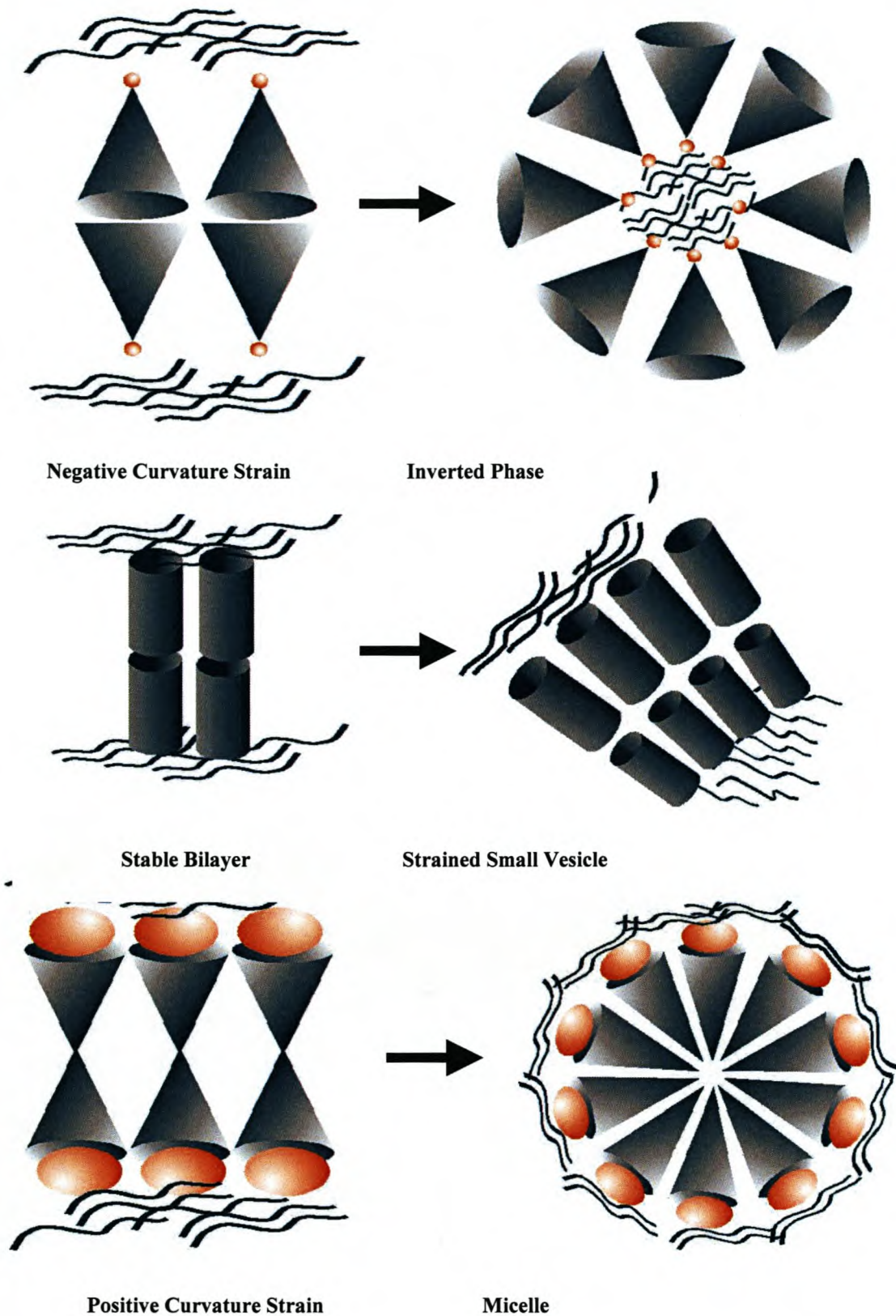


Figure 1.1 The figures on the left-hand side (top to bottom) represent three alternative bilayer motifs. The lipid shapes have been exaggerated in order to emphasize the consequences of packing into a flat structure with: a small head group (negative curvature strain), a head group comparable to the cross-section of the acyl chains (stable bilayer), and a large head group (positive curvature strain). The right-hand side represents the type of curved structures that can form if the bilayer stress reaches a critical point. The wavy lines indicate the presence of water.

a lipid component can be stabilised or destabilised by interaction with an antimicrobial peptide, depending on its specific structural properties. Calorimetry has been used to monitor whether a peptide stabilises or destabilises membranes by showing an increase or decrease in the lamellar (L_{α}) to inverse hexagonal (H_{ii}) transition temperature (T_H) respectively. Wasp venom mastoporan [70] and antimicrobial magainin [64] were shown to increase the L_{α} - H_{ii} transition temperature of dipalmitoleoylphosphatidylethanolamine. In another study, melittin was shown to stabilise PE membranes by decreasing the negative curvature stress [71-73]. Gramicidin S was shown to increase the negative curvature, destabilising PE membranes towards the formation of non-lamellar structures [74]. Alamethicin has also recently shown to exhibit similar destabilising of PE membranes [75].

These examples indicate that the selectivity of antimicrobial peptides is influenced by the specific lipid composition of the target membrane and that the extent of structural complementarities, which occurs between peptide and lipid, can be a fundamental factor influencing the mechanism of action used (detailed in Chapter 3).

1.1.3 Mechanism of action

1.1.3.1 Structural parameters

Several structural parameters can modulate the biological activity and mechanism of action of linear α -helical peptides. It is, however, difficult to determine the individual importance of each of these parameters, as they often influence each other. Nevertheless, certain trends have emerged from studies with naturally occurring peptides and model peptides:

1.1.3.1.1 Helicity: Studies indicate that helicity is essential for activity against zwitterionic membranes (eukaryotes), but less important for activity against negatively charged membranes (prokaryote). Various D-amino acid substitution-studies on melittin [76], pardaxin [77] and Lys-Leu model peptides [78] were used to disrupt helix formation. Compared to their wild-types, the diastereomers did not bind to zwitterionic model membranes, but retained their affinity for negatively charged membranes. This in turn correlated with a loss of haemolytic ability, while retaining antimicrobial activity. In contrast, non-haemolytic magainin lost all of its antimicrobial activity after helix disruption by two consecutive D-amino acid substitutions [79], but retained its permeabilising activity on negatively charged PG membranes [80].

1.1.3.1.2 Amphipathicity: Amphipathicity of a peptide is a measure for the spatial separation between hydrophilic and hydrophobic side chains. It is generally determined by calculating the hydrophobic moment, which is defined as the vector sum of the hydrophobicities of each amino acid residue [81]. Studies using peptides consisting of repeating motifs of Lys-Leu-Ala-Leu (KLAL-peptides) indicate that the hydrophobic moment plays a minor role in the permeabilisation of negatively charged membranes but substantially influences their effect on neutral membranes [82]. This parameter strongly influences hydrophobic peptide-lipid bilayer interactions [83], and although it has been a key feature in the *de novo* design of simple peptides, peptides with increased antimicrobial activity and high selectivity still remain limited [84].

1.1.3.1.3 Hydrophobicity: A peptide's hydrophobicity reflects the intrinsic capability to move from an aqueous phase into a hydrophobic phase. It can be expressed as the mean hydrophobicity, defined as the average of the numeric hydrophobicity values of all residues [85]. Natural antimicrobial peptides show a wide range of hydrophobic moments and mean hydrophobicities. Several studies on model peptides [86-87], cathelicidin-derived peptides [88], and analogues of brevenin 1E [89] indicate that high mean hydrophobicities correlate with high cytotoxic activity against the neutral membranes of mammalian cells. Further studies on histatin- and magainin-derivatives [90] confirmed that haemolytic activity was strongly correlated with mean hydrophobicity, independent of amphipathicity or net positive charge. Other studies have addressed the relationship between hydrophobicity and antibacterial activity, showing that no strong correlation exists [87, 91-92]. In contrast, cecropin A-melittin studies [93] and studies using analogues of CAMELO (a 15-residue antibacterial peptide) [94] do show a correlation between hydrophobicity and antibacterial activity, however difficulties arise when interpreting results from different peptide studies as they often vary in more than one parameter. KLAL-peptide analogues addressed this problem, and the results indicated that there is a more direct relationship between hydrophobicity and haemolytic activity than with antibacterial activity [84]. One explanation is that electrostatic accumulation of the peptides near the negatively charged bacterial membranes reduces the relative contribution of hydrophobicity to the overall effect [84].

1.1.3.1.4 Hydrophobic and hydrophilic angles: The angles subtended by the hydrophobic and hydrophilic faces influence membrane binding, independent of the hydrophobicity and the hydrophobic moment [84]. Furthermore, they also affect the induction of positive or negative

membrane curvature strain, thereby influencing the destabilisation of lipid bilayer membranes [84]. Brasseur *et al.* [95] suggested that peptides with small hydrophilic angles and high mean hydrophobicities tend to form trans-membrane pores. A recent study [96] used model peptides $\theta p100$ and $\theta p180$ with polar angles of 100° and 180° respectively, to show that despite its somewhat lower affinity, $\theta p100$ exhibited higher permeabilisation activity, a greater flip-flop rate, as well as more antimicrobial activity than $\theta p180$ due to a higher pore formation rate. Furthermore, the number of peptides constituting the $\theta p100$ pore was less than that of $\theta p180$, and the $\theta p100$ pores involved less lipid molecules [96]. In other studies on magainin and KLAL peptide analogues (whereby the hydrophobicity, hydrophobic moment and the number of charged residues were maintained constant) showed that changes in the hydrophilic angle had little effect on the neutral lipid membranes of erythrocytes, whereas the permeabilisation of highly charged membranes was decreased upon increase of the polar angle [84]. It should, however, be noted that the modulating potential of the polar angle is generally connected with the magnitude of other structural parameters.

1.1.3.1.5 Charge: Various studies using δ -hemolysin [97], magainin [98-99], and pardaxin [100] have shown that an increase in positive charge correlates to an increase in antibacterial activity, whereas a gradual reduction in positive charge decreases antibacterial activity [99-100]. However, if the peptide's positive charge is increased too far, membrane activity may decrease as strong electrostatic interactions anchor the peptide to the lipid head group disrupting insertion into the hydrophobic core [80,101]. Furthermore, repulsion between the positively charged side-chains (intra- or intermolecular) may obstruct the formation of pores. Although there is no simple correlation between peptide charge and biological activity, studies indicate that a sensitive balance between electrostatic and hydrophobic interactions determine peptide-membrane interactions [82]. Peptide charge seems to modulate the initial membrane interaction and selectivity, whereas biological activity appears to be driven by the hydrophobic interaction between non-polar amino acids and the hydrophobic core of the lipid bilayer [47].

1.1.3.1.6 Oligomerisation: Pardaxin, LL-37, and peptides from the dermaseptin family are examples of peptides that are highly positive and yet show no selectivity between bacteria and mammalian cells [47]. A study on their mode of action revealed that peptide oligomerisation in solution and in the membrane was an additional important parameter that controlled their selectivity to specific targets [47]. It was revealed that those peptides which bound as oligomers, showed no selectivity between zwitterionic and negatively charged membranes,

whereas those peptides that were in monomer form showed selectivity for negatively charged membranes [47]. A recent study [102] compared model peptides to their cyclic counterparts. They found that cyclisation abolished oligomerisation of the linear peptide in solution and in sodium dodecyl sulphate (SDS), and increased selectivity between bacteria and human erythrocytes by substantially decreasing the haemolytic activity of the cyclic peptides. Furthermore, the linear peptide was only active toward gram-positive bacteria, whereas the cyclic monomer peptide was active towards gram-positive and gram-negative bacteria.

Each structural parameter plays a role in the combined influence over selectivity. A summary of all currently accepted studies can be represented by the following:

- peptides with a moderately high positive charge and a small polar angle, which exist as monomers in solution, show high antibacterial and low haemolytic activity;
- peptides with a large hydrophobic moment, high mean hydrophobicity and a low positive charge, which oligomerise in solution, show high antibacterial and high haemolytic activity.

These structural trends have been incorporated into proposed models for the mechanism of action of antimicrobial peptides. In the following section, we will highlight the most accepted models.

1.1.3.2 “Barrel-stave” model for transmembrane channel/pore formation

The barrel-stave mechanism [103] describes the formation of transmembrane channels/pores by bundles of amphipathic α -helices, such that their hydrophobic surfaces interact with the lipid core of the membrane and their hydrophilic surfaces point inward, producing an aqueous pore (Fig. 1.2). Other distinct structures such as bundles of β -sheets, or combinations of α -helices and β -sheets are also included in this model of pore formation [47]. The structures are orientated perpendicular to the membrane surface after insertion. The following criteria must be fulfilled for a peptide to act *via* this mechanism [47]: (1) peptides bind to the membrane in a monomeric or multimeric form, (2) monomers recognise each other in the membrane-bound state at low surface density of bound peptide. However, if they reach the membrane as small oligomers they do not dissociate in the membrane, (3) peptides insert in the hydrophobic core of the membrane, (4) progressive recruitment of additional monomers or small oligomers occurs to increase the size of the pore.

A crucial step in this mechanism requires peptides to recognise each other in the membrane-bound state. Peptide-assembly can occur on the surface of the membrane [104-105], or within the hydrophobic core [104-105], since it would be energetically unfavourable for a single amphipathic helix to transverse the membrane as a monomer [47]. It can be assumed that since these peptides can insert into the hydrophobic core of the membrane, their interactions with target membranes are predominantly driven by hydrophobic forces [47]. Furthermore, if they adopt an α -helical structure, their net charge along the peptide backbone should be close to neutral. Peptides using this model tend to be toxic towards bacteria and erythrocytes. Examples include pardaxin [106-107], alamethicin [108], and the helix $\alpha 5$ of δ -endotoxin [109-110].

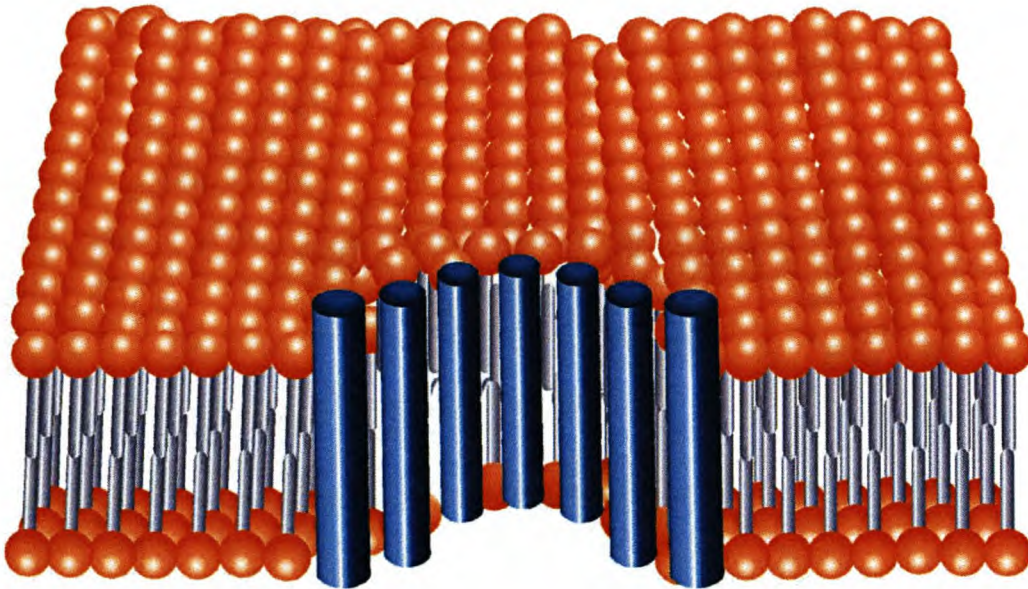


Figure 1.2. Graphical representation of the barrel-stave mechanism during multimeric perpendicular insertion of α -helical peptides (cylinders) into the hydrophobic core of a bilayer membrane. The orange spheres and grey rods represent the lipid head groups and acyl side chains of a bilayer membrane respectively.

1.1.3.3 “Carpet” model for membrane disruption

This model was initially proposed for dermaseptin S [111] and describes a situation where lytic peptides are in contact with the phospholipid head groups throughout the entire process of membrane permeation. According to this model (Fig. 1.3), lytic peptides initially bind onto the surface of the target membrane and cover it in a carpet-like manner (Fig. 1.2). Initial interaction with the negatively charged target membrane is electrostatically driven, and therefore most active peptides with this type of mechanism are positively charged [47]. A high local concentration of membrane-bound peptide must be reached for membrane permeation to occur. Higher peptide concentrations can lead to membrane disintegration. High local concentration on the surface of the membrane depends on the type of target membrane and can occur either after all the surface of the membrane is covered with peptide monomers, or alternatively, after there is an association between membrane-bound peptides which form a local carpet [47]. Contrary to the “barrel-stave” model, peptides are not inserted into the hydrophobic core of the membrane; neither do they assemble with their hydrophilic surfaces facing each other [47]. Furthermore, a peptide that permeates the membrane using the “carpet” model does not require a specific length or the adoption of a secondary structure and can be linear or cyclic upon binding to the membrane [47]. The four steps proposed to be involved in this model are [47]: (1) preferential binding of peptide monomers to the phospholipid head group, (2) alignment of the peptide monomers on the surface of the membrane so that their hydrophilic surface is facing the phospholipid head groups or water molecules, (3) rotation of the peptide monomers leading to orientation of the hydrophobic residues toward the hydrophobic core of the membrane (4), permeating or disintegrating the membrane by disrupting the bilayer curvature to such an extent that vesicles form. It has been proposed that peptides using the “carpet” mechanism have a high net charge, which is spread along the peptide chain, and they bind weakly (or not at all) to zwitterionic membranes, limiting haemolytic activity [47]. However, highly charged peptides can lyse erythrocytes if they form oligomers in solution. The “carpet” mechanism has been used to describe the mode of action of natural analogues of dermaseptin [112-113], cecropins [114-116], LL-37 [102], caerin 1.1 [117], trichogin GA IV [118], and diastereomers of various lytic peptides [47].

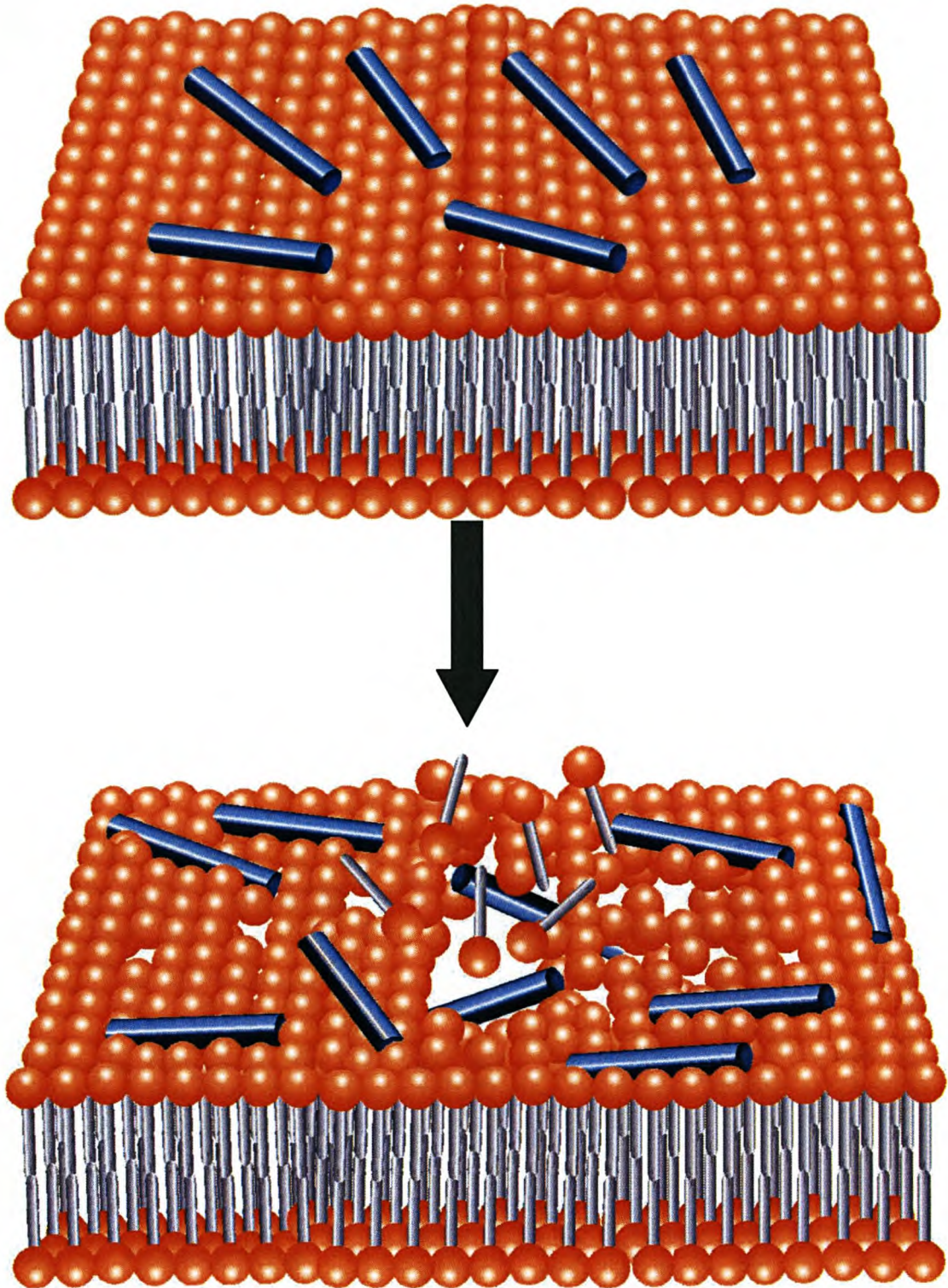
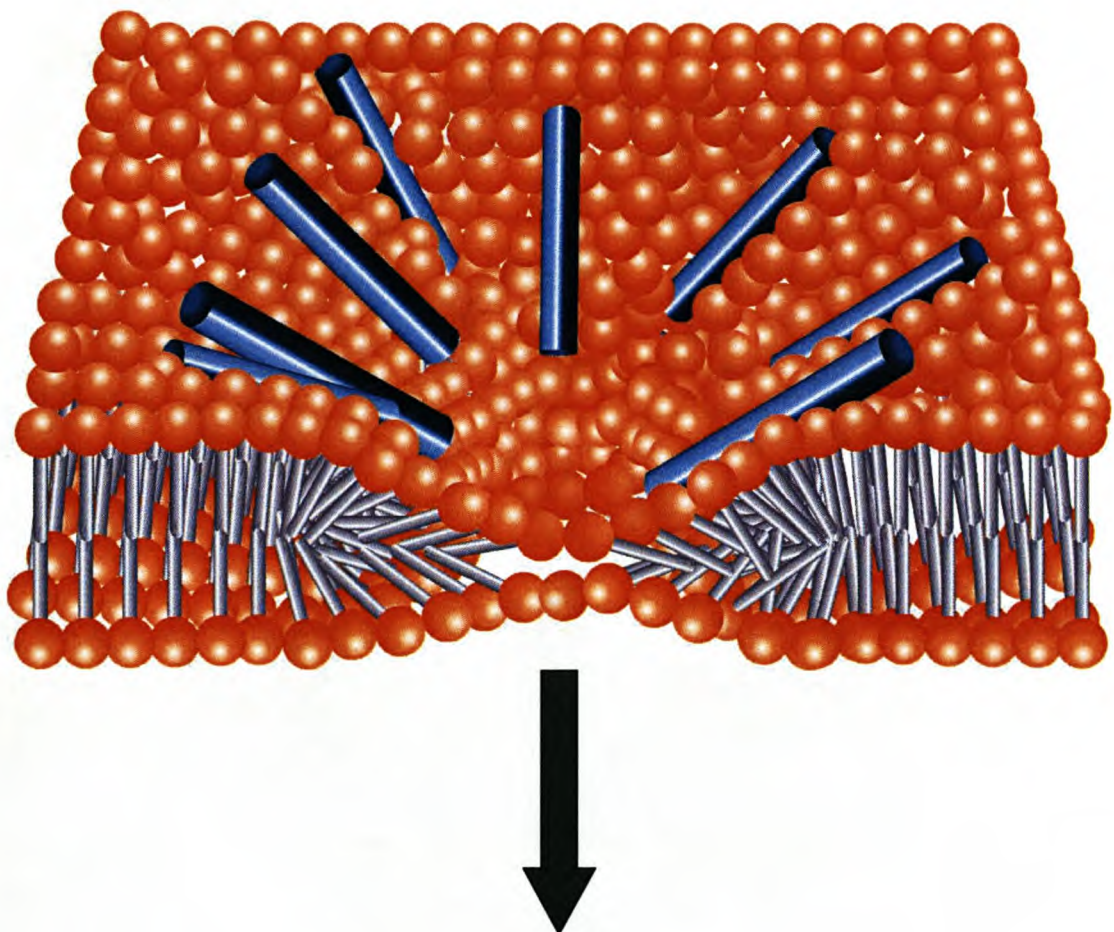


Figure 1.3 Graphical representation of the carpet mechanism illustrating the process of lipid perturbation due to monomeric peptide insertion in a parallel orientation. The blue cylinders represent the monomeric peptides. The orange spheres and grey rods represent the lipid head groups and acyl side chains of a bilayer membrane respectively.

1.1.3.4 “Toroidal” model

The “toroidal” (or wormhole) model [11,65] describes the formation of transient holes in the membrane surface (Fig. 1.4). It is a variation on the lysis phase of the “carpet” model, before the collapse of the membrane packing. These holes would enable the passage of low molecular weight molecules prior to complete membrane lysis. The model describes changes in peptide orientation during insertion, from horizontal to vertical, while maintaining contact with the lipid head group. Consequently, the lipid monolayer bends inwards with the peptide, from the top leaflet to the bottom leaflet, so that unlike the “barrel-stave” model, both the lipid head groups and the peptides line the pore. The “toroidal” model has been proposed for the mode of action of dermaseptin [119] magainin [11,65,120,121], protegrin [122], and recently melittin [123].

These holes may allow the passage of peptide molecules from the outer membrane into the inner membrane of for example, gram-negative bacteria in a process that may be referred to as self-promoting uptake (see 1.1.3.8) [124-126].



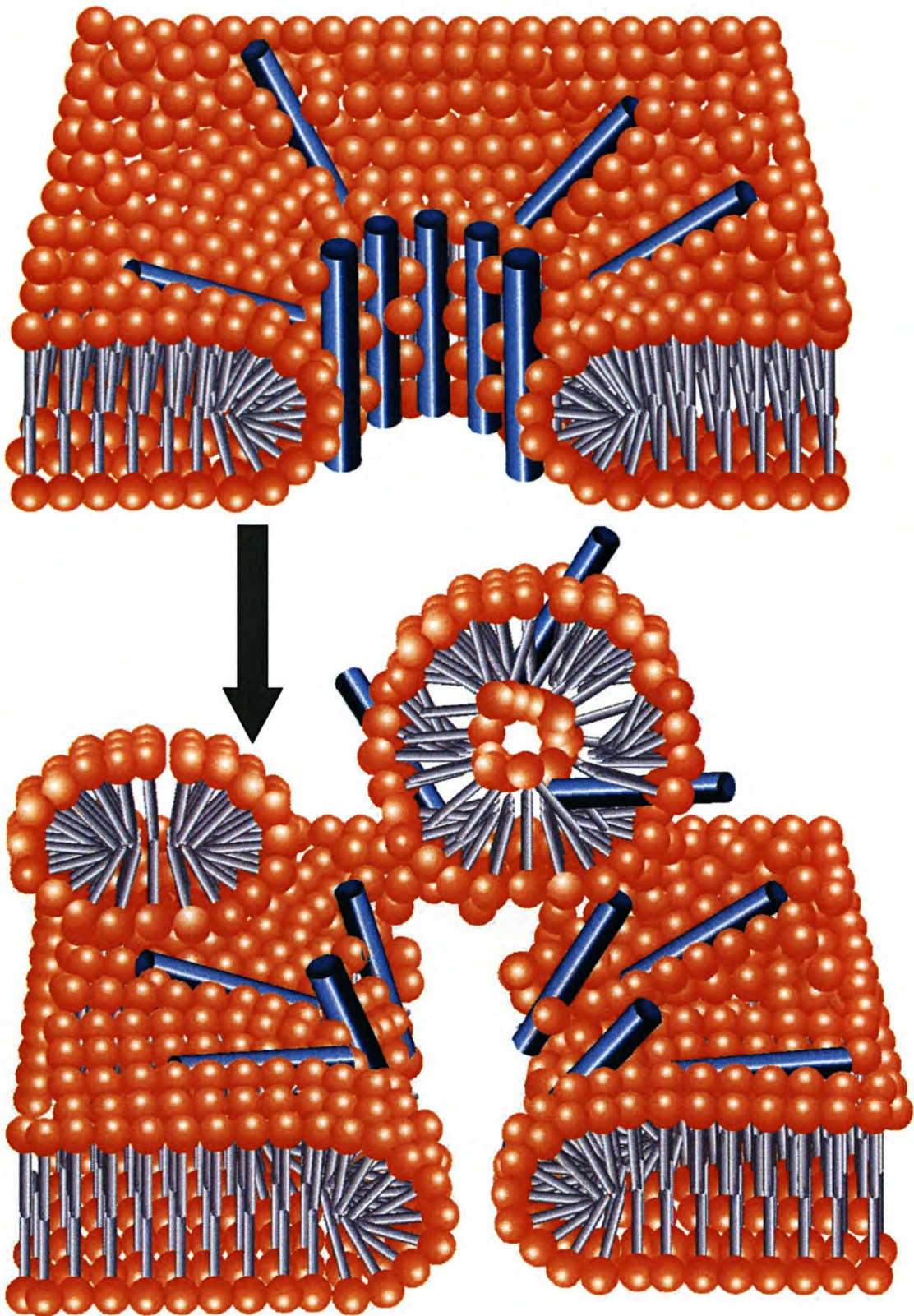


Figure 1.4. Graphical representation of the toroidal mechanism illustrating the intercalation of peptides into the hydrophobic core by a parallel to perpendicular transition. The blue cylinders represent the monomeric peptides. The orange spheres and grey rods represent the lipid head groups and acyl side chains of a bilayer membrane respectively.

1.1.3.5 “Detergent-like” effects

It has been proposed that as an extension of the “carpet” model, some peptides can form destructive peptide-lipid micelle-like structures after accumulating on the surface of membranes in a parallel configuration [127].

Experiments were performed to test the properties of magainin 2 and the micelle-forming detergents Triton-100 and octyl glucoside [128]. The results showed the specific activities of magainin 2 and the detergents were similar in their ability to induce leakage of carboxyfluorescein from PS vesicles [128]. The onset of dye leakage took place at a magainin concentration of approximately 3 mole %. Similar results were obtained with Triton-100 and octyl glucoside. The addition of magainin at high concentration to phospholipid bilayers resulted in the appearance of large water-filled bilayer disruptions [11]. ³¹P solid state NMR spectroscopy detected the optical clearing of dense suspensions and the formation of isotropic phases [10]. Membrane disruptive properties have also been observed for apolipoproteins [129], myelin basic protein [130], glucagon [131], and model peptides [132]. A recent study on melittin [133] showed that release of markers from zwitterionic palmitoylcholine vesicles was highly selective, whereas release from negatively charged palmitoylphosphatidylglycerol vesicles was non-selective and detergent-like.

1.1.3.6 The aggregate channel model

The aggregate channel model [134] proposes that after binding to the lipid head groups, the peptides insert into the membrane and cluster into unstructured aggregates that span the membrane. These aggregates are proposed to have water molecules associated with them, creating channels for the leakage of ions and possibly larger molecules through the membrane. This model differs from the “barrel-stave” and “carpet” models because short-lived trans-membrane clusters of an undefined nature are formed, which allow the peptides to cross the membrane without causing significant membrane depolarisation. Once inside, the peptides find intracellular targets to exert their killing activities [134].

1.1.3.7 Intracellular targets of antimicrobial peptides

A number of studies indicate that the biological activity of certain antimicrobial peptides is due to interference with intracellular targets or processes. The glycine-rich attacins block the transcription of the *omp* gene in *Escherichia coli* [135], whereas magainins and cecropins induce selective transcription of *E. coli* stress-related genes *micF* and *osmY* at sublethal concentrations [136]. Bac 5 and Bac 7 inhibit protein and RNA synthesis of *E. coli* and *Klebsiella pneumoniae* by inhibition of respiration, in addition to their potential to disturb the membranes of these bacteria [88]. Buforin II [137] and PR-39 [138,26] also bind to the cell membranes of *E. coli* without causing permeabilisation and subsequently destroys the bacteria by stopping both DNA and protein synthesis. Histatin 5 and histatin 3 can pass the cytoplasmic membrane of *Candida albicans* [139-141], and histatin 5 targets the mitochondria [140].

1.1.3.8 Self-promoting uptake pathway of gram-negative bacteria

In gram-positive bacteria, cytoplasmic membranes are surrounded by several layers of peptidoglycan containing lipoteichoic acid (LTA), whereas the cytoplasmic membrane of Gram-negative bacteria are surrounded by outer lipid membranes containing cell-surface lipopolysaccharides (LPS). It has been suggested that LPS plays a role in the transport of peptides through this outer membrane [142]. In the proposed self-promoting uptake pathway, cationic peptides bind to LPS, competitively replacing Ca^{2+} and Mg^{2+} , essential for cell surface stability, from their divalent binding sites. This is thought to cause openings in the LPS surface through which small molecules and peptides can pass [142]. This pathway putatively explains the synergy found between several antimicrobial peptides and classic antibiotics acting against gram-negative bacteria [142-144]. However, synergistic effects between peptides and antibiotics have also been found for gram-positive bacteria [145] and *C. albicans* [146].

1.1.3.9 Antiviral Activity

Several antimicrobial peptides also display antiviral activity *in vitro*. Defensins neutralise herpes simplex virus (HSV), vesicular stomatitis virus, and influenza virus [146]. Tachyplesins [147], polyphemusins [147], melittin [14], cecropin [14], and indolicin [148] display anti-HIV activity. The generally accepted mechanism of antiviral action is analogous to the pore-forming models suggested for antibacterial activity, whereby interaction of the

peptides with the virus envelope leads to permeation and lysis of the virus particle. However, other mechanisms have been proposed for peptide T22 that inactivates HIV-1 *in vitro* by binding to the gp120 protein of the virus and the CD4 receptor of T-helper cells. This binding of T22 may block virus-cell fusion in the early stage of the infection [147]. Melittin and cecropins inhibit the replication of HIV-1 by suppression of the expression of the long terminal repeat gene [14].

Each structural parameter plays a role in the combined influence over the mechanism of action of a specific peptide, with the “barrel-stave” model and the “carpet” model representing the opposing poles of all currently accepted models. Many studies are still required before our understanding of the mechanism of action of antimicrobial peptides reaches the level of widespread therapeutic development. The main limiting factor is that the techniques being used are most effective in model membrane systems and therefore alternative methods for the study of natural membrane targets should be explored.

1.2 Visualisation of antimicrobial activity

The availability of analytical and preparative techniques has allowed the application of many biophysical methods for determining the orientation, conformation, and interaction of peptides with lipid membranes, in an attempt to unravel the mechanism of action [10]. These include X-ray crystallography [121,149], nuclear magnetic resonance (NMR) in solution [150] and in the presence of lipid bilayers [150], as well as Fourier transform infrared (FTIR) [151], Raman- [10], fluorescence- [10,151] and circular dichroism (CD) spectroscopy [10,152]. The main reason for the difficulties in establishing a direct correlation between the lipid interaction and the conformation and orientation of peptides is the lack of experimental model systems that mimic the complexity of natural cell membranes. Model systems fail to capture biological features such as lipid heterogeneity, the presence of membrane proteins and relevant features in the periplasm adjacent to the membrane (proteins, negatively charged membrane-derived oligosaccharides, osmolarity, and pH), as well as membrane potential and the pH gradients across the cytoplasmic membrane, etc. Furthermore, methanol, ethanol, acetonitrile, 1,1,1,3,3,3-hexafluoroisopropanol, SDS, and trifluoroethanol (TFE) are the most frequently used membrane-mimetic organic co-solvents to determine the induced conformations relevant to antimicrobial activity [153-154]. However, the induced conformations do not necessarily reflect the peptide conformation upon interacting with lipid surfaces. For example, pardaxin

was shown to adopt a helical or β -sheet conformation depending on whether lipid vesicles or different concentrations of TFE or SDS were used in the experiments [100,155]. The secondary structure of magainin differed between TFE-water mixtures and lipid environments [156,157]. Another example is the significantly different conformations reported for melittin in the presence of detergent micelles and TFE [158].

Even though the structure of many peptides are well established by means of the above-mentioned techniques, the orientation and structure of these peptides in membranes remains controversial (Table 1.3), and conclusions regarding the mechanism of action vary, depending on the experimental methodology. An alternative could lie in combining the structural information obtained from these indirect techniques with the latest advances in microscopy to validate antimicrobial peptide mechanism of action. After all, seeing is believing.

Model Membrane	Peptide:Lipid Ratio	Orientation of bulk of melittin molecules	Reference
DPhPC	1:30	Parallel (23°C)	123
DMPC	1:100	Perpendicular (35°C)	123; 151
DMPC	1:100	Parallel (15°C)	151
DLPC	1:30	Perpendicular (23°C)	123
DOPC	1:100	Parallel (23°C)	189
POPC	1:15	68% perpendicular (23°C)	123
POPC	1:40	85% parallel (23°C)	123
POPC	1:50	Perpendicular (45°C)	133

Table 1.3 Variations in the orientation of melittin because of changes in lipid composition and peptide concentration.

Abbreviations: 1,2-diphytanoyl-*sn*-glycero-3-phosphocholine (DPhPC), 1,2-dimyristoyl-*sn*-glycero-3-phosphocholine (DMPC), 1,2-dilauroyl-*sn*-glycero-3-phosphocholine (DLPC), dioleoylphosphatidylcholine (DOPC), 1-palmitoyl-2-oleoyl-*sn*-glycero-3-phosphocholine (POPC).

1.2.1 Microscopy

To visualise the effects of antimicrobial peptides on target membranes resolution in the nanometer range is required. Many techniques are available with resolution that ranges from micrometers in the case of light microscopy, through to the sub-nanometer range for electron microscopy. Electron microscopes are now available that give point-to-point resolutions of less than 0.2 nanometers [159], but the sample needs to be treated or fixed. In the case of cell membranes, it would result in conformational changes of the peptide and membrane surfaces. This limits the applications and conclusions concerning the mechanism of action of antimicrobial peptides. Various other microscopy techniques are available (polarizing, reflecting, phase-contrast, fluorescence and acoustic microscopy to name a few), but sample treatment is always required to obtain resolution in the nanometer range [160]. However, the last decade has seen rapid development in the field of scanning probe microscopy [161].

Scanning probe microscopes can create three-dimensional (3D) images down to the atomic scale. They function in air, liquid as well as in vacuum, and use a technique for which biological specimens need no staining or fixing [162]. In addition, they can map electronic, mechanical, and optical properties, furthermore, they can even manipulate a surface to the level of moving atoms one by one. The entire scanning microscopy family is based on the invention of scanning tunnelling microscopy (STM) by Binnig *et al.* [163] in 1982. All these techniques are based on a deceptively simple principle whereby a sharp probe interacts with a specimen by raster scanning its surface, providing three-dimensional information in the form of a computer generated image.

Many different physical principles have been used for imaging. These include photo tunnelling with a fibre-optic tip (scanning near-field optical microscopy) [164-165] magnetic interaction with a magnetised probe (scanning magnetic microscopy) [166-167], surface repulsive forces (atomic force microscopy, AFM) [168-169], and ion conduction with a glass pipette [170]. The resolution of these different techniques varies from micrometers into the sub-nanometer range and depends critically on the geometry of the tip and the nature of the interaction. AFM [168] and STM [163] are arguably the most versatile and widely applied in the various fields of research.

Historically, there is normally a long delay for any new imaging method to make headway in biological research. A well-known example is electron microscopy [171]. Even after the first images of biological samples were published, the general perception amongst biologists was not very positive [160]. The reason is that most biological structures were thought of as very delicate and could easily be damaged, raising the question whether the information gathered was entirely relevant to *in vivo* biological structures. It took many years of persistent effort in the development of specimen preparatory techniques and in cross-corroboration with other methods that finally established electron microscopy as a credible method in biology [171-173]. Nowadays, electron microscopy is an essential part of structural research in cell biology and is becoming increasingly important in obtaining structural information, even at atomic resolution. This slow evolution was in sharp contrast with the case of STM and AFM in biology. It took only a few years after the invention of STM before the first images of a biological sample (DNA) were published, claiming the resolution of the double helix pitch or even of the individual bases [174-175]. These images stirred a burst of enthusiasm among researchers from a broad-spectrum of backgrounds [176]. However, because STM requires that a current be passed through the sample, artefacts due to substrate deformation and the inability to understand the contrast formation in these non-conductive structures, generated serious doubts about the validity of the STM images [177]. Admittedly, many of these earlier images were poorly reproducible and the experiments were not conducted with rigorous control [176]. Since AFM does not require that a current be passed through the sample, it became the favoured choice for biological imaging. However, reproducibility due to sample deformation was still a problem but the mechanism of image formation was simpler. These earlier difficulties created a rather negative perception about STM and AFM in general, and the future of these novel technologies in biology was seriously questioned [176-177].

The real breakthrough came with improved preparative methodologies. In 1992, Bustamante *et al.* [178] published the first credible DNA images in air, with a resolution favourably comparable with that of conventional electron microscopy [179]. Within a few months, several other reports of DNA were also published with similar or different preparatory methods at a similar resolution [180], strongly supporting the validity and reproducibility of AFM. From these results, it became clear that AFM was not responsible for the difficulties, but rather the methods of sample preparation, which lead to a rapid development of different techniques, that continues today [181].

At this stage, the emphasis of scanning probe microscopy (SPM) has almost entirely shifted to AFM, with many interesting images being published and resolution improving into the nanometer domain [181]. This rapid development is mainly because structural information about macromolecules can be obtained under physiological conditions at a spatial resolution better than that obtainable with light microscopy [182]. No other structural probe can surpass this performance at the single molecule level. The rapid increase in the number of publications released each year has firmly established AFM as a major contender in structural biology. This is almost unparalleled progress if you consider that AFM was only introduced 16 years ago.

1.2.2 Atomic force microscopy

AFM is the most widely used of the SPM techniques. Invented by Binnig *et al.* [168] in 1986, it is also conceptually the most straightforward. AFM could be compared to a blind person scanning the environment with a stick to explore the path ahead. Deflections of the stick are recorded and used to assemble an image in the brain. In AFM, the sample is scanned with a cantilever whose deflections are monitored by laser and recorded by a computer, which generates a 3D image of the sample's surface (Fig. 1.5). The greatest advantage of AFM is its ability to image the surface of cells and even bio-macromolecules *in situ*, if not *in vivo*, which opens an exciting new approach to visualisation in structural biology. It is not surprising that AFM has become the focus for many novel biological applications in recently published studies [183].

Recently, topographs of α -hemolysin packed into supported lipid bilayers were recorded at 1nm lateral resolution and show that α -hemolysin exists as a hexamer when associated with a lipid bilayer [184]. The functions of the protein complexes were unimpaired, as the topographs were recorded in physiological buffer by low-force contact. This application was utilised in another study on the outer membrane of gram-negative bacteria. These membranes are often assembled from regularly packed protein channels and have been the subject of extensive electron microscopic analyses. Using AFM, changes in an outer membrane pore of *E. coli* (porin OmpF) were recorded [185]. The study showed that pore changes were triggered by a change in pH from 7 to 3, as well as by an external electric field. Another study has also imaged gadolinium-induced pore formation on erythrocytes using 1.5% glutaraldehyde in Tris buffer [186].

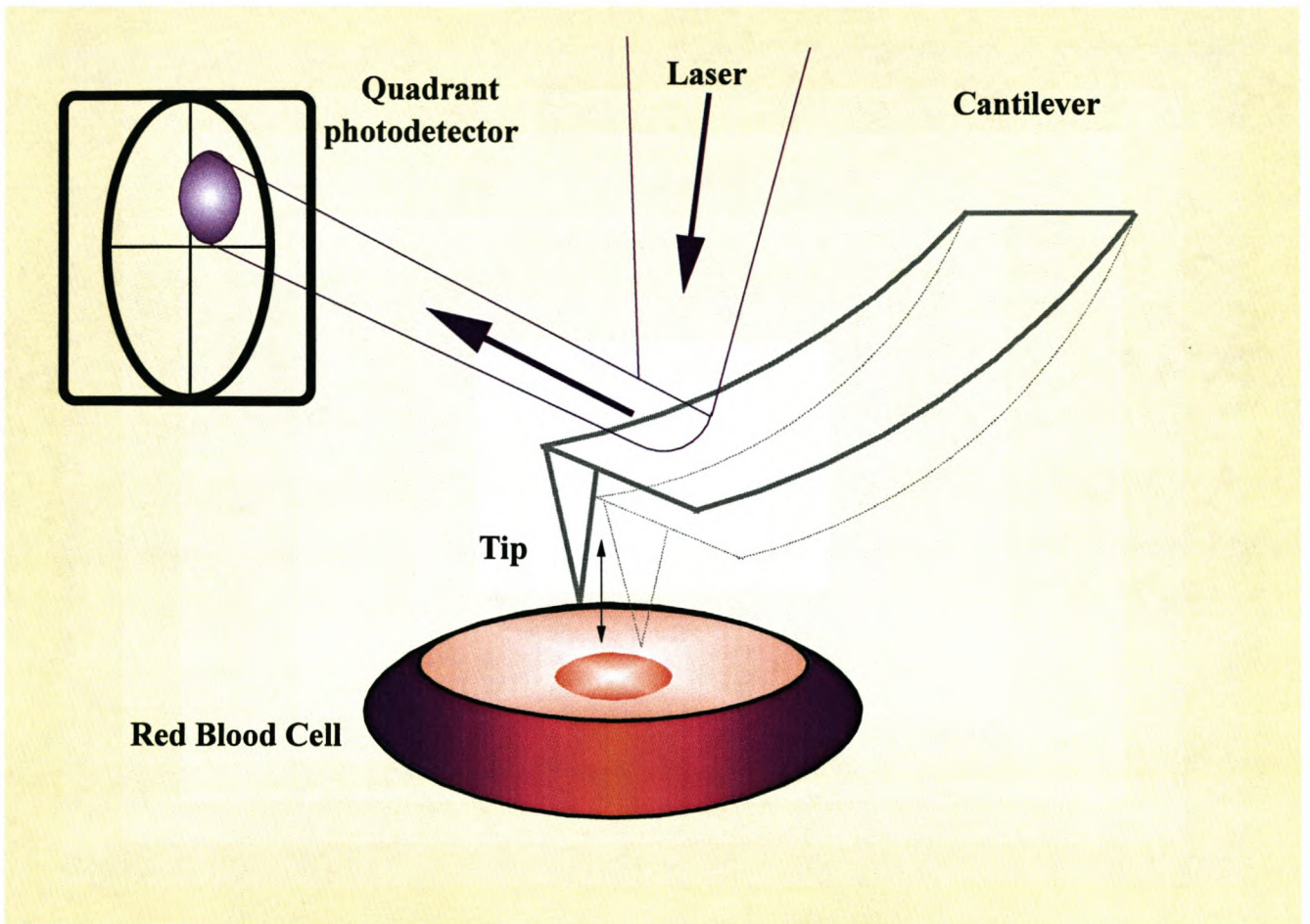


Figure 1.5. Diagram illustrating the atomic force microscope scanning process

These examples highlight the reliable images of eukaryote and bacterial cells that have recently been obtained [187,188] in the nanometer range. This opens a new approach to studying the interaction of antimicrobial peptides with target cell membranes.

We used AFM as a novel approach for studies on antimicrobial peptides and their interaction with target cell membranes. Methods were developed to image the interaction of antimicrobial peptides with target membranes. A comparison was made of the structural changes induced by synthetic magainin (non-toxic) (synthesis and purification described in Chapter 2) and isolated bee-venom melittin (toxic) on different cell membranes (Chapter 3). Dose response effects were observed with both biological activity assays and AFM. Specifically, the activity of these peptides was characterised in terms of lytic activity on eukaryotic cells (goat erythrocytes) and both lytic activity and inhibition of growth of bacterial cells (*E. coli*). Furthermore, we suggest a hypothetical model, based on conclusions drawn from previous model membrane studies and our AFM results (Chapter 4).

1.3 References

1. Bonomo R.A. (2000) *Clin. Infect. Dis.* **31** 1414-1422
2. Wong A.H., Wenzel R.P. and Edmond M.B., (2000) *Am. J. Infect. Control* **28** 277-281
3. G. Kreil; "Antimicrobial peptides from amphibian skin: an overview" in: *Antimicrobial Peptides*; Ciba Foundation Symposium 186, John Wiley & Sons, New York, 1994, pp. 77-90
4. Zasloff M. (1987) *Proc. Natl. Acad. Sci. USA* **84** 5449-5453
5. Zasloff M., Martin B. and Chen H.C. (1988) *Proc. Natl. Acad. Sci. USA* **85** 910-913
6. Gwadz R.W., Kaslow D., Lee J.Y., Maloy W.L., Zasloff M. and Miller L.H. (1989) *Infect. Immun.* **57** 2628-2633
7. Cruciani R.W., Baker J.L., Zasloff M., Martin B., Chen H.C. and Calamonic O. (1991) *Proc. Natl. Acad. Sci. USA* **88** 3792-3796
8. Ohsaki Y., Gazdar A.F, Chen H.C. and Johnson B.E. (1992) *Cancer Res.* **52** 3534-3538

9. Baker M.A., Maloy M.L., Zasloff M. and Jacob I. (1993) *Cancer Res.* **58** 3052-3057
10. Bechinger B. (1997) *J. Membr. Biol.* **156** 197-211
11. Ludtke S.J., He K., Heller W.T., Harroun T.A., Yang L. and Huang H.W. (1996) *Biochemistry* **35** 13723-13728
12. Steiner H., Hultmark D., Engstrom A., Bennich H. and Boman H.G. (1981) *Nature* **292** 246-248
13. Hultmark D., Steiner H., Rasmuson T. and Boman H.G. (1980) *Eur. J. Biochem.* **106** 7-16
14. Wachinger M., Kleinschmidt A., Winder D., von Pechmann N., Ludvigsen A., Neumann M., Holle R., Solmans B., Erfle V. and Brack-Werner R. (1998) *J. Gen. Virol.* **79** 731-740
15. Marcos J.F., Beachy R.N., Houghten R.A., Blondelle S.E. and Pérez-Payá E. (1995) *Proc. Natl. Acad. Sci. USA* **92** 12466-12469
16. Baghain A., Jaynes J., Enright F. and Kousolas K.G. (1997) *Peptides* **18** 177-183
17. Epand R.M and Vogel H.J. (1999) *Biochim. Biophys. Acta.* **1462** 11-28
18. Sansom M.S.P. (1991) *Prog. Biophys. Mol Biol* **55** 139-235
19. Wooley G.A. and Wallace B.A. (1992) *J. Membr. Biol.* **129** 109-136
20. Cross T.A. (1997) *Methods Enzymol.* **289** 672-696
21. Oppenheim F.G., Xu T., McMillan F.M., Levitz S.M., Diamond R., Offner G.D. and Troxler R.F. (1988) *J. Biol. Chem.* **263** 7472-7477
22. Brewer D., Hunter H. and Lajoie G. (1998) *Biochem. Cell. Biol.* **76** 247-256
23. Frank R.W., Gennaro R., Schreider K., Przybylski M. and Romeo D. (1990) *J. Biol. Chem* **263** 9573-9575
24. Skerlavaj B., Romeo D. and Gennaro R. (1990) *Infect. Immun.* **58** 3724-3730
25. Shi, Ross C.R., Leto T.L., Stytle M.J., Mcvey D.S. and Blecha F. (1996) *Proc. Natl. Acad. Sci. USA* **93** 6014-6018
26. Boman H.G., Agerberth B. and Boman A. (1993) *Infect. Immun.* **61** 2978-2984
27. Lawyer C., Pai S., Watabe M., Borgia P., Mashimo T., Eagleton L. and Watabe K. (1996) *FEBS Lett.* **390** 95-98
28. Selsted M.E., Novotny M.J., Morris W.L. Tang Y.Q., Smoth W. and Cullen J.S. (1992) *J. Biol. Chem.* **267** 4292-4295

29. Simmaco M., Mignogna G., Barra D. and Bossa F. (1994) *J. Biol. Chem.* **269** 11956-11961
30. Park J.M., Jung M-E. and Lee B.J., (1994) *Biochem. Biophys. Res. Commun.* **205** 948-954
31. Clark D.P., Durell S., Maloy L.W. and Zasloff M. (1994) *J. Biol. Chem.* **269** 10849-10855
32. Sahl H-G. and Bierbaum G. (1998) *Annu. Rev. Microbiol.* **52** 41-79
33. Tam J.P., Lu Y.A., Yang J.L. and Chiu K.W. (1999) *Proc. Natl. Acad. Sci. USA* **96** 8913-8918
34. Gustafson K.R., Sowder R.C., Henderson L.E., Parsons T.C., Kashman Y., Candellina J.H., McMahon J.B., Buckheit R.W., Pannell L.K. and Boyd M.R. (1994) *J. Am. Chem. Soc.* **116** 9337-9338
35. Lehrer R.I. and Ganz T. (1999) *Curr. Opin. Immunol* **11** 23-27
36. Rautenbach M. and Hastings J.W. (1999) *Chemica oggi* **11/12** 81-87
37. Spencer J.H. (1992) *Advan. Enzyme Regul.* **32** 117-129
38. Bevins C.L. and Zasloff M. (1990) *Annu. Rev. Biochem.* **59** 395-414
39. Hoffmann J.A. and Hetru C. (1992) *Immun. Today* **13** 411-415
40. Broekaert W.F., Cammue B.P.A., De Bolle M.F.C., Thevissen K., De Samblanx G.W. and Osborn R.W. (1997) *Crit. Rev. Plant Sci.* **16** 297-323
41. Matsuzaki K., Yoneyama S., Fujii N., Miyajima K., Yamada K., Kirino Y. and Anzai K. (1997) *Biochemistry* **36** 9799-9806
42. Tamamura H., Kuroda M., Masuda M., Otaka A., Funakoshi S., Nakashima H., Yamamoto N., Waki M., Matsumoto A., Lancelin J.M., Kohoda D., Tate S., Inagaki F. and Fujii F. (1993) *Biochim. Biophys. Acta* **1163** 209-216
43. Kokryakov V.N., Harwig S.S. Panyutich E.A., Shevchenko A.A., Aleshina G.M., Shamova O.V., Korneva H.A. and Lehrer R.I. (1997) *FEBS Lett.* **327** 231-236
44. Cho Y., Turner J.S., Dinh N.N. and Lehrer R.I. (1998) *Infect. Immun.* **66** 2486-2493
45. Nisin and novel lantibiotics, G. Jung and H.-G. Sahl Eds; ESCOM, Leiden, The Netherlands, 1991
46. Montville T.J. and Chen Y. (1998) *Appl. Microbiol. Biotechnol.* **50** 511-519
47. Shai Y. and Oren Z. (2001) *Peptides* **22** 1629-1641

48. Bessalle R., Kapitkovsky A., Gorea A., Shalit I. and Fridkin M. (1990) *FEBS Lett.* **274** 151-155
49. Hetru C., Letellier L., Oren Z., Hoffman J.A. and Shai Y. (2000) *Biochem. J.* **345** 653-654
50. Merrifield R.B, Juvvadi P., Andreu D. Ubach J., Boman A. and Boman H.G. (1995) *Proc. Natl. Acad. Sci. USA.* **92** 3449-3453
51. Wade D., Boman A., Wahlin B., Drain C.M., Andreu D., Boman H.G. and Merrifield R.B. (1990) *Proc. Natl. Acad. Sci. USA* **87** 4761-4765
52. Breukink E., Wiedemann I., van Kraaij C., Kuipers O.P., Sahl H. and de Kruijff B. (1999) *Science* **286** 2361-2364
53. Brock T.D. *Biology of microorganisms.* 2nd ed. Englewood Cliffs (NJ): Prentice-Hall Inc. 1974
54. Verklij A.J, Zwaal R.F., Roelofsen B., Comfurious P., Kastelijn D. and Deenen L.V. (1973) *Biochim. Biophys. Acta.* **323** 178-193
55. Gazit E., Lee W.J., Brey P.T. and Shai Y. (1994) *Biochemistry* **33** 10681-10692
56. Matsuzaki K., Sugishita K. and Miyajima K. (1999) *FEBS Lett.* **449** 221-224
57. Strahilevitz J., Mor A., Nicolas P. and Shai Y. (1994) *Biochemistry* **33** 10951-10960
58. Latal A., Degovics G., Epand R.F., Epand R.M. and Lohner K. (1997) *Eur. J. Biochem.* **248** 938-946
59. Oren Z., Hong J. and Shai Y. (1999) *Eur. J. Biochem* **259** 360-360
60. Oren Z., Lerman J.C., Gudmundsson G.H., Agerberth B. and Shai Y. (1999) *Biochem. J.* **341** 501-513
61. Oren Z. and Shai Y. (1996) *Eur. J. Biochem.* **237** 303-310
62. Choung S-Y., Kobayashi T., Takemoto K., Ishitsuka H. and Inoue K. (1988) *Biochim. Biophys. Act.* **940** 180-187
63. Matsuyama K. and Natori S. (1990) *J. Biochem.* **108** 128-132
64. Matsuzaki K., Sugishita K., Ishibe N., Ueha M., Nakata S., Miyajima K. and Epand R.M. (1998) *Biochemistry* **37** 11856-11863
65. Matsuzaki K., Murase O., Fujii N. and Miyajima K. (1996) *Biochemistry* **35** 11361-11368

66. S.G. Wilkinson; *Microbial Lipids*, vol. 1, C. Ratledge, S.G. Wilkinson Eds.; Academic Press, London, 1988, pp. 299-488
67. W.M. O'Leary and S.G. Wilkinson; *Microbial Lipids*, vol. 1, C. Ratledge, S.G. Wilkinson Eds.; Academic Press, London, 1988, pp. 117-201
68. M.A. Yorek, in: G. Cevc (Ed.), *Phospholipid Handbook*, Marcel Dekker, New York, 1993, pp. 745-775
69. Epand R.M. (1998) *Biochim. Biophys. Acta* **1376** 353-368
70. Tytler E.M., Segrest J.P., Epand R.M., Nie S.-Q., Epand R.F., Mishra V.K., Venkatachalapathi Y.V. and Anantharamaiah G.M. (1993) *J. Biol. Chem.* **268** 22112-22118
71. Batenburg A.M., van Esch J.H. and deKruiff A. (1988) *Biochemistry* **27** 2324-2331
72. Colotto A., Lohner K. and Laggner P. (1991) *J. Appl. Cryst.* **24** 847-851
73. Charvolin J. (1985) *J. Phys. (Paris) Colloq.* **46** 173-190
74. Prenner E.J., Lewis R.N.A.H., Neuman K.C., Grunner S.M., Kondejewski L.H., Hodges R.S. and McElhaney R.N (1997) *Biochemistry* **36** 7906-7916
75. Keller S.L., Gruner S.M. and Gawrisch K. (1996) *Biochim. Biophys. Acta* **1278** 241-246
76. Oren Z. and Shai Y. (1997) *Biochemistry* **36** 1826-1835
77. Shai Y. and Oren Z. (1996) *J. Biol. Chem.* **271** 7305-7308
78. Oren Z., Hong J. and Shai Y. (1997) *J. Biol. Chem.* **272** 14643-14649
79. Dathe M., Schümann M., Wieprecht T., Winkler A., Beyermann M., Krause E., Matsuzaki K., Murase O. and Bienert M. (1996) *Biochemistry* **35** 12612-12622
80. Wieprecht T., Dathe M., Schümann M., Krause E., Beyermann M. and Bienert M. (1996) *Biochemistry* **35** 10844-18853
81. Eisenberg D. (1984) *Annu. Rev. Biochem.* **53** 595-623
82. Dathe M., Wieprecht T., Nikolenko H., Handel L., Maloy W.L., MacDonald D.L., Beyermann M. and Beinert M. (1997) *FEBS. Lett.* **403** 208-212
83. Dathe M., MacDonald D.L., Maloy W.L., Beyermann M., Krause E., Beinert M., in *Peptide Science- Present and Future*; Y. Shimonishi (Ed), Kluwer Academic Publishers, Dordrecht, 1999, pp 684-686
84. Dathe M. and Wieprecht T. (1999) *Biochim. Biophys. Acta* **1462** 71-87

85. Eisenberg D., Scharz E., Komaromy M. and Wall R. (1984) *J. Mol. Biol.* **179** 125-42
86. Ohmori N., Niidome T., Hatakeyama T., Mihara H. and Aoyagi H. (1998) *J. Pept. Res.* **51** 103-109
87. Blondelle S.E. and Houghten R.A. (1992) *Biochemistry* **31** 12688-12694
88. Skerlavaj B., Gennaro R., Bagella L., Merluzzi L., Risso A. and Zanetti M. (1996) *J. Biol. Chem.* **271** 28375-28381
89. Kwon M.Y., Hong S.Y. and Lee K.H. (1998) *Biochim. Biophys. Acta* **1387** 239-248
90. Helmerhorst E.J., Reijnders I.M., Van't Hof W., Veerman E.C.I. and Nieuw Amerongen A.V. (1999) *FEBS Lett.* **449** 105-110
91. Bessalle R., Gorea A., Shalit I., Metzger J.W., Dass C., Desiderio D.M. and Fridkin M. (1993) *J. Med. Chem.* **36** 1203-1209
92. Ohmori N., Niidome T., Hatakeyama T., Mihara H. and Aoyagi H. (1998) *J. Pept. Res.* **51** 103-109
93. Juvvadi P., Vunnam S., Merrifield E.L., Boman H.G. and Merrifield R.B. (1996) *J. Pept. Sci.* **2** 223-232
94. Mee R.P., Auton T.R. and Morgan P.J. (1997) *J. Pept. Res.* **49** 89-102]
95. Brasseur R., Pillot T., Lins J., Vandekerckhove J. and Rosseneu M. (1997) *Trends Biochem. Sci.* **22** 167-17
96. Uematsu N. and Matsuzaki K. (2000) *Biophys. J.* **79** 2075-2083
97. Dhople V.M. and Nagaraj R. (1995) *Protein Eng.* **8** 315-318
98. Bessalle R., Haas H., Gorla A., Shalit I. and Fridkin M. (1992) *Agents Chemother.* **36** 313-317
99. Matsuzaki K., Sugishita K., Harada M., Fujii N. and Miyajima K. (1997) *Biochim. Biophys. Acta* **1327** 119-130
100. Thennarasu S. and Nagaraj R. (1996) *Protein Eng.* **9** 1219-1224
101. Wieprecht T., Dathe M., Beyermann M., Krause E., Maloy W.L., MacDonald D.L. and Bienert M. (1997) *Biochemistry* **36** 6124-6132
102. Oren Z. and Shai Y. (2000) *Biochemistry* **39** 6103-6114
103. Ehrenstein G. and Lecar H. (1977) *Q. Rev. Biophys.* **10** 1-34
104. Efraim I.B. and Shai Y. (1997) *Biophys. J.* **72** 85-96
105. Shai Y. (1995) *Trends Biochem. Sci.* **20** 460-464

106. Rapaport D. and Shai Y. (1991) *J. Biol. Chem.* **266** 23769-23775
107. Shai Y., Bach D. and Yanovsky A. (1990) *J. Biol. Chem.* **265** 20202-20209
108. Rizzo V., Stankowski S. and Schwarz G. (1987) *Biochemistry* **26** 2751-2759
109. Gazit E., Bach D., Kerr I.D., Sansom M.S., Chejanovsky N. and Shai Y. (1994) *Biochem. J.* **304** 895-902
110. Gazit E. and Shai Y. (1993) *Biochemistry* **32** 3429-3436
111. Pouny Y., Rapaport D., Mor A., Nicolas P. and Shai Y. (1992) *Biochemistry* **31** 12416-12423
112. Ghosh J.K., Shaool D., Guillaud P., Ciceron L., Mazier D., Kustanovich I. and Y. Shai (1997) *J. Biol. Chem.* **272** 31609-31616
113. Strahilevitz J., Mor A., Nicolas P. and Shai Y. (1994) *Biochemistry* **33** 10951-10960
114. Gazit E., Boman A., Boman H.G. and Shai Y. (1995) *Biochemistry* **34** 11479-11488
115. Gazit E., Lee W.J., Brey P.T. and Shai Y. (1994) *Biochemistry* **33** 10681-10692
116. Gazit E., Miller I.R., Biggin P.C., Sansom M.S.P. and Shai Y. (1996) *J. Mol. Biol.* **258** 860-870
117. Wong H., Bowie J.H. and Carver J.A. (1997) *Eur. J. Biochem.* **247** 545-557
118. Monaco V., Formaggio F., Crisma M., Toniolo C., Hanson P. and Millhauser G.L. (1999) *Biopolymers* **50** 239-253
119. Mor A. and Nicolas P. (1994) *J. Biol. Chem.* **269** 1934-1939
120. Matsuzaki K., Murase O. and Miyajima K. (1995) *Biochemistry* **34** 12553-12559
121. Yang L., Weiss T.M., Lehrer R.I. and Huang H.W. (2000) *Biophys. J.* **79** 2002-2009
122. Heller W.T., Waring A.J., Lehrer R.I. and Huang H.W. (1998) *Biochemistry* **37** 17331-17338
123. Yang L., Harroun T.A., Weiss T.M., Ding L. and Huang H.W. (2001) *Biophys. J.* **81** 1475-1485
124. Sawyer J.G., Martin N.L and Hancock R.E. (1988) *Infect. Immun.* **56** 693-698
125. Piers K.L. and Hancock R.E. (1994) *Mol. Microbiol.* **12** 951-958
126. Falla T.J., Karunaratne D.N. and R.E.W. Hancock (1996) *J. Biol. Chem.* **271** 19298-19303
127. Oren Z. and Shai Y. (1998) *Biopolymers* **47** 451-463

128. Grant Jr. E., Beeler T.J., Taylor K.M., Gable K. and Roseman M.A. (1992) *Biochemistry* **31** 9912-9918
129. Segrest J.P., Garber D.W., Brouillette C.G., Harvey S.C. and Anantharamaiah G.M. (1994) *Adv. Protein Chem.* **45** 303-309
130. Roux M., Nezil F.A., Monck M. and Bloom M. (1994) *Biochemistry* **33** 307-311
131. Jones A.J.S., Epand R.M., Lin K.F., Walton D. and Vail W.J. (1978) *Biochemistry* **17** 2301-2307
132. Reynaud J.A., Grivet J.P. Sy D. and Trudelle Y. (1993) *Biochemistry* **32** 4997-5008
133. Ladokhin A.S. and White S.H. (2001) *Biochim. Biophys. Acta.* **1514** 253-260
134. Hancock R.E.W. and Chappie D.S. (1999) *Antimicrob. Agents Chemother.* **43** 1317-1323
135. Carlsson A., Engström P., Palva E.T. and Bennich H. (1991) *Infect. Immun.* **59** 3040-3045
136. Oh J., Cajal Y., Skowronska E.M., Belkin S., Chen J., Van Dyk T.K., Sasser M. and Jain M.K. (2000) *Biochim. Biophys. Acta* **1463** 43-54
137. Park C.B., Kim H.S. and Kim S.C. (1998) *Biochem. Biophys. Res. Commun.* **244** 253-257
138. Cabiaux V., Agerberth B., Johansson J., Homble F., Goormaghtigh E. and Ruyschaert J.M. (1994) *Eur. J. Biochem.* **224** 1019-1027
139. Edgerton M., Koshiukova S.E., Lo T.E., Chrzan B.G., Straubinger R.M. and Raj P.A. (1998) *J. Biol. Chem.* **273** 20438-20447
140. Helmerhorst E.J., Breeuwer P., Van't Hof W., Walgreen-Weterings E., Oomen L.C.J.M., Veerman E.C.I., Nieuw Amerongen A.V. and Abee T. (1999) *J. Biol. Chem.* **274** 7286-7291
141. Xu Y., Ambudkar I., Yamagishi H., Swaim W., Waish T.J. and O'Connell B.C. (1999) *Antimicrob. Agents Chemother.* **43** 2256-2262
142. Hancock R.E.W. (1997) *Peptide antibiotics, Lancet* **349** 418-422
143. Giacometti A., Cirioni O., Barchiesi F., Fortuna M. and Scalise G. (1999) *J. Antimicrob. Chemother.* **44** 641-645
144. Scott M.G., Gold M.R. and Hancock R.E. (1999) *Infect. Immun.* **67** 6445-6453
145. Nykanen A., Vesanen S. and Kallio H. (1998) *Lett. Appl. Microbiol.* **27** 345-348

146. Van't Hof W., Veerman E.C.I., Helmerhorst E.J. and Niew Amerongen A.V. (2001) *J. Biol. Chem.* **382** 597-619
147. Tamamura H., Ishihara T., Otaka A., Murakami T., Ibuka T., Waki M., Matsumoto A., Yamamoto N. and Fujii N. (1996) *Biochim. Biophys. Acta.* **1298** 37-44
148. Robinson W., McDougall B., Tran D. and Selsted M.E. (1998) *J. Leukoc. Biol.* **63** 94-100
149. Terwilliger T.C., Weissman L. and Eisenberg D (1982) *Biophys. J.* **37** 353-361
150. Bechinger B. (1999) *Biochim. Biophys. Acta* **1462** 157-183
151. Blondelle S.E., Lohner K. and Aguilar M-I. (1999) *Biochim. Biophys. Acta* **1462** 89-108
152. Hwang P.M. and Vogel H.J. (1998) *Biochem. Cell Biol.* **76** 235-246
153. Zhong L. and Johnson Jr. W.C. (1992) *Proc. Natl. Acad Sci. USA* **89** 4462-4465
154. Jasanoff A. and Fersht A.R. (1994) *Biochemistry* **33** 2129-2135
155. Thennarasu S. and Nagaraj R. (1997) *Biopolymers* **41** 635-645
156. Matzusaki K., Harada M., Funakoshi S., Fujii N. and Miyajima K. (1991) *Biochim. Biophys. Acta* **1063** 162-170
157. Matzusaki K., Nakamura A., Murase O., Sugishita K., Fujii N. and Miyajima K. (1997) *Biochemistry* **36** 2104-2111
158. Okada A., Wakamatsu K., Miyazawa T. and Higashijima T. (1994) *Biochemistry* **33** 9438-9446
159. www.Britannica.com
160. Shao Z., Mou J., Czajkowsky D.M., Yang J. and Yuan J-Y. (1996) *Adv. Phys.* **45** 1-86
161. Miles M. (1997) *Science* **277** 1845-1847
162. Salmeron M. (1997) *Chem. Rev.* **97** 1163-1194
163. Binnig G., Rohrer H., Gerber Ch. and Wiebel E. (1982) *Appl. Phys. Lett.* **40** 178-180
164. Durig U., Pohl D.W. and Rohner F. (1986) *J. Appl. Phys.* **59** 3318-3327
165. Betzig E. and Chichester R.J. (1993) *Science* **262** 1422-1425
166. Martin Y. and Wickramasinge H.K. (1987) *Appl. Phys. Lett.* **50** 1455-1458

167. Saenz J.J., Garcia N., Grutter P., Meyer E., Heinzelmann H., Wiesendanger R., Rosenthaler L., Hidber H.R. and Guntherodt H.J. (1987) *J. Appl. Phys.* **63** 4293-4295
168. Binnig G., Quate C.F. and Gerber C. (1986) *Phys. Rev. Lett.* **56** 930-933
169. Quate C.F. (1994) *Surf. Sci.* **299-300** 980-995
170. Hansma P.K., Drake B., Marti O., Gould S.A. and Prater C.B. (1989) *Science* **243** 641-643
171. Oatley C.W., McMullan D. and Smith K.C.A. (1985) *The Development of the Scanning Electron Microscope*, in *The Beginnings of Electron Microscopy*, ed P W Hawkes. *Advances in Electronics and Electron Physics Suppl.* **16** (London: Academic Press) pp 443-482
172. Dykstra M. J., 1992 *Biological Electron Microscopy: Theory, Techniques and Troubleshooting*, Plenum Press, New York, NY.
173. Kühlbrandt W. (1994) *Curr. Opin. Struct. Biol.* **4** 519-528
174. Amrein M., Durr R., Staslak A., Gross H. and Travaglini G. (1989) *Science* **243** 1708-1711
175. Arscott P.G., Lee G., Bloomfield V.A. and Evans D.F. (1989) *Nature* **339** 484-486
176. Engel A. (1991) *A. Rev. Biophys. biophys. Chem.*, **20** 79-108
177. Clemmer C.R. and Beebe Jr. T.P. (1991) *Science* **251** 640-642
178. Bustamante C., Vesenka J., Tang C.L. Rees W., Guthod M. and Keller R. (1992) *Biochemistry* **31** 22-26
179. Kleinschmidt A.K. (1968) *Methods in Enzymology*, Vol XII (Grossman L., and Moldave K. eds.) Academic Press, New York, pp361-377
180. Henderson E. (1992) *Nucleic Acids Res.* **20** 445-447
181. Engel A., Gaub H.E. and Müller D (1999) *Curr. Biol.* **9** 133-136
182. T. Wilson, *Confocal Microscopy*. San Diego, CA: Academic Press Ltd., 1990
183. Engel A., Lyubchenko Y. and Müller D. (1999) *Trends Cell Biol.* **9** 77-80
184. Czajkowsky D.M. and Shao Z. (1998) *FEBS Lett.* **430** 51-54
185. Müller D.J. and Engel A. (1999) *J. Mol Biol* **285** 1347-1351
186. Cheng Y., Liu M., Rongchang L., Wang C., Bai C. and Wang K. (1999) *Biochim. Biophys. Acta.* **1421** 249-260
187. Yamashina S. and Katsumata O. (2000) *J. Electron Microscopy* **49** 445-451

188. Bolshakova A.V., Kiselyova O.I., Filonov A.S., Frolova O.Y., Lyubchenko Y.L. and Yaminsky I.V. (2001) *Ultramicroscopy* **86** 121-128
189. Hristova K., Dempsey C.E. and White S.H. (2001) *Biophys. J.* **80** 801-811

Chapter 2

Synthesis and purification of magainin 2

2.1 Introduction

Since the turn of the last century, peptide synthesis has been a great challenge to organic chemists, when the pioneering success of Curtius [1] and later Fischer [2] stimulated new theories in protein structure [3,4]. By the early 1950s it was realised that other important biological molecules had simpler amino acid sequences resulting in the subsequent isolation and synthesis of the first biologically active peptide called oxytocin, a lactogenic nonapeptide amide hormone [5]. This stimulated a surge of interest in the scientific community resulting in the synthesis of numerous biologically active peptides. Pharmaceutical companies also realised the market potential, but classical methods of solution peptide synthesis were hard pressed to meet the explosive increase in demand. In 1962 R.B. Merrifield proposed a solution to the problem [6] with a new procedure called solid phase peptide synthesis (SPPS). The method was initially criticised because of its potential for many side-reactions and contaminants. However, by 1964 Merrifield had substantially developed the technique [7] to the extent that he was able to synthesise the naturally occurring nonapeptide bradykinin in four days (instead of four weeks) and isolated, purified, and fully characterised it in a further five days. Merrifield's technique was well timed and adopted with enthusiasm by biochemists, pharmacologists, and others who saw an answer to their pressing need for synthetic analogues of the many natural peptides being discovered.

Solid phase peptide synthesis has predominant advantages over solution peptide synthesis because of the simplicity of separation from reagents and solvents by filtration and washing, as well as the consequent savings in time and labour. Physical losses are also kept to a minimum, excess reagents can be utilized to drive the reactions to completion, and subsequently many of the operations are open to automation. This approach does, however, have its limitations: by-products formed from either incomplete reactions, side-reactions, or impure reagents will accumulate on the resin during chain assembly and contaminate the final product. This has serious implications with regard to product purification, because the

impurities generated are often very similar to the desired peptide and therefore extremely difficult to separate. The principles of solid phase synthesis are illustrated in Figure 2.1.

The two main techniques used in solid phase peptide synthesis are the Merrifield and the 9-fluorenylmethoxycarbonyl-based (Fmoc-based) techniques respectively. The principal features of the Merrifield technique [8-10] are illustrated in Figure 2.2.

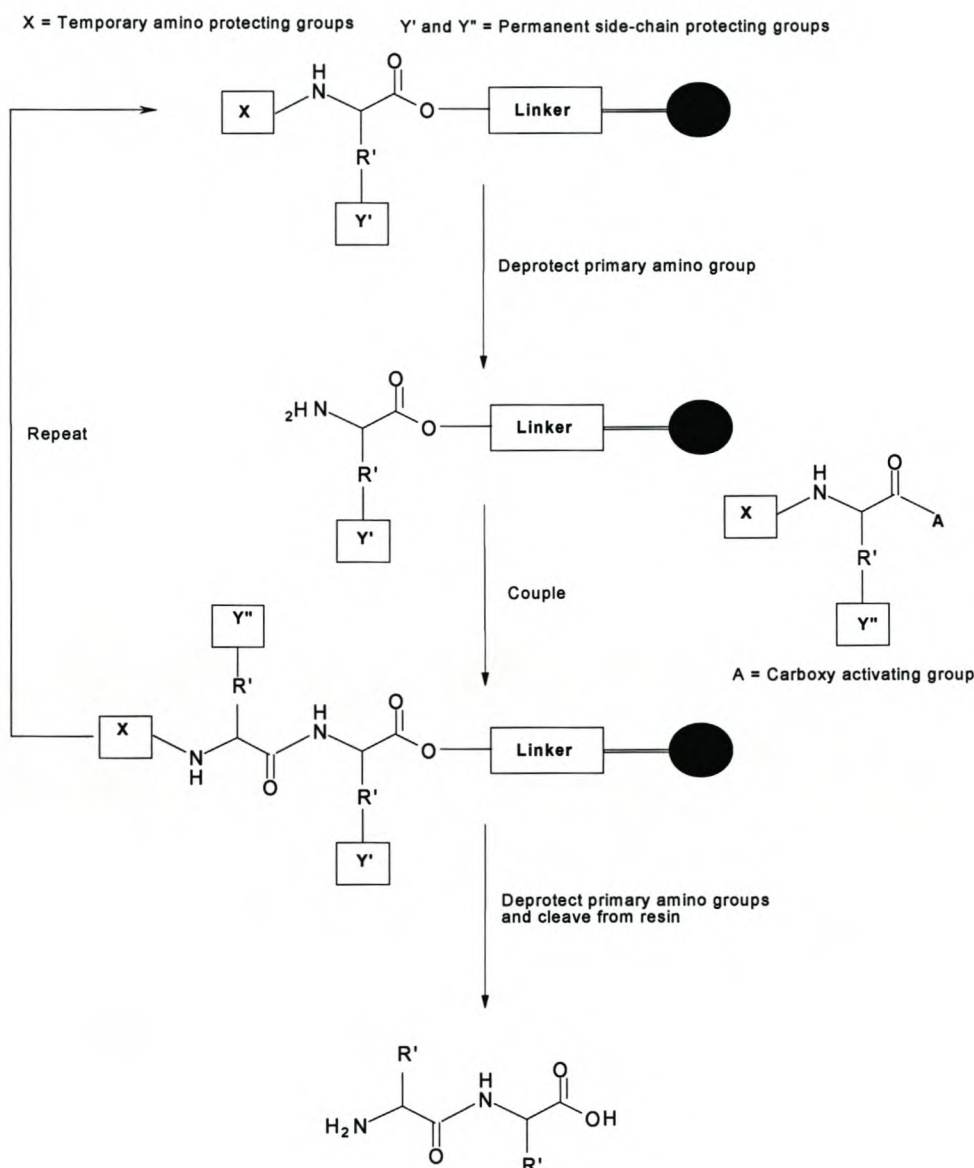


Figure 2.1 Principles of SPPS: The carboxyl group of the first C-terminal amino acid residue is attached with an ester-bond to the linker of the insoluble support. Any functional amino acid groups must be masked with permanent protecting groups that are not affected by the reactions conditions used during peptide synthesis. The temporary protecting groups masking the α -amino groups during the initial loading of the resin are removed.

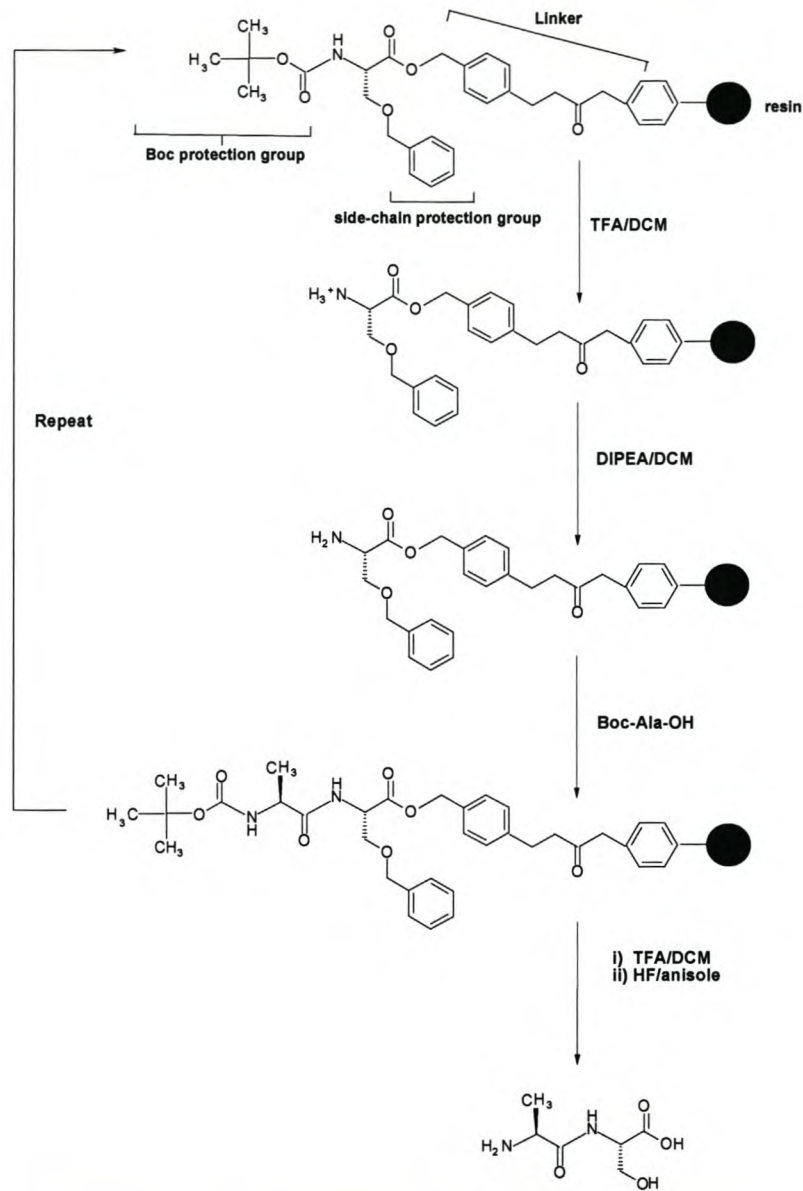


Figure 2.2 Merrifield SPPS: The C-terminal is anchored to the support through the formation of a benzyl ester with hydroxymethylphenylacetamidomethyl polystyrene (PAM resin). The tert-butoxycarbonyl (Boc) group is used for temporary protection of the α -amino group and trifluoroacetic acid (TFA) or TFA in dichloromethane (DCM) is used to liberate it from the amino acid. The resulting trifluoroacetate is neutralised prior to coupling using diisopropylethylamine (DIPEA) in DCM. Coupling is mostly carried out using pre-formed amino acid symmetrical anhydrides or benzotriazolyl esters in *N,N'*-dimethylformamide (DMF) or *N*-methylpyrrolidone (NMP). The side-chains are protected using a wide range of benzyl-based protecting groups. Anhydrous hydrogen fluoride is used for release of the peptide from the resin and for removal of the side-chain protection groups.

Improvements in the quality of base-resin material, tert-butoxycarbonyl (Boc)-protecting amino acids, and the introduction of improved hydrogen fluoride (HF) cleavage procedures has made this technique an extremely powerful tool in the last few years. However, the need

to use highly toxic liquid HF in a special polytetrafluoroethylene (PTFE)-lined apparatus has generally deterred most newcomers to the field from using this technique.

Unlike the Merrifield approach that makes use of graduated acidolysis (Fig. 2.2), Fmoc-based SPPS (Fig. 2.3), developed in the late 1970s [11] is based on an orthogonal protecting group strategy. A base labile *N*-Fmoc group was used for protection of the α -amino group and acid-labile side-chain protection groups and resin-linkage agents. Since removal of the temporary and permanent protection is effected by completely different chemical mechanisms, side-chain protecting groups and linkage agents can be employed that are removed under considerably milder conditions than those used in the Merrifield method. *t*-butyl- and trityl-based side-chain protection and alkoxybenzyl-based linkers are used, as they can be removed using TFA. This reagent is an excellent solvent for peptides. It can be used with standard laboratory glassware and being volatile, is readily removed by evaporation. The results of an unprecedented survey paper [12] by the Association of Biomolecular Research Facilities highlighted the superiority of the Fmoc strategy, confirming its undoubted status as the most popular method for SPPS and a well-established method in our laboratory. The principle features of the Fmoc-based SPPS [13,14] are illustrated in Figure 2.3.

We used the Fmoc-based SPPS to synthesise Magainin 2 ($M_r=2466.93$; **GIGKFLHSAKKFGKAFVGEIMNS**). We chose this peptide because of its unique and well-documented mechanism of action, as well as its broad-spectrum of activity and lack of toxicity [15,16]. Magainin's structural parameters do not favour haemolytic interactions, as the positive charges are spread over the whole peptide and the hydrophobicity and hydrophobic moment are moderate [17]. However, electrostatic interactions do promote antimicrobial activity towards gram-negative and gram-positive bacteria [18,19].

We used melittin purchased from Sigma (M_r 2846.50; **GIGAVLKVLTTGLPALISWIKRKRQQ-amide**) as a control peptide during our AFM studies. We chose this peptide because of its lack of selectivity between mammalian and bacterial cells [20]. Melittin's structural parameters favour haemolytic activity, as the N-terminal is strongly hydrophobic with a large hydrophobic angle, promoting deep penetration into the hydrophobic membrane surface, which might favour the association of membrane bound peptides to form pores [17,21]. In addition, it has an amphipathic highly positive C-terminal sequence, which contributes to its activity against gram-positive and gram-negative bacteria [17].

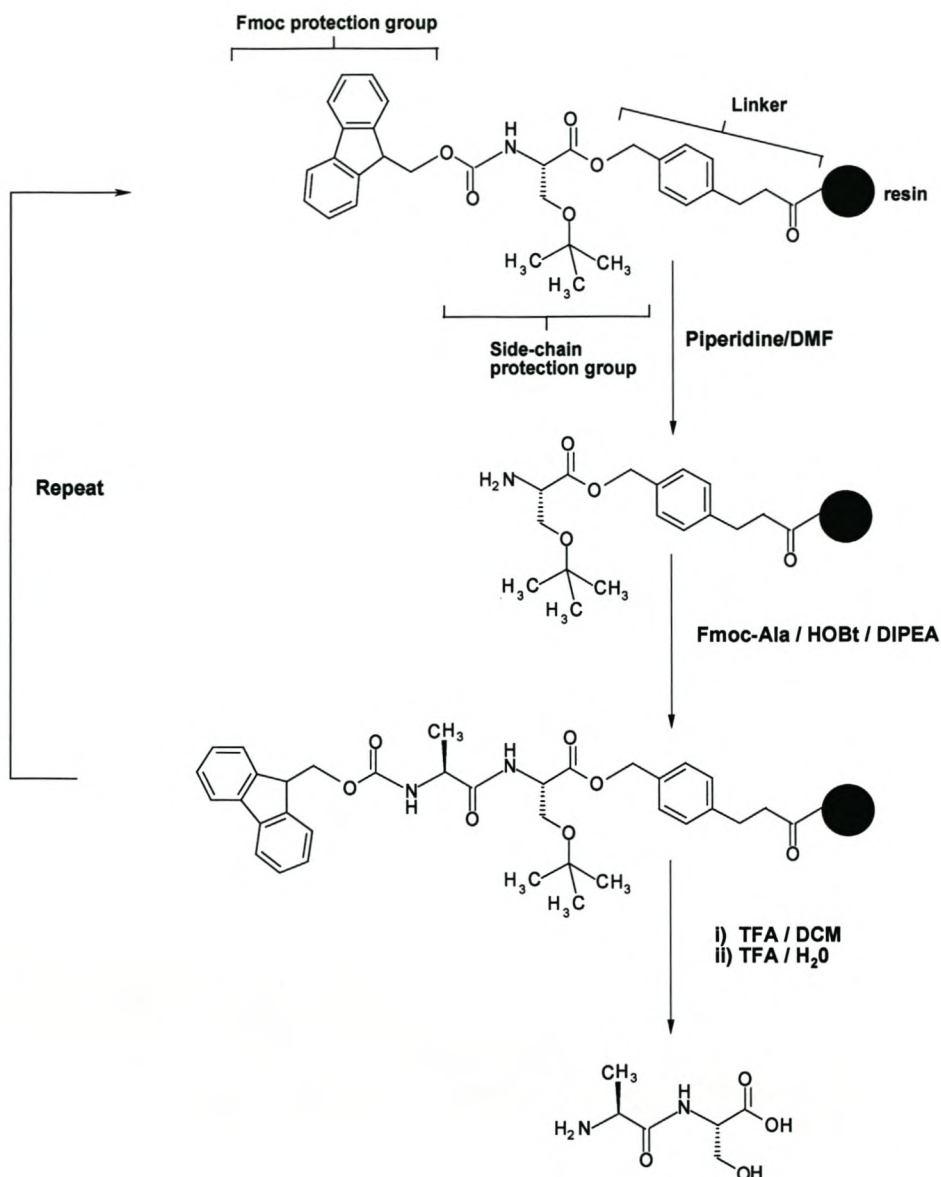


Figure 2.3 Fmoc-based SPPS: The C-terminal of the first residue is anchored to a TFA-labile linkage agent. The side-chains are protected with TFA-labile protecting groups. The temporary N^α -Fmoc protecting group is removed with 20% piperidine in DMF. Coupling is typically carried out in DMF or NMP with pre-formed active esters or using activation reagents that generate benzotriazolyl esters. Cleavage of side-chain protecting groups and the peptide from the resin is achieved with 95% TFA.

2.2 Materials

2.2.1 General reagents and solvents

N, N'-dimethylformamide (DMF; 99.5%), ethyl acetate (99.5%), glacial acetic acid (99.8%), sodium carbonate (anhydrous), phosphorus-pentoxide, molecular sieve (4 Å beads approximately 3.2 mm) and self-indicating silica gel were purchased from Saarchem (Krugersdorp, South Africa). Diethyl ether (99.5%), *n*-hexane (99.8%), tert-amylalcohol (>99%), ethanol (99.8%), piperidine (98%), pyridine (99.5 %), trifluoroacetic acid (TFA; >98% and 99.5%), potassium cyanide (KCN), ninhydrin, 1-fluoro-2,4-dinitrobenzene (FDNB) and phenol were purchased from Merck (Darmstadt, Germany). Piperidine (99%), pyridine (99.9%) and TFA (>98%) were also purchased from Sigma (Steinheim, Germany). Thioanisol and 1, 2-ethanedithiol were from Fluka (Steinheim, Germany). Nitrogen gas was provided by Afrox, South Africa.

2.2.2 Derivatives, catalysts and resins for peptide synthesis

Pepsyn KA-resin (0.15 & 0.2 meq/g), Fmoc-L-Ala-OPfp¹, Fmoc-L-Gly-OPfp, Tboe-Gly-OH, Fmoc-L-His-(Boc)-OH, Fmoc-L-Ile-OH, Fmoc-L-Ile-Opfp, Fmoc-L-Leu-OPfp, Fmoc-L-Leu-OH, Fmoc-L-Lys-OPfp, Fmoc-L-Met-OH, Fmoc-L-Phe-OH, Fmoc-L-Phe-OPfp, and Fmoc-L-Val-OH were from Milligen-Millipore (Milford, USA). Fmoc-L-Asn-OPfp, Fmoc-L-Asn-(Mbh)-OH, Fmoc-Glu-(tBu)-OH, Fmoc-L-Gly-OH, Fmoc-L-Leu-OH, Fmoc-L-Lys-(Boc)-OH, Fmoc-L-Ser-(tBu)-OH, Fmoc-pentafluorophenol, and N, N'-diisopropylethyl amine (DIPEA) were purchased from Sigma (Steinheim, Germany). Benzotriazol-1-yl-oxy-trispyrrolidinophosphonium hexafluorophosphate (PyBOP[®]) and 1-hydroxybenzotriazole (HOBt) were supplied by Calbiochem-Novabiochem Co. (La Jolla, USA).

2.2.3 Reagents and solvents for chromatography

Methanol (HPLC-grade, UV cut-off 205 nm), acetonitrile (HPLC-grade, UV cut-off 190 nm) were from Romil LTD (Cambridge, UK). Nova-Pak analytical HPLC columns, 0.45 micron

¹ OPfp = pentafluorophenyl ester; activated α -carbonyl group

HV membrane filters were provided by Waters-Millipore (Milford, USA). Polygosil (C₁₈, 60 Å, irregular particles) packing material was supplied by Macherey-Nagel (Düren, Germany). Sephadex G10 was from Pharmacia Fine Chemicals (Uppsala, Sweden), and CM-Separose (CL-6B) was purchased from Sigma, USA. Analytical grade water was prepared by filtering glass-distilled water through a Millipore Milli Q[®] water purification system.

2.2.4 Drying and storage of reagents and products

Fmoc-amino acids and peptide synthesis resins were stored at 4°C in desiccators with silica gel as drying agent. The FDNB was stored at <10°C and the PYBOP[®] and the HOBt at -20°C, both with silica gel (with indicator) as drying agent. Before use, amino acid derivatives, resins, PyBOP[®] and HOBt were dried overnight under high vacuum, with phosphorous-pentoxide as drying agent. The freshly distilled DMF was stored over molecular sieve (4 Å beads approximately 3.2 mm) at room temperature. Peptides were stored at room temperature, under vacuum in a desiccator, with silica gel as drying agent. All other reagents were stored at room temperature.

Great care was taken to avoid detergent contamination of glassware, because this type of contamination of a peptide preparation could influence its bioactivity. Detergent contamination could easily be detected with electrospray ionisation mass spectrometry (ESI-MS) as most laboratory detergents contain highly charged compounds. The glassware, returned from the regular wash, was rinsed three times with distilled water, three times with 60% ethanol and then rinsed three times with analytical grade water. It was placed in an oven to dry at temperature ranging between 110°C and 140°C. Bottles for amino acid derivatives and purified peptides were also prepared in the same way and then pyrolysed at 565-570°C for 2 hours.

2.3 Methods

All the SPPS methods are standard peptide synthesis procedures refined or developed in the BIOPEP laboratory [23]. Variations to these standard protocols have been included here.

2.3.1 Preparation of solvents

2.3.1.1 Distillation of *N, N'*-dimethylformamide

DMF is an excellent solvent both for protected amino acids derivatives and for most reagents used in peptide synthesis. It is the principal solvent used in Fmoc-polyamide solid phase peptide synthesis and it is imperative that it is always freshly distilled and highly pure. Impure DMF is often contaminated with secondary amines and H₂O, which can react with the Fmoc- and active ester groups of the peptide. DMF reacts with water to form dimethylamine and formic acid [22,23]. DMF was shaken up with 10-20 g/L dry potassium hydroxide pellets to remove residual water, or stored for at least one week on activated molecular sieve (4Å beads approximately 3.2mm). Impurities such as volatile secondary amines were removed by fractional distillation under vacuum (high vacuum; 5-7mm Hg) and dry nitrogen bleed. The first 10-15% of the distillate was discarded and the constant boiling fraction was collected. Only the DMF that passed the Sanger's test for amines was used (see below), otherwise it was redistilled.

2.3.1.2 Sanger's test for amines

Secondary amines in DMF can cleave the base-labile Fmoc-group from the N-terminus of the peptide or from the Fmoc-amino acid, causing unwanted polymerisation during peptide chain elongation. Sanger's reagent is used to test for the presence of amines and determine the quality of DMF prior to use [10]. It was performed by mixing equal volumes of FDNB (1.0 mg/mL in 95% ethanol) and DMF at room temperature for 30 minutes and subsequently determining the absorbance of the reaction mixture at 381 nm. FDNB (0.5 mg/mL in 95% ethanol) was used as a blank and measured in the region of 0.2 absorbance units. DMF with an absorbance of 0.025-0.05 units higher than the blank was used in the coupling procedure as well as in the washing steps prior to coupling procedure. Lower quality DMF with an absorbance of 0.05-0.08 units higher than the blank was used for the other washing steps.

To ensure the removal of all traces of piperidine used in the deblocking steps during the peptide synthesis protocol, the Sanger test was also performed on DMF samples from the final washing step, before the coupling of the next amino acid. The samples were incubated with an equal volume of FDNB (0.5 mg/mL in 95% ethanol) for 2-3 minutes, compared to a blank solution (DMF/FDNB; 1:1), and accepted as piperidine-free if they were no more than 0.01 absorbance units higher than the blank.

2.3.1.3 Distillation of piperidine and pyridine

Piperidine was purified by distillation over dry potassium hydroxide (10-20 g/L) and a dry nitrogen bleed at atmospheric pressure. The first 10-15% of the distillate was discarded and the constant boiling fraction (105°C) was collected. The distilled piperidine was stored in dark bottles and used within three months [22]. Pyridine for use in the Kaiser-ninhydrin test was distilled in the same way [23].

2.3.1.4 Distillation of *N, N'*-diisopropylethyl amine

N, N'-diisopropylethyl amine was initially distilled over ninhydrin (1-2 g/L) and then redistilled over dry potassium hydroxide pellets (5-10 g/L). Distillation was performed at atmospheric pressure under dry nitrogen bleed. A small forerun was discarded, and the constant boiling fraction with boiling point between 125-127°C was collected. Small volumes (± 4 mL) were aliquoted into amber vials, flushed with dry N₂, sealed and stored at -20°C. Small volumes were distilled because of the instability of the reagent [24].

2.3.2 Preparation and quality control of the amino acid derivatives

2.3.2.1 Melting Point Determination

The melting point of all derivatives and catalysts (PyBOP[®], HOBT) were determined before peptide synthesis. A small amount of derivative was placed in the bottom of a capillary tube and the melting point determined using a Gallenkamp melting point apparatus. The amino acid derivatives and catalysts were only used in peptide synthesis if their melting points were 3-5°C higher or lower than their literature values [13].

2.3.2.2 Purification of Fmoc amino acid derivatives

Amino acid derivatives showing positive Kaiser tests (see 2.3.3.4) or incorrect melting points were purified and reassessed prior to use in a synthesis. Fmoc-amino acids without acid labile side-chain protection were suspended in 1% acetic acid (0.1% acetic acid, if an acid labile side chain protection group was present) and the undissolved Fmoc-amino acid derivative was collected by filtration. The precipitate was then washed with water, ice-cold methanol, ethyl acetate, and diethyl ether and dried thoroughly under vacuum. If the Kaiser test remained positive, the derivative was re-crystallised from hexane/ethyl acetate. The OPfp activated Fmoc amino acid derivatives were re-crystallised from hexane and/or washed with ice-cold ethyl acetate and n-hexane.

Table 2.1 Operations for one cycle of the peptide synthesis procedure (Table reproduced with kind permission from M. Rautenbach [23])

Synthesis Step	Time	Volume	Monitoring	Comment
1. Swelling of resin	20 min.	4 bed volumes		Bed volume = 5mL/gram resin
2. Anchoring of first amino acid <i>via</i> activated Fmoc-amino acid to resin	2 hours	< ¹ / ₂ bed volume	Fmoc-test	Refer to section 2.3.3.1 and 2.3.3.5
3. DMF wash		Minimum of 6 x 3 bed volumes		
4. Resin sample A			Kaiser test (2.3.3.4)	If test is positive, extend or repeat coupling step in elongation.
5. Removal of Fmoc group(deblocking) with 20% piperidine in DMF.	30 min.	3 bed volumes	Absorbance at 290	Refer to sections 2.3.3.3 & 2.3.3.5
6. DMF wash		Minimum of 10 x 3 bed volumes		
7. DMF wash sample		0.5 mL	Sanger test (2.3.1.2)	Wash until test is negative
8. Resin sample B			Kaiser test (2.3.3.4)	If test is negative, repeat deblocking
9. Coupling of next amino acid <i>via</i> activated Fmoc-amino acid	60 min.	< ¹ / ₂ bed volume		Refer to sections 2.3.3.1 & 2.3.3.2 Repeat steps 3, 4 & 9 if necessary
10. Repeat steps 3-8				
11. Repeat steps 9 & 10 for α -amino acids in sequence				
12. Washing & drying of resin				Refer to 2.3.3.3
13. Liberation of peptide acid from resin				Refer to 2.3.3.6

2.3.3 Synthesis of the peptides

The peptides were synthesised at room temperature (20-25°C) according to the Fmoc-based protocol using a shake flask procedure [23]. Two full-length syntheses and one extension of a resin-bound magainin without its four N-terminal residues (magainin 2 N¹⁹) were performed. The protocol for a complete cycle of operations including washing, coupling, deblocking, and sample steps is set out in Table 2.1.

2.3.3.1 Coupling of the first amino acid

Pepsyn KA-resin (capacity of 0.15 or 0.2 milli-equivalents per gram resin) was used in the syntheses, to which the first amino acid was coupled via the PyBOP[®] method (described next). The coupling efficiency was evaluated using the Fmoc-test (section 2.3.3.5), and the coupling step was repeated until the resin was completely saturated². Prior to synthesis, the resin was swollen for approximately 20 minutes in high purity DMF (20 mL/g).

2.3.3.2 Elongation of the peptide chain

The reagent quantities used during the elongation steps were calculated from the resin capacity of 0.15 or 0.2 milli-equivalents per gram of dry resin. The OPfp activated derivatives of the Fmoc-amino acids were coupled with HOBt as a catalyst and trapping agent [25,26] using a 3-7 fold molar excess for each. Fmoc-amino acids were coupled using the PyBOP[®] method in the following manner: a 3-7 fold molar excess of the protected amino acid and HOBt, were each dissolved in a minimum volume of DMF (0.5-1.0 mL), combined and added to the resin. PyBOP[®] was subsequently mixed at 3-7 fold molar excess with a 6-14 fold molar excess of DIPEA, both in a minimum volume of DMF (0.5-1.0 mL) and the combination added to the resin [23,27]. Complete acylation was obtained after 60-120 minutes as determined with the Kaiser test and/or Fmoc-test.

2.3.3.3 Removal of the Fmoc-group from the attached amino acid

Once the coupling was completed, as shown by a negative Kaiser test, the resin was washed to remove excess active amino acid derivative and catalyst. The Fmoc-group was subsequently removed from the coupled amino acid by incubation with at least three bed volumes of piperidine (20% DMF) for 30 minutes. After each deblocking step, the absorbance

² It should be noted that the first amino acid coupled to the resin is the last amino acid (S23) in the magainin peptide sequence.

was recorded at 290nm. Each absorbance value was compared to the absorbance values obtained from previous deblocking steps to show the extent of deblocking. After the piperidine was removed, the resin was thoroughly washed with DMF until an acceptable Sanger test was obtained (section 2.3.1.2).

2.3.3.4 The Kaiser Test

The Kaiser test is specific to primary amino groups [28] and consists of three solutions: (a) 500mg ninhydrin in 10mL 95% ethanol, (b) 40g phenol in 10mL 95% ethanol and (c) 2mL 0.001M KCN solution diluted to 100mL with distilled pyridine. The Kaiser test was used during peptide synthesis to evaluate the deblocking process, as well as the coupling of each amino acid. The test proceeds as follows: 4-5 resin beads were dried using diethyl ether and 3-5 drops of each solution was then added to the beads. This was incubated for 1-10 minutes in a water bath at 80-90°C and the colour of the resin beads and the reaction mixture was subsequently evaluated using a magnified eyepiece. A positive result, as expected after deblocking, caused the beads to change colour varying from light to dark blue depending on the amino acid. Exceptions were found with G (beads changed to a yellow-brown colour), S and N (beads changed to a brown/orange colour). A negative result, as expected after coupling, showed no change in the colour of the beads or reaction mixture.

Quality control of the Fmoc-amino acid derivatives was also done using the Kaiser test. Five milligrams of the dried derivative was dissolved in 100µl DMF, after which 100µl of each of the Kaiser test solutions were added. Colours were evaluated after five minutes incubation at 90°C. To determine the extent of contamination of a derivative, its Kaiser test result was compared to a standardised colour chart.

2.3.3.5 The Fmoc-test

To evaluate the coupling of an Fmoc-amino acid, and specifically the coupling of the first amino acid, the UV absorbance character of the liberated Fmoc-fulveen group was exploited [25,29]. An analytical test was developed in our laboratory [30-32] whereby the concentration of the Fmoc-groups released, subsequent to the deblocking step, could be used to calculate the percentage of coupling. The linear relationship between the percentage liberated Fmoc and the absorbance at 290 nm was as follows:

$$A_{290} = 0.002848 \times \% \text{ liberated Fmoc-groups} - 0.009975$$

This test proved to be useful as an alternative to amino acid analysis, a time consuming procedure. To evaluate a coupling step, 10-15mg of resin was removed, washed with DMF

and diethyl ether and dried for 60 minutes. The resin was then analytically weighed and deblocked with a volume of 20% piperidine in DMF that was equivalent to 20mL per 0.1mmol of expected Fmoc-groups. After deblocking, a 100 times dilution (in triplicate determinations) was made of the deblocking mixture and the absorbance determined at 290nm. The absorbance values were entered into the previously determined standard curve equation and the percentage coupling determined.

2.3.3.6 Removal of the completed peptide from the resin

After the deprotection and DMF wash of the final amino acid, the resin was washed with t-amyl alcohol, glacial acetic acid, again with t-amyl alcohol, and finally dried with diethyl ether [24,25,32]. The peptides were cleaved from the resin using reagent K (82.5% TFA, 5% phenol, 5% H₂O, 5% thioanisol, and 2.5% 1,2-ethanedithiol) [33] and separated from the resin by filtration. The resin was washed with TFA, glacial acetic acid, and analytical grade H₂O and the filtrate collected. The resin was subsequently washed with ether and vacuum dried. The filtrates, containing peptide, were concentrated under vacuum using a Buchi Rotavapor at 45°C. The peptide concentrate was then dissolved in 50mL analytical grade water and extracted three times with 50mL diethyl ether. The combined ether fractions were then washed with 50mL analytical grade water to recover any peptide in the ether. The combined aqueous fractions were freeze-dried.

2.3.4 Purification of the peptides

2.3.4.1. Gel-permeation chromatography

The peptides were initially purified by Sephadex G10 gel permeation chromatography using analytical grade water as eluant. Freeze-dried crude peptide preparations were dissolved in 2-3 mL of water, equivalent to 1.7-2.5 % of the column bedvolume (39 x 2cm; 122.5 cm³), their absorbance measured at 230nm and 257nm³ and then loaded (10mg/mL) onto the Sephadex G10 column. Flow rates were 10-14 mL/hour and the major absorbing fractions were collected and freeze-dried.

3 Phenylalanine forms part of the magainin peptide sequence, and absorbs maximally at 257 nm.

2.3.4.2 Cation exchange chromatography

A CM-Sepharose CL-6B column utilising a 0.35–0.45M ammonium acetate (pH. 6.00) gradient was used for further purification of the peptides.

The column was regenerated by running a linear 0.35 – 0.45 M ammonium acetate (pH. 6.00) gradient, followed by equilibration with three bedvolumes of 0.35M ammonium acetate (pH. 6.00). Freeze dried peptide preparations were dissolved in 2-2.3 mL of equilibration buffer equivalent to 10-12% of the column bed volume (11 x 1.5 cm; 20.32 cm³), and loaded onto the column (10-12mg/mL). The flow rate was ±14mL/hour. Elution was started with the equilibration buffer, and after an hour (±14mL eluant) a linear gradient was introduced with the highest concentration of ammonium acetate (0.45M; pH.6.00) as the final concentration. The eluted fractions were monitored at 230nm and 257nm and the major absorbing fractions were collected and freeze-dried.

2.3.4.3 Semi-preparative high performance liquid chromatography

Semi-preparative HPLC was used as a final purification step in order to achieve magainin 2 of high purity. Peptide samples (5mg/mL) were dissolved in 50% acetonitrile in analytical grade water. All samples were then centrifuged for 5 minutes, using a STRATAGENE Picofuge™, to remove particulate. Sample volumes loaded varied between 50-150µL. The HPLC system consisted of the following components: two Waters 510 pumps, a Waters Model 440 detector (monitoring at 254nm), a WISP 712 sample processor, a controller system with MAXIMA software, and a semi-preparative C₁₈ Polygosil HPLC column (irregular particle size, 60 Å pore size, 8 x 250 mm). A linear gradient (3 mL/min flow rate) was created using eluant A (0.1% TFA) and eluant B (90% acetonitrile and 10% eluant A) as shown in Table 2.2 [32]. Peptide fractions were collected, and freeze-dried for further analysis.

2.3.5 Analysis of purified peptides

2.3.5.1 Analytical high performance liquid chromatography

Analytical reverse phase high performance liquid chromatography was used to determine the purity of the synthetic peptides. A C₁₈ Nova-Pak HPLC column (3.9 x 150mm) was used with the system described under section 2.3.4.3. The chromatography was monitored at 254nm and the same gradient was employed as for preparative HPLC, but the flow rate was reduced to 1.0mL/min (Table 2.2), loading 20µL samples at 2 mg/mL (Table 2.2).

Table 2.2 Gradient program used for the HPLC of the peptide preparations

Time (min)	Flow rate; preparative HPLC (mL/min)	Flow rate; analytical HPLC (mL/min)	%A	%B
0	3.0	1.0	80	20
0.5	3.0	1.0	80	20
13	3.0	1.0	15	85
13.1	3.0	1.0	0	100
14	3.0	1.0	0	100
20	3.0	1.0	80	20
25	3.0	1.0	80	20

2.3.5.2 Mass spectrometry

A Micromass Quattro triple quadrupole mass spectrometer, fitted with an electrospray ionisation source, was used for electrospray ionisation mass spectrometry (ESI-MS). Peptide samples (0.2-0.3 mg/mL) were dissolved in 50% acetonitrile in analytical grade water modified with 0.01 % TFA. Ten μ l of the sample was introduced into the ESI-MS at 20 μ L/minute using a Rheodyne injector valve. The applied capillary voltage was 3.5 kV and a cone voltage of 50 V with the skimmer lens offset at 5 V was used in all the analysis. The source temperature was 80°C. Data was acquired in the positive mode for these cationic peptides, scanning the first analyser (MS₁) through a m/z (molecular mass to charge ratio) of between 100 and 1500 at a scan rate of 5 sec/scan atomic mass units/second. Combining a number of scans across the elution peak and subtracting the background produced representative spectra.

2.4 Results and Discussion

2.4.1 Synthesis 1 of Magainin 2

2.4.1.1 Coupling of the first amino acid

Serine (S23), the last amino acid in the magainin 2 sequence⁴, was esterified to the 4-hydroxymethylbenzoic acid linker of the 0.2 mmol Pepsyn KA resin in a previous study performed by Gertrude Lourens. It came to our attention that some of the Fmoc-groups were liberated after coupling, due to erroneous short-term exposure to piperidine. It had been determined that only 75% of the S23 N-terminal primary amino groups were still Fmoc-protected. To ensure that the resin was fully saturated with the first amino acid, the unprotected amine groups were blocked again by incubating the S23-resin with an excess of Fmoc-OPfp and HOBt for 90 minutes using freshly distilled DMF as solvent. It was confirmed that the exposed N-terminal primary amino groups of S23 were re-protected with a negative Kaiser test and a 103% yield according to the analytical Fmoc test, which has an accuracy of $\pm 5\%$.

2.4.1.2 Elongation of the peptide chain

Asparagine (N22) was the second amino to be coupled and a negative Kaiser test was obtained after 90 minutes of incubation with the resin. The deblocking procedure for N22 appeared problematic with a negative Kaiser test after 30 minutes, which indicated that the Fmoc-groups had not been liberated from the N-terminal of the peptide chain. The resin was deblocked for an additional 30 minutes before complete deprotection and a positive Kaiser test was obtained. Although the absorbance of the liberated Fmoc-group, at 290nm, had dropped by 12% we continued with the coupling of methionine (M21). The resin showed a negative Kaiser test after 90 minutes of coupling, but the Fmoc-absorbance subsequently dropped by another 43%. The resin was again deblocked for another 30 minutes, but no or little additional Fmoc-groups were liberated. Although the synthesis had been compromised, the Fmoc group of M21 was recoupled using fresh peptide to reassess coupling percentage. The Fmoc-absorbance was still 17% lower than that obtained for N22. During the rest of the

⁴ Amino acid derivatives for the synthesis of the magainin 2 sequence (M_{23}) will be annotated as follows throughout chapter:

G1 I2 G3 K4 F5 L6 H7 S8 A9 K10 K11 F12 G13 K14 A15 F16 V17 G18 E19 I20 M21 N22 S23

synthesis constant Fmoc liberation and negative Kaiser tests were obtained for all the remaining couplings, using a three-fold excess concentration of amino acid derivative (see 2.3.3.2).

2.4.1.3 Purification and analysis of synthesis 1 peptide products

Low molecular mass impurities and solvents that accumulated during synthesis and peptide cleavage were separated from the peptide using Sephadex G10 gel-permeation chromatography (Fig. 2.4). The major absorbing fraction ($V_e = 51$ ml; V_e is the elution volume) that eluted from the Sephadex G10 column was conservatively pooled into fractions and analysed using ESI-MS (Fig 2.5).

The ESI-MS results indicated that Magainin 2 (M_{23}) had been synthesised (Fig. 2.5). The correct m/z (molecular mass/charge ratio) in multiply charge forms were present, namely 617.29 ($[M_{23}+4H]^{4+}$), 823.3 ($[M_{23}+3H]^{3+}$), and 1234.53 ($[M_{23}+2H]^{2+}$). The fractions were, however, contaminated with oxididated side-products 828.67 ($[M_{23}+O+3H]^{3+}$) and 3 additional triply charged deletion analogues ($m/z = 756.22$, 706.33, and 668.29). The major contaminant appeared to be as a result of the exclusion of N22 and S23 with an m/z of 756.22 ($[M_{23}-N22-S23+3H]^{3+}$). The early contamination and subsequent dramatic loss in yield experienced with the N22 exclusion is possibly the result of a common side chain reaction that occurs during Asn-Ser sequence peptides. The long exposure to piperidine together with the possible liberation of the tBu and trityl side-chain protection groups of S23 and N22 respectively can result in aspartimide formation on N22 [24]. The reaction involves the attack of the nitrogen on the side-chain ester of N22 and the subsequent formation of an amide (Fig. 2.6). This intermediate can suffer a number of fates resulting in dramatic loss in peptide yield. This in turn could be responsible for the difficulty experienced with the coupling of M21.

Due to the low crude yield obtained, it was decided re-synthesise the peptide implementing additional controls to solvents and derivatives to reduce contamination and product loss. The concentration of amino acid derivatives was increased from a three fold to a 5-7 fold excess to drive the reactions to completion.

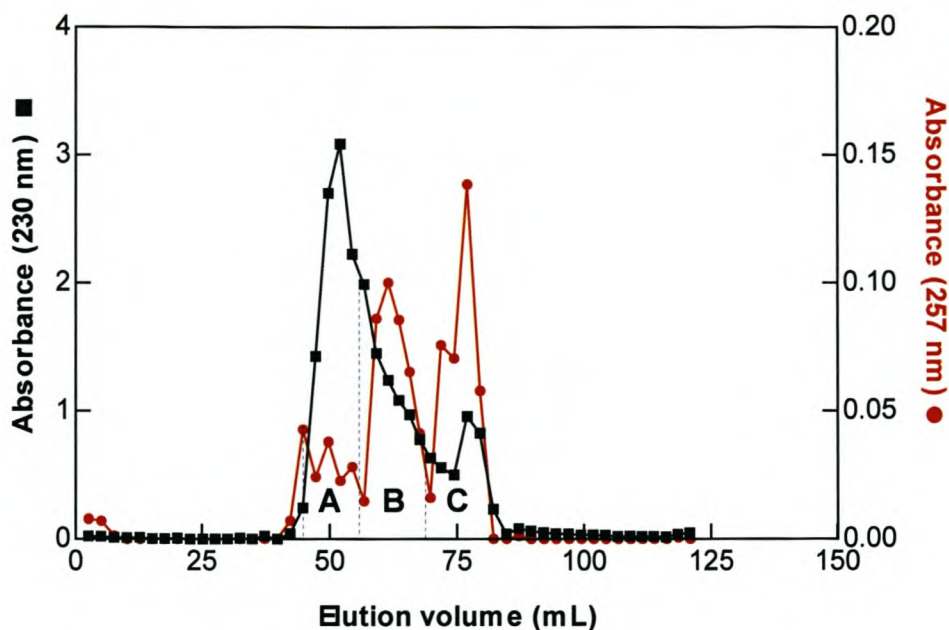


Figure 2.4 An example of the Sephadex G10 chromatography elution profile generated by the crude magainin 2 peptide during *synthesis 1*. The crude peptide mass was 30 mg. Peak B contained the main peptide fraction (ESI-MS: figure 2.5), whereas peak A and C contained the main deletion analogue fractions.

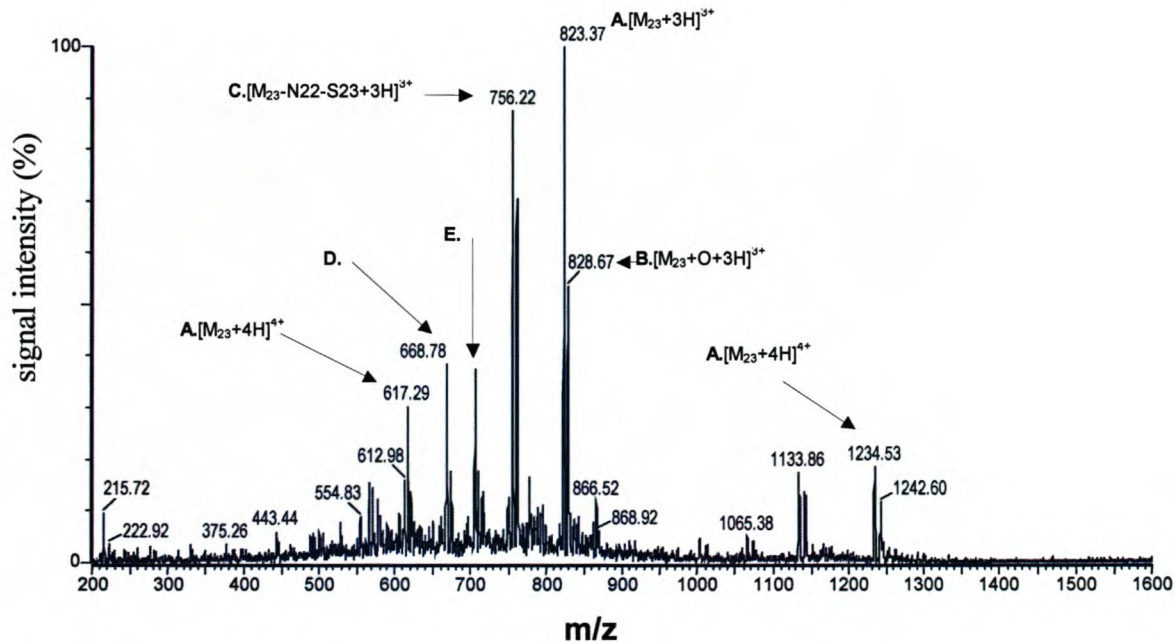


Figure 2.5 Positive mode ESI-MS of fraction B (see figure 2.4) of the peptide mixture collected after Sephadex G10 chromatography: **A** representing magainin 2, **B** is its oxidized side-product, and **C-E** are the deletion analogues.

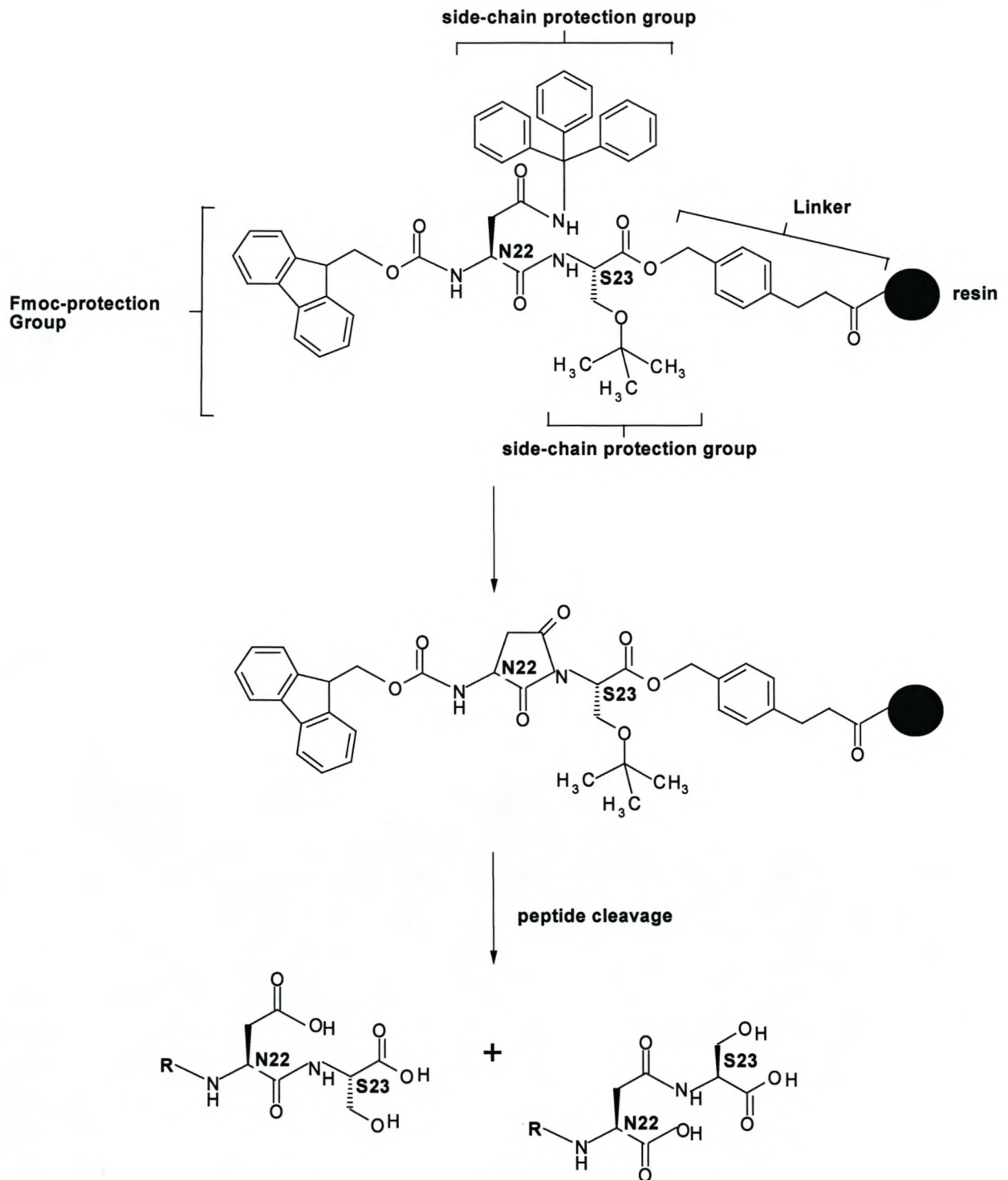


Figure 2.6 Possible aspartimide formation on N22 during *synthesis 1* : the five-membered imide can undergo ring opening during Fmoc-removal and later hydrolyse in solution to form the corresponding α - and β -apartyl peptides.

2.4.2 Synthesis 2 of Magainin 2

2.4.2.1 Coupling of the first amino acid

Pepsyn KA resin (0.15mmol) was incubated with the first amino acid derivative, Fmoc-Serine(tBu)-OH (S23) for 24 hours and the resultant Fmoc test indicated an 83% coupling. The resin was washed and re-incubated with fresh derivative for a further 24 hours, however coupling only increased to 87%, probably due to steric hindering. To insure that no deletion analogues were formed as experienced in synthesis 1, we blocked the remaining OH groups of the resin with the smaller tBoc-Gly-OH. The acid labile tBoc protection group of Gly would remain attached during the rest of the synthesis because of the mild reaction conditions of the Fmoc method and the liberated Gly would be easy to purify from our main peptide product. To ascertain whether the tBoc-Gly-OH coupling and blocking was completed we performed three additional Fmoc-tests to compare with the original Fmoc-test of 87% (see Figure 2.7a). The first Fmoc-test was a positive control, coupling Fmoc-Gly-OH to an S23-resin test sample prior to incubation with tBoc-Gly-OH. The result showed a 98% coupling indicating that there were open OH groups on the resin that required protection. The second Fmoc-test was after the incubation of tBoc-Gly-OH with the S23-resin and showed a coupling of 87% as expected. The third Fmoc-test was taken on a tBoc-Gly-S23-resin test sample that was incubated with Fmoc-Gly-OH and also gave an 87% coupling, confirming that the tBoc-Gly-OH had blocked all the remaining open OH groups on the resin and that the next amino acid could be coupled.

2.4.2.2 Elongation of the peptide

Stringent Kaiser tests and melting point tests were performed on all amino acid derivatives and activating agents before coupling commenced, using a 5-7 times excess concentration. Satisfactory Kaiser tests and were obtained for all couplings, although some of the Fmoc liberations over the last third of the peptide (S8-G1) appeared problematic (Fig. 2.7b). The peptide was successfully cleaved from the resin.

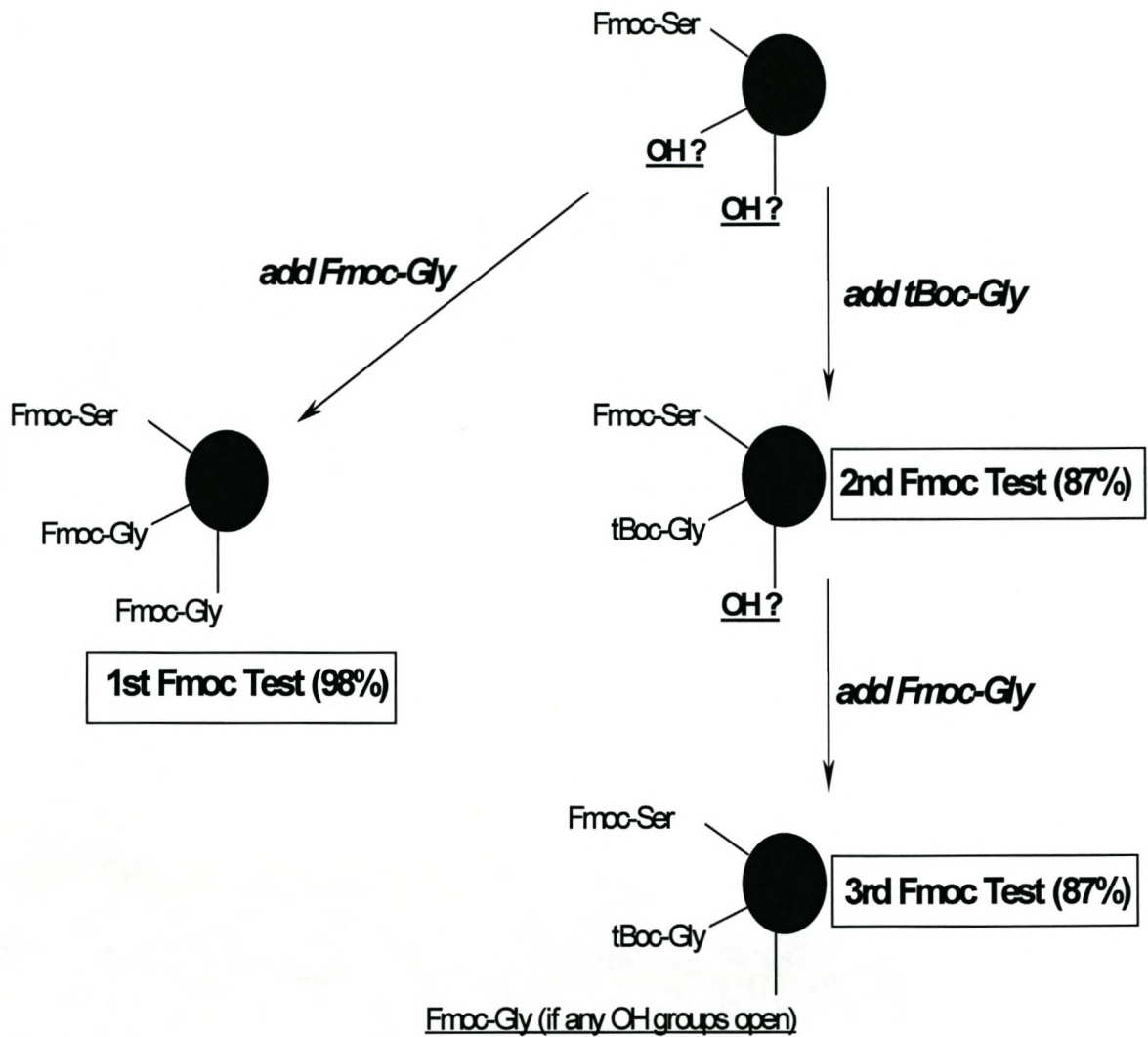


Figure 2.7a A flow diagram illustrating the test procedure followed to ascertain whether the tBoc-Gly-OH had completely blocked all open binding sites on the resin beads during *synthesis 2*.

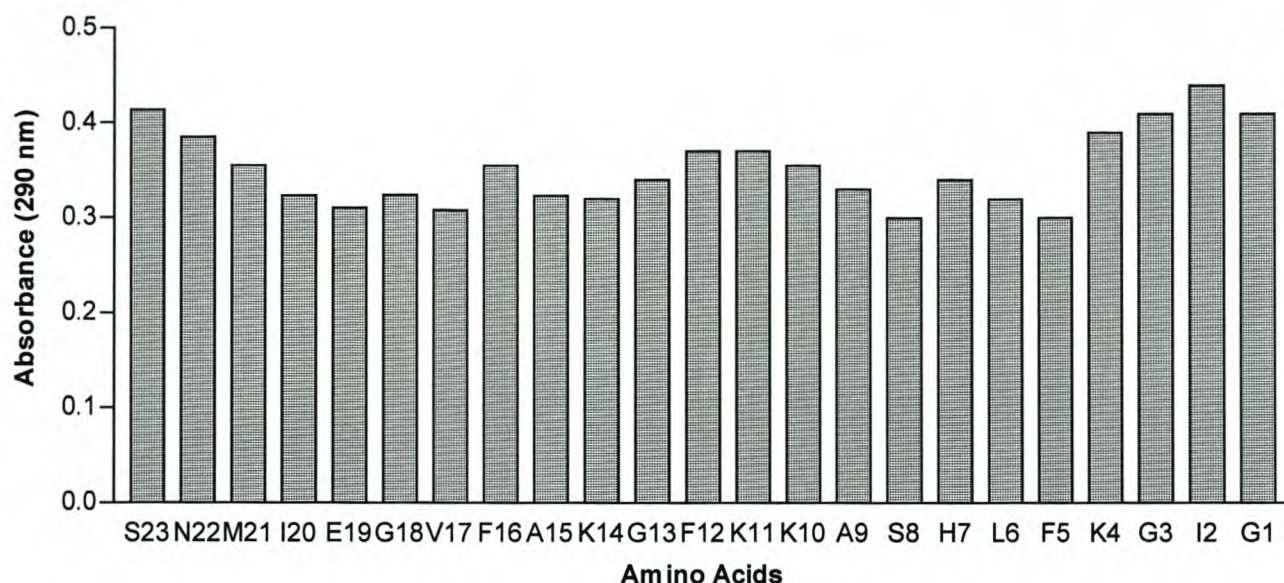


Figure 2.7b Fmoc absorbance measurements after deblocking of each amino acid coupling during synthesis 2

2.4.2.3 Purification and analysis of synthesis 2 peptide products

Low molecular mass impurities were removed using gel-permeation chromatography (Fig. 2.8). A major absorbing fraction ($V_e = 51$ mL) was eluted from the Sephadex G10 column and was conservatively pooled and analysed using ESI-MS (Fig. 2.9). The ESI-MS results showed that the major peptide fractions were still contaminated with a Met-oxidised side-product, an insertion analogue ($M_{23}+G1/G3$) and a deletion analogue ($M_{23}-S8-G3-G1$).

We decided to attempt purify both the oxidised side-product and magainin 2 from the insertion and deletion analogues for later analysis. A sample was chromatographed on a CM Sepharose CL-6B cation-exchange column using an optimised linear 0.35-0.45M ammonium acetate (pH6) gradient. Two major absorbing fractions eluted at 25mL (0.364M) and 39mL (0.376M) respectively (Fig. 2.10). We tested each individual fraction collected with ESI-MS before pooling the fractions together. Unfortunately the results indicated that neither the insertion or deletion analogues nor the oxidative side-product had separated from Magainin 2 (Fig. 2.11). This indicated that there was no discernible difference in charge between the products, which lead us to attempt purification based on their polarity differences using HPLC. Analytical HPLC was used to optimise a gradient that would best suit the separation of the contaminants from magainin 2. We used the optimised gradient for semi-preparative HPLC (Fig. 2.12) and separated the oxidised side-product and the insertion analogue (Fig. 2.13; ESI-MS shown) from magainin 2 (Fig. 2.13; ESI-MS shown) but were still unable to separate the deletion analogue.

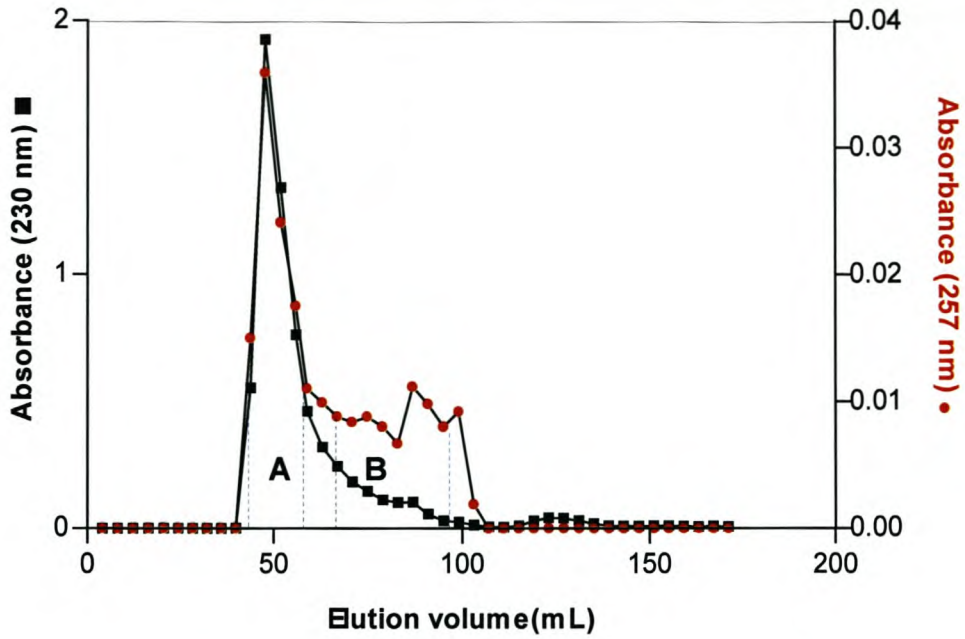


Figure 2.8 An example of the Sephadex G10 chromatography elution profile generated by the crude magainin 2 peptide during *synthesis 2*. The crude peptide mass was 30 mg. Peak A contained the main peptide fraction, which was analysed using ESI-MS (see figure 2.9), whereas Peak B contained the major deletion analogue fraction.

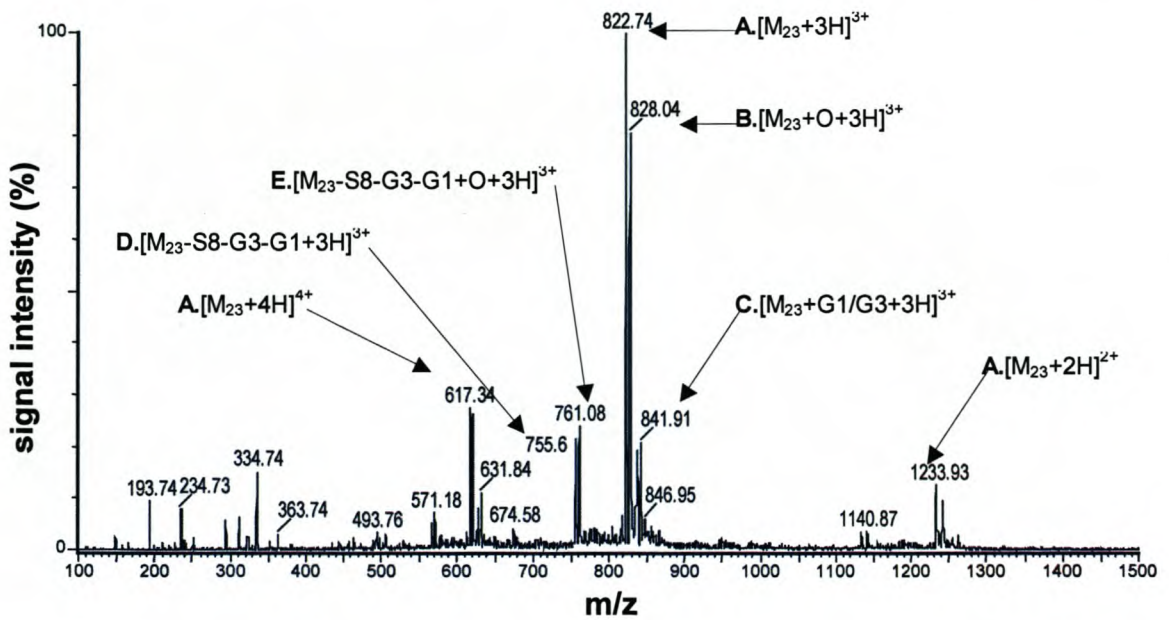


Figure 2.9 Positive mode ESI-MS of peak A (see Figure 2.8) of the peptide mixture collected after Sephadex G10 chromatography: **A** representing magainin 2, **B** is its oxidised side-product, **C** is an insertion analogue, **D** is a deletion analogue, and **E** is its oxidised side-product.

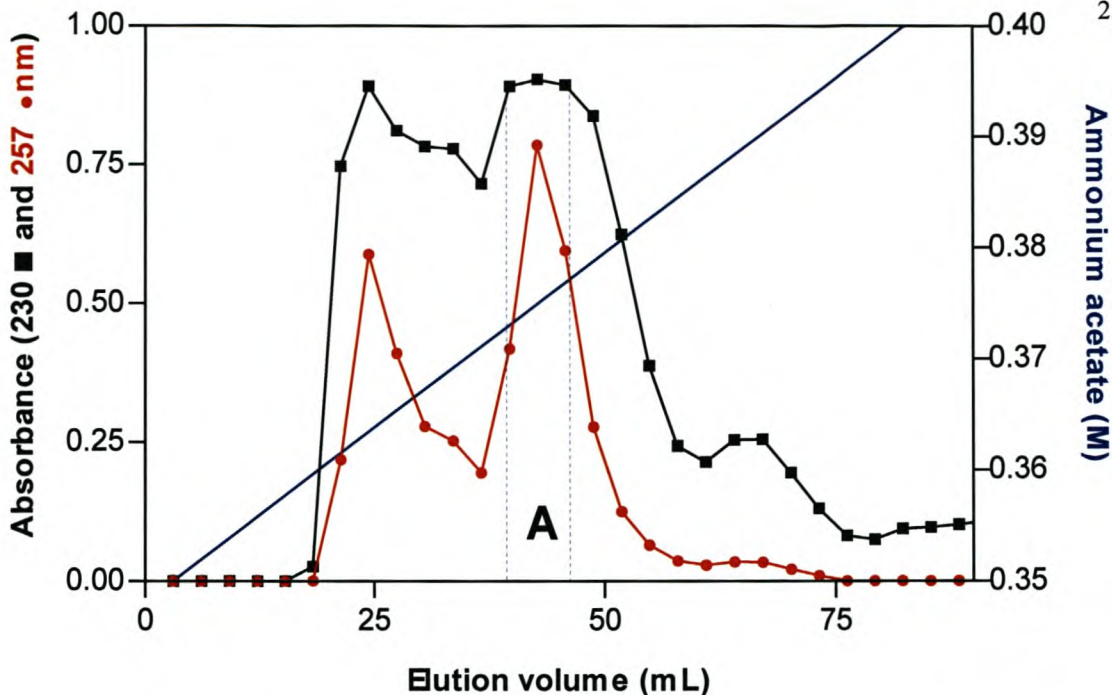


Figure 2.10 CM-Sepharose CL-6B cation exchange chromatography of peak A (see figure 2.8 and 2.9) during *synthesis 2*. The main peptide fraction is indicated by **A**, which was analysed using ESI-MS (see figure 2.11).

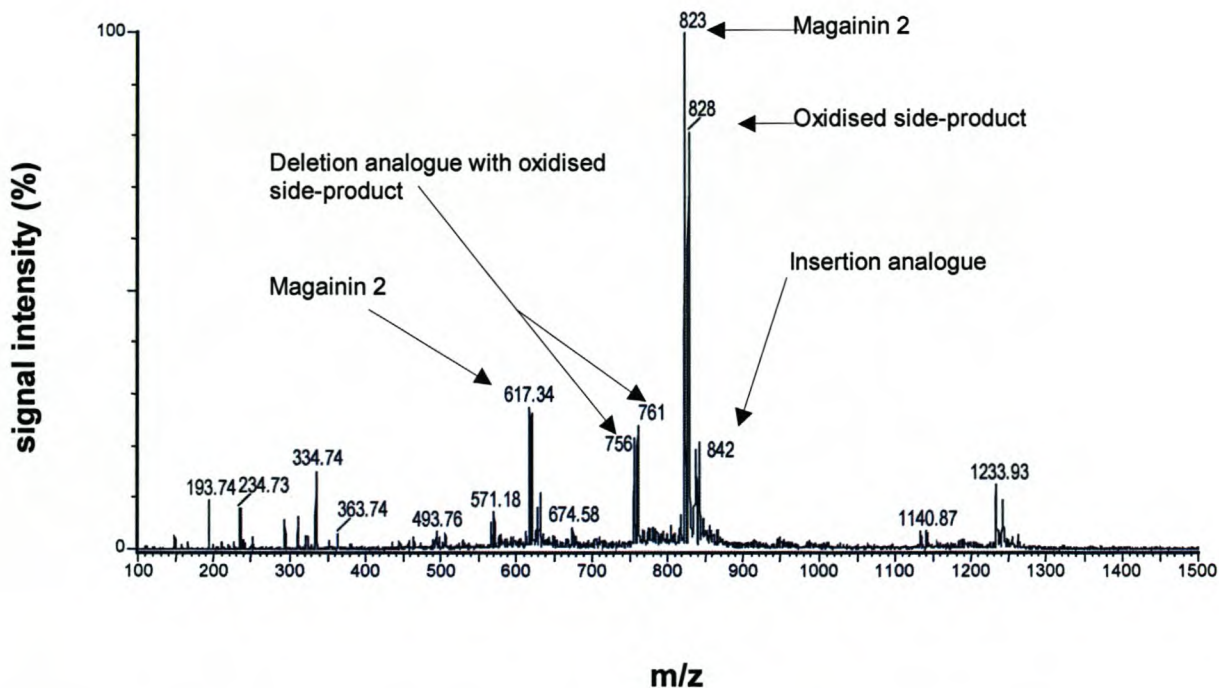


Figure 2.11 Positive mode ESI-MS of fraction A (see Figure 2.10) of the peptide mixture collected after CM-Sepharose CL-6B cation exchange chromatography indicating the unsuccessful separation of magainin 2 from its oxidised side-product, the minor insertion analogue, and the deletion analogue with its oxidised side-product.

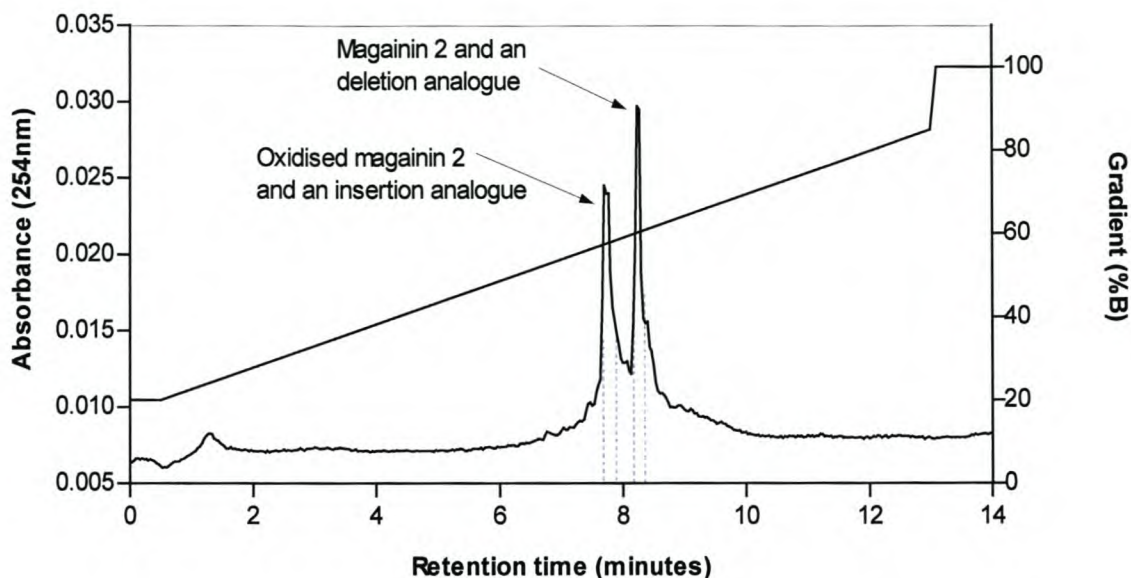


Figure 2.12 A semi-preparative HPLC chromatogram of peak A (see figure 2.8), with the dashed line representing the respective fractions collected. The gradient was developed over 13.1 minutes with 0.1% TFA in water as solvent A and acetonitrile with 10% A as solvent B with a flow rate of 3 mL/min.

Although the problems experienced in synthesis 1 were successfully solved a new problem was experienced. From an analysis of the ESI-MS results (Fig. 2.9) and the absorbance measurements after Fmoc removal (Fig 2.7b) obtained during coupling it became evident that the major reason for this new contamination was possibly due to molecular crowding, caused by using a five- to seven-fold excess concentration of incubated amino acid per coupling, instead of the recommended three-fold excess, resulting in the M_{23} -S8-G3-G1 deletion analogue and the $M_{23}+G1/G3$ insertion analogue (calculated using ESI-MS firm spectral data). Molecular crowding typically occurs with growing peptide chains because of steric crowding and intersite side-reactions. Furthermore, this leads to incomplete solvation of the peptide-resin complex, sudden shrinkage of the gel matrix, and reduced reagent penetration ultimately resulting in failure of the acylation reaction [24]. It resulted in deletion and insertion analogues that could not be purified from the main product. To solve the overcrowding problem we commenced a third synthesis with a resin-bound magainin 2 N^{19} using the recommended three-fold excess.

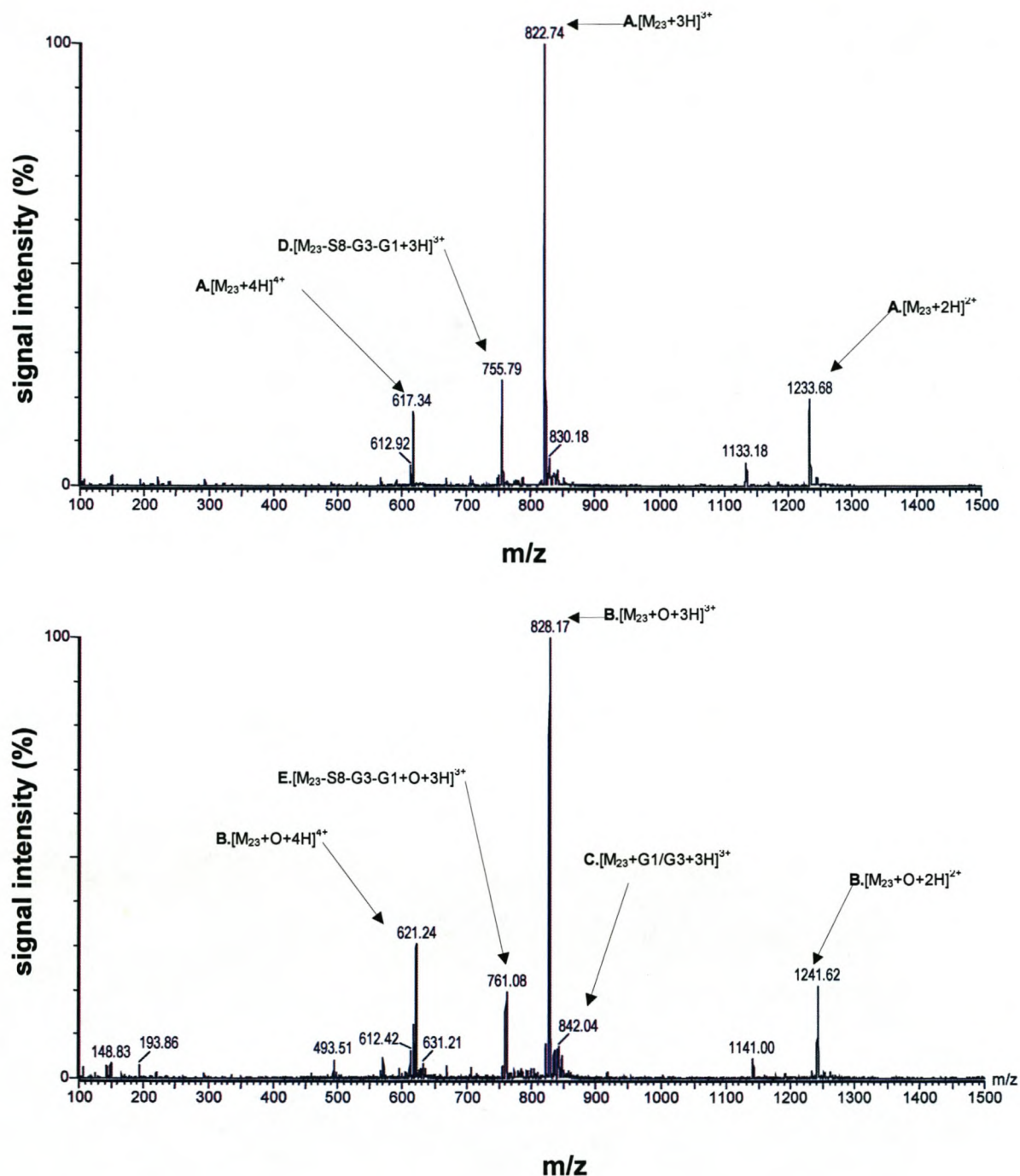


Figure 2.13 Positive mode ESI-MS of the HPLC separation (see Figure 2.12) of magainin 2 and its deletion analogue (top) from the oxidised magainin 2 and insertion analogue (bottom): **A** representing magainin 2, **B** is its oxidised side-product, **C** is the insertion analogue, **D** is a deletion analogue, and **E** is its oxidised side-product.

2.4.3 Synthesis 3 of Magainin 2 from Magainin 2 N¹⁹

Due to time constraints Magainin 2 N¹⁹ was used for the final synthesis.

2.4.3.1 Elongation of the peptide

Magainin 2 N¹⁹ on Pepsyn KA; 0.2 mmol, graciously donated by E.A. du Toit, was extended with K4, G3, I2 and G1. Using a three-fold excess of the activated Fmoc-amino acids, satisfactory Kaiser tests were obtained for all four couplings and the peptide was successfully cleaved from the resin.

2.4.3.2 Purification and analysis of synthesis 3 peptide products

Low molecular mass impurities that accumulated during peptide synthesis and cleavage were removed using gel-permeation chromatography (Fig. 2.14). The Sephadex G10 column eluted a major peptide fraction at a V_e of 48mL that was conservatively pooled into fractions and analysed using ESI-MS.

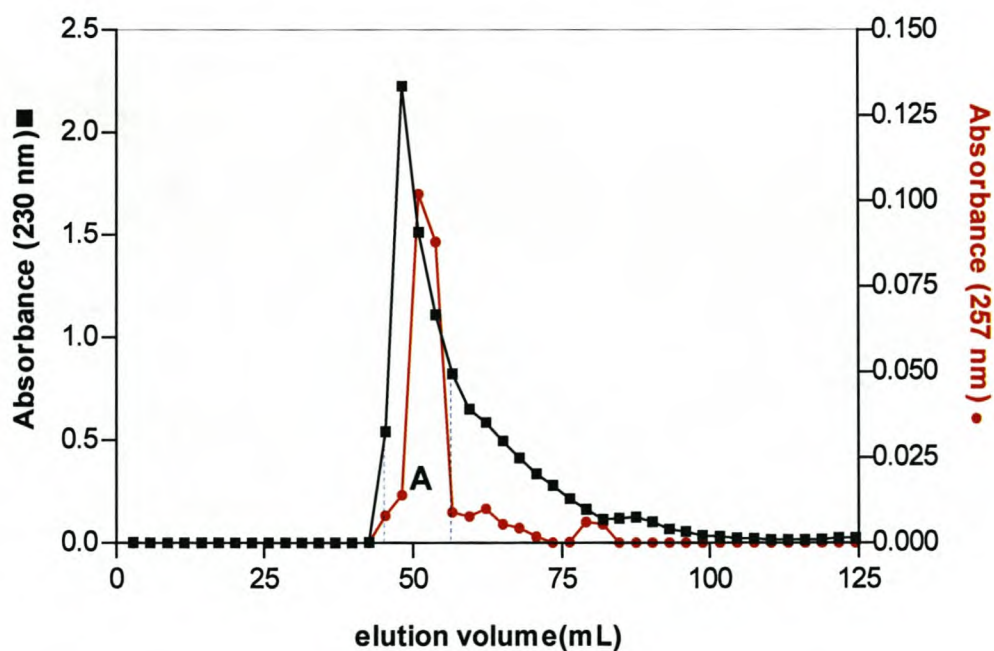


Figure 2.14 An example of the Sephadex G10 chromatography elution profile generated by the crude magainin 2 peptide during *synthesis 3*. The crude peptide mass was 30 mg. Peak A contained the main peptide fraction, which was analysed using ESI-MS (see figure 2.15).

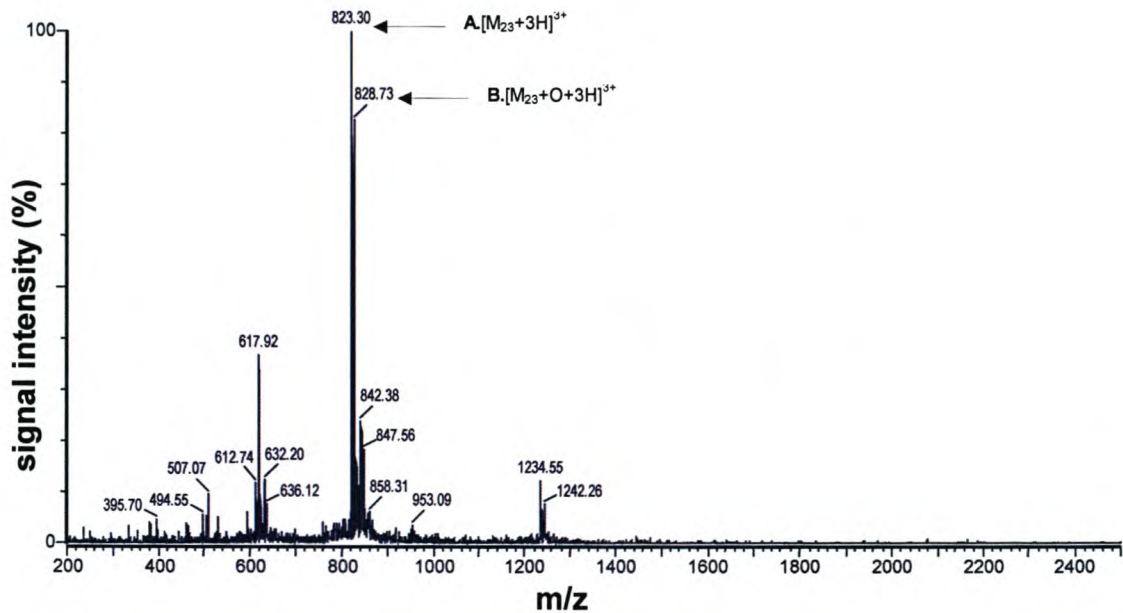


Figure 2.15 Positive mode ESI-MS of the Sephadex G-10 separation (see Figure 2.14): **A** representing magainin 2 and **B** its oxidative side-product.

These results showed that magainin 2 had been successfully synthesised without deletion analogues, however the fractions were still contaminated with methionine sulphoxide (Met-oxidised side-product) (Fig. 2.15). During the TFA cleavage process, highly reactive cationic species are generated from the protecting groups and resin linkers which can, unless trapped, react with and modify, those amino acids containing electron-rich functional groups such as tyrosine, tryptophan, methionine and cysteine [24]. For this reason various nucleophilic reagents, known as scavengers, are added to TFA to quench these ions. Subsequently, Met-oxidation is normally suppressed by thioanisole, and 1,2-ethanedithiol present in the reagent K cleavage cocktail. However, an explanation may be that the scavengers were degraded resulting in the oxidised side-product. (Fig. 2.16).

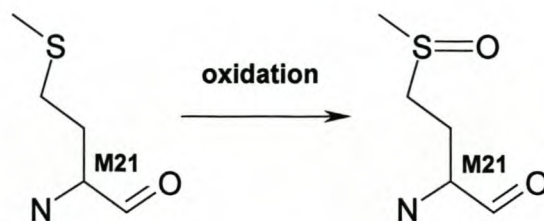


Figure 2.16 Sulphoxide formation on the methyl group (M21) of magainin 2.

Although the oxidised side-product could be reduced [11] we decided to purify this side-product for later analysis. Semi-preparative HPLC, based on the gradient optimisation of synthesis 2, (Fig. 2.17) was used to separate the oxidated side-product from magainin 2. Semi-preparative HPLC (Fig. 2.18) and ESI-MS (Fig. 2.19) revealed a highly purified magainin 2 with the correct multiple charged species with m/z 411.92 ($[M_{23}+6H]^{6+}$), m/z 494.14 ($[M_{23}+5H]^{5+}$), m/z 617.3 ($[M_{23}+4H]^{4+}$), m/z 822.74 ($[M_{23}+3H]^{3+}$), and m/z 1233.80 ($[M_{23}+2H]^{2+}$).

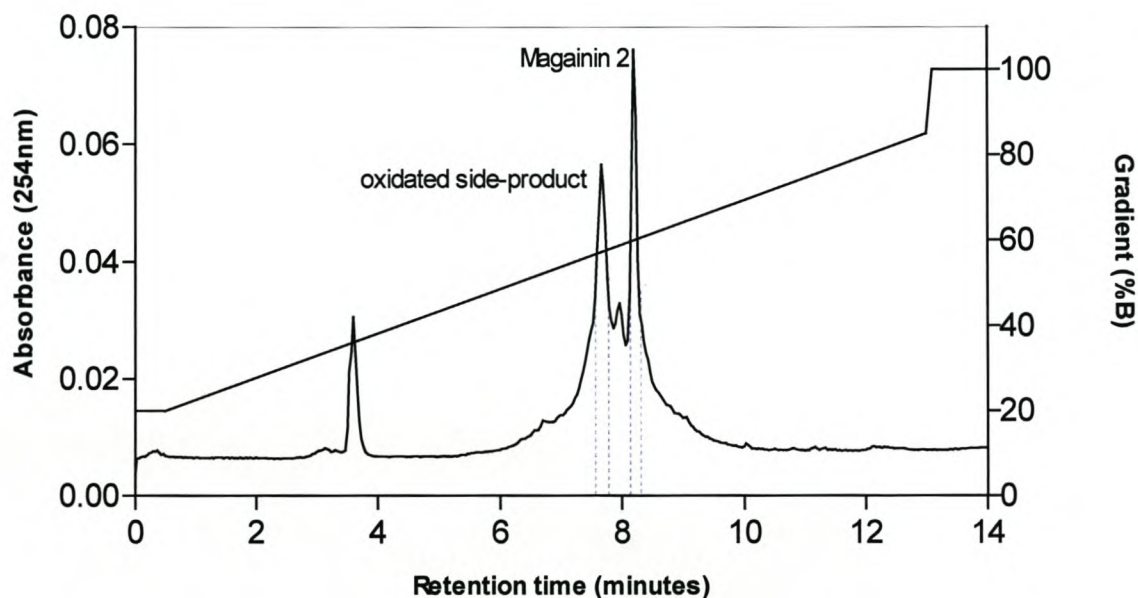


Figure 2.17 A semi-preparative HPLC chromatogram of peak A (see figure 2.14), with the dashed line representing the respective fractions collected. The gradient was developed over 13.1 minutes with 0.1% TFA in water as solvent A and acetonitrile with 10% A as solvent B with a flow rate of 3 mL/min.

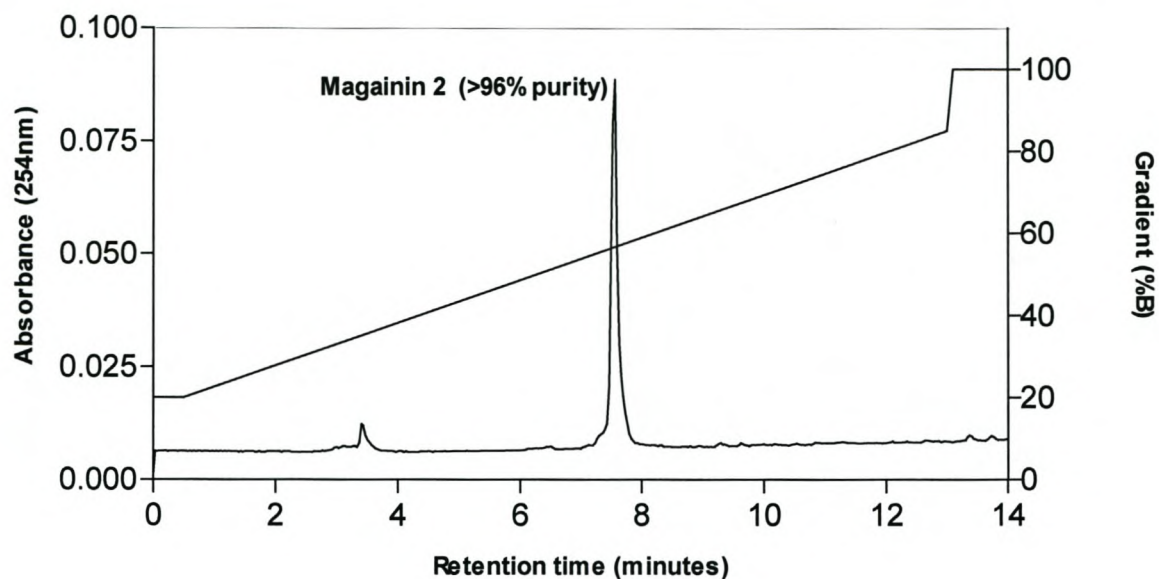


Figure 2.18 Semi-preparative HPLC chromatogram of magainin 2 (>96 % purity) from *synthesis 3*. The gradient was developed over 13.1 minutes with 0.1% TFA in water as solvent A and acetonitrile with 10% A as solvent B with a flow rate of 3 mL/min.

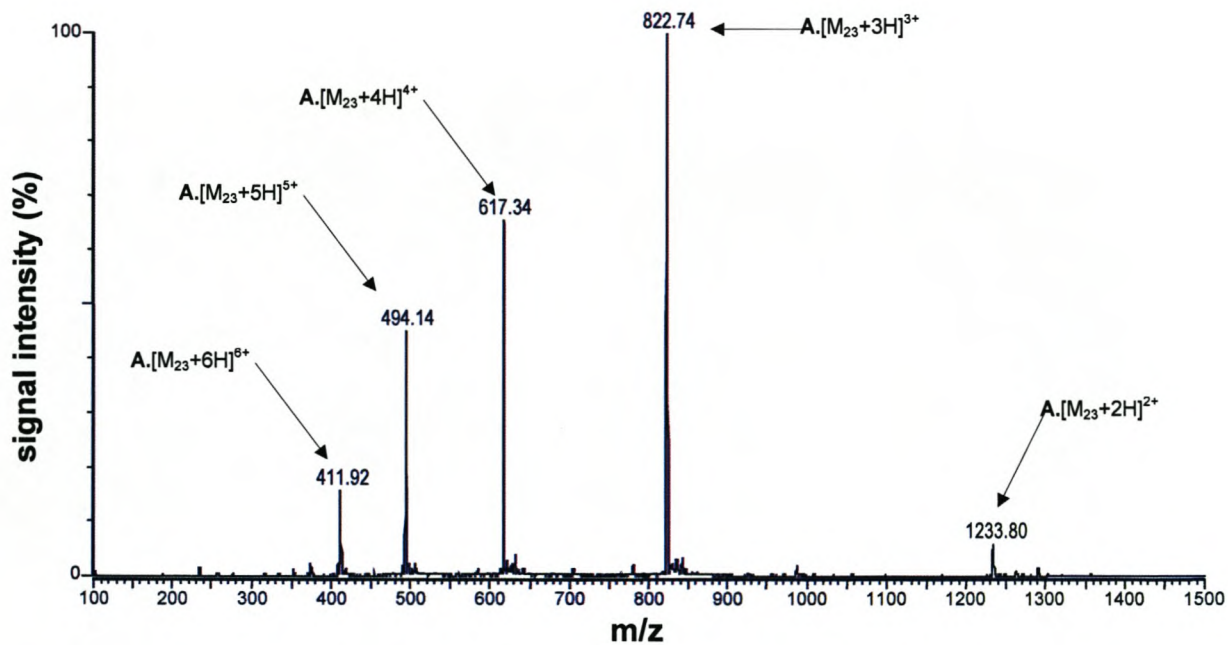


Figure 2.19 Positive mode ESI-MS of purified magainin 2 from *synthesis 3*.

2.5 Conclusions

The main objectives of this chapter were to optimise and synthesise pure magainin 2 for biological use.

In order to ensure a successful synthesis it is necessary for quality control checks on all derivatives, even newly acquired ones, prior to synthesis. There are many reasons for the degradation of derivatives, of which the most prevalent are storage conditions, for example: temperature, moisture, light, volatile organic and inorganic contamination of reagents. During our first synthesis, the aspartimide reaction on N22 was probably due to loss of side-chain deprotection of S23, resulting in additional unwanted analogues and a decrease in peptide yield. This highlights the importance of using high purity derivatives. The aspartimide reaction can also be partially suppressed by the inclusion of 0.1 M HOBt in the deprotection mixture [34]. In the second synthesis this problem was prevented by rigorously testing all derivatives and activating agents, however attachment of the first C-terminal amino acid to the resin linker is also particularly important. The extent of this first reaction will determine the yield of final peptide, and sites on the resin not reacted in this initial process can potentially become acylated in subsequent cycles, leading to the formation of related C-terminally truncated by-products. Extreme care was taken during coupling of the first amino acid for the second synthesis of magainin 2. The open hydroxyl groups on the resin, which were most likely due to steric hindrance, were blocked using tBoc-Gly-OH. These safety measures were effective in preventing the problems experienced in the first synthesis. We were also cautious of incomplete couplings decreasing peptide yield and subsequently overcompensated on amino acid excess concentrations. It worked in driving the reaction cycles to completion over the first two-thirds of the peptide, but caused coupling and deblocking problems over the last third. Coupling concentrations were decreased to the recommended three-fold excess during a third synthesis, which prevented subsequent steric-crowding and the formation of any truncated by-products, while still maintaining rigorous testing on all the derivatives and activating agents. The oxidised magainin 2, although easily separated, can be prevented in future syntheses by ensuring that the components of the reagent K cleavage cocktail are of high quality.

These measures allowed us to finally synthesise magainin 2 of very high purity (>96%) for use in biological experiments. In Chapter 3 I shall report on the optimisation of the AFM technique and the visualisation of the effects of magainin 2 and melittin on target membranes.

2.6 References

1. Curtius T. (1881) *J. Prakt. Chem.* **24** 239
2. Fischer E. (1902) *Ber. dtsh. Chem. Ges.* **35** 1095
3. Hofmeister F. (1902) *Ergeb. Physiol. Biol. Chem. Exp. Pharmacol.* **1** 759
4. Fischer E. (1906) *Ber. dtsh. Chem. Ges.* **39** 530
5. du Vignaud V., Ressler C., Swann J.M., Roberts C.W., and Katsoyannis P.G. (1954) *J. Amer. Chem. Soc.* **76** 3115
6. Merrifield R. B. (1962) *Fed. Proc. Fed. Amer. Soc. Exp. Biol.* **21** 412
7. Merrifield R. B. (1964) *Biochemistry* **3** 1385
8. Kent S.B.H. (1988). *Ann. Rev. Biochem.* **57** 957
9. Barany G., Kneib-Cordnier N. and Mullen D.G. (1987) *Int. J. Peptide Protein Res.* **1987** 705
10. Stewart J. M. and Young J.D. (1984) *Solid phase peptide synthesis*, 2nd edition, Pierce Chem. Co. Rockford, Illinois, pp. 69-70
11. Atherton E., Fox H., Harkiss D., Logan C. J., Sheppard R. C. and Williams B. J. (1978) *J. Chem. Soc., Chem. Commun.* **4** 539
12. Jung G and Bayer E. (1988) *Proc. 20th European Peptide Symposium*, Walter de Gruyter, Berlin, pp. 199-200
13. Fields G. B. and Noble R.L. (1990) *Int. J. Peptide Protein Res.* **35**, 161
14. Grant, G. (1992) *Synthetic peptides*, W. H. Freeman & Co., New York
15. Zasloff M. (1987) *Proc. Natl. Acad. Sci. USA* **84** 5449-5453
16. Zasloff M., Martin B., and Chen H.C. (1988) *Proc. Natl. Acad. Sci. USA* **85** 910-913
17. Dathe M. and Wieprecht T. (1999) *Biochim. Biophys. Acta* **1462** 71-87
18. Bechinger B. (1997) *J. Membr. Biol.* **156** 197-211

19. Ludtke S.J., He K., Heller W.T., Harroun T.A., Yang L. and Huang H.W. (1996) *Biochemistry* **35** 13723-13728
20. Steiner H., Hultmark D., Engstrom A., Bennich H. and Boman H.G. (1981) *Nature* **292** 246-248
21. Yang L., Harroun T.A., Weiss T.M., Ding L. and Huang H.W. (2001) *Biophys. J.* **81** 1475-1485
22. Gait M.J. (1984) Oligonucleotide synthesis, In: Practical Approach Series (Eds. Rickwood D. and Hames D.D.) IRL Press, Washington D.C., p.99
23. Rautenbach M. (1999) The synthesis and characterisation of analogues of the antimicrobial peptide iturin A₂, Ph.D. Thesis (Biochemistry), University of Stellenbosch, pp.28-31
24. Atherton E. and Sheppard R.C. (1989) Solid phase synthesis: A practical approach, In: The practical approach series (Series Eds., Rickwood D., and Hames B.D.), IRL Press, Oxford University Press, Oxford, pp.1-61
25. Gloor A.P., Hoare S.M., Lawless K., Steinauer R.A., White P., Young C.W. (1994/1995) Novabiochem 94/95 Catalogue and Peptide Synthesis handbook, ppS1-S42
26. Bodasky M. (1984) Principles of peptide synthesis (Eds. Hafner K., Rees C.W., Trost B.M., Lehn J., Von Ragne Schleyer P., Zahradnik R.), Springer Verlag, Berlin, pp. 9-52
27. Høeg-Jensen T., Jakobsen M.H., Olsen C.D. and Holm A. (1991) *Tetrahedron Lett.* **32** 7617-7620
28. Kaiser E., Colescott R.L., Bossinger C.D. and Cook P.I. (1970) *Anal. Biochem.* **34** 595-598
29. Carpino L.A. and Han G.Y. (1972) *J.Org. Chem.* **37** 3404-3406
30. Lourens G.D. (1999) The influence of immobilisation and peptide structure on the bioactivity of model antimicrobial peptides, M.Sc. Thesis (Biochemistry), University of Stellenbosch, pp. 2.11-2.12

31. Du Toit E.A. (1999) The development of an antimicrobial assay and its use in the investigation of the combined effect of tetracycline and synthetic antimicrobial peptides on strains of *Escherichia coli*, M.Sc. Thesis (Biochemistry), University of Stellenbosch, pp. 2.12-2.13
32. Rautenbach M. (1989) The synthesis and characterisation of antigenic peptide determinants, M.Sc. Thesis (Biochemistry), University of Pretoria, pp.11-25, 28-33, 80-82
33. King D.S., Fields C.G. and Fields G.B. (1990) *Int. J. Peptide Protein Res.* **36** 255-266
34. Lauer J.L., Fields C.G. and Fields G.B. (1994) *Lett. Pept. Sci.*, **1** 197

Chapter 3

Imaging the action of membrane-active peptides on different target cells using Atomic Force Microscopy

3.1 Introduction

Over a decade ago, it was realised that antimicrobial peptides played a crucial role in nature as a means of “front-line” defence against invading organisms [1,2]. With the increasing problem of pathogenic organisms that are resistant to conventional antibiotics, there is growing interest in the application of antimicrobial peptides to treat infection. Research is currently focused on understanding the mechanism of action of these antimicrobial peptides to improve their potency and specificity, which will allow the development of the next generation of antibiotic [1].

This aim is complicated by the structural diversity found among antimicrobial peptides, and the different mechanisms of action they utilise [3-7]. For example, two well-known membrane-active peptides, melittin and magainin, differ widely in their target specificity and proposed mechanisms of action. Magainin, a 23-residue antimicrobial peptide, was discovered from the granular gland of the skin of the African clawed frog *Xenopus laevis* [8], and exhibits a broad spectrum of activity against bacteria, fungi, and protozoa typically in the concentration range of 10-100 $\mu\text{g/mL}$ [9-13]. In contrast, more than 1 mg/mL of magainin is required to lyse erythrocytes [14], indicating selective toxicity against microorganisms. Melittin, a bee venom 26-residue peptide amide, does not share the selective bioactivity properties of magainin. It is extremely haemolytic and shows minimal selectivity towards a broad range of microbial target cells [15].

Studies using model membrane systems have been used to better understand the influence of an antimicrobial peptide's structure on its toxicity and mechanism of action. The most

substantiated models (see Section 1.1.3) for toxic peptides (i.e. melittin) and non-toxic peptides (i.e. magainin) include the “barrel-stave” [16], “carpet” [17] and “wormhole/toroidal” pore models [18]. These studies also prompted the realisation that the mechanism of action was not only influenced by the structural properties of the peptide, but also by the variation in lipid composition and structure found among different target cell membranes. Biological membranes are predominantly arranged in a bilayer with the polar head groups facing outwards and the non-polar acyl chain tails pointing inward, however alternative non-lamellar phases also exist. This is because the structural properties of some lipids can be positive or negative-curvature inducing [19]. Lipids with small head groups promote negative curvature strain (see Section 1.1.2), which can form inverted phases if the bilayer stress reaches a critical point [19]. Alternatively, large head groups promote positive curvature strain (see Section 1.1.2), which can form micelles, if the bilayer stress reaches a critical point [19].

So if we analyse human and goat erythrocyte membranes (see Table 3.1), which can be considered representative of mammalian cell membranes, we find that the outer leaflet of the membrane consists mainly of the choline phosphatides, phosphatidylcholine (PC) and sphingomyelin (SM) [20,21]. The inner leaflet of the membrane is mainly composed of the aminophosphatides, phosphatidylethanolamine (PE) and phosphatidylserine (PS) [20,21]. In contrast, *E. coli* (Table 3.1) shows an outer membrane consisting mainly of lipopolysaccharides [22-24], while the inner membrane is mainly composed of cardiolipin (CL), phosphatidylglycerol (PG) and PE [25,26]. The specific properties of these structural components will influence erythrocyte and *E. coli* cell membranes towards positive or negative curvature strain.

Peptides can also influence the tendency of lipids to form non-lamellar phases [19] by inducing positive or negative curvature strain. Peptides that promote positive curvature strain on membranes can be associated with the formation of pores or lesions, depending on the orientation of the peptide [27]. In contrast, peptides that promote negative curvature strain can be associated with membrane collapse [27].

Table 3.1 Lipid composition in human and goat erythrocytes and in *E. coli* [21,22].

Phospholipid	% in erythrocyte plasma membranes Human; Goat	% in <i>E. coli</i> cell membrane (inner membrane)
CL	0; 0	12
PG	0; 0	6
PE	28.4; 27.8	82
PS	13.4; 20.8	0
PC	31; 0	0
SM	23.5; 45.9	0
Other	3.7; 5.5	0

Clearly, the combined influence of diverse peptide structure and target membrane complicates our understanding of the mechanism of action. However, the availability of efficient analytical and preparative techniques [see reviews 28-31] has allowed the application of many biophysical methods to determine the orientation, conformation, and interaction of peptides with model membranes. Through these model membrane studies, various membrane permeation models have been proposed for different peptide classes [29]. However, some peptides have also shown bactericidal activity *via* alternative mechanisms other than membrane permeation. For example, Park *et al* [32] compared the mechanism of action of buforin II with magainin 2. It was shown that unlike magainin 2, buforin II killed *E. coli* without lysing the cell membrane, even though both are structurally similar linear amphipathic α -helical peptides (for more examples see Section 1.1.3.5-1.1.3.9). This example highlights the fact that there are still many uncertainties surrounding our understanding of the mechanism of action of even this well-studied group of peptides. One reason for this is that although model membrane studies provide a wealth of information, they do not mimic the complexity of natural cell membranes. Model membrane studies cannot determine the combined curvature properties of all the phospholipid and protein components of a cell membrane, nor decipher the influence of peptide structure on the mechanism of action of a target cell membrane.

An alternative is to combine data obtained from model membrane studies with defined target cell studies. For example, the latest advances in microscopy allow us to visualise the effects of antimicrobial peptides on target cell membranes in the nanometer range. A number of microscopy techniques are available with resolution ranging from micrometers in the case of light microscopy, through to the sub-nanometer range for electron microscopy. In most of these methods the samples need to be coloured or fixed. In the case of cell membranes, treatment could result in conformational changes of the peptides and membrane surfaces. This limits the applications and conclusions concerning the mechanism of action of antimicrobial peptides. However, the last decade has seen rapid development in the field of scanning probe microscopy [33], more specifically atomic force microscopy, which has opened new and exciting applications in the natural sciences.

In the May 2000 edition of *Nature Structural Biology* [34], Feng briefly described the applications of atomic force microscopy (AFM) and how samples can be imaged (to nanometer resolution, without fixing) in air or under water. In AFM, the sample is scanned with a cantilever and the deflections are recorded by a computer, which generates a 3D image of the sample's surface [35]. This technique can provide us with new insights into understanding the mechanism of action of antimicrobial peptides.

We developed a method for using AFM to image the morphological changes induced by the linear α -helical peptides, melittin¹ and magainin 2¹, on target membranes without using fixing agents. Increasing peptide dose-responses were compared to the AFM images of the target-membranes obtained. From these images we were able to correlate our results with current membrane-permeation models and furthermore conclude that lipid composition plays a fundamental role in the mechanism of action and selectivity of antimicrobial peptides.

¹ Melittin and magainin were chosen for this study because of their contrasting selective properties. The structural details for these two peptides are highlighted in Section 2.1.

3.2 Materials

Escherichia coli (HB101) and erythrocytes isolated from freshly drawn goat blood were used as peptide target cells in all experiments. Melittin was from Sigma-Aldrich Chemie (Steinheim, Germany). Magainin 2 was synthesised at room temperature (20-25°C) according to the Fmoc-polyamide protocol [36] (see Chapter 2). Analytical quality water was prepared by filtering glass-distilled water through a Millipore Milli Q[®] water purification system. Glucose was purchased from BDH Chemicals (Poole, England), and trisodium citrate was from B&M Scientific cc. (Cape Town, South Africa). Sodium chloride and glacial acetic acid were from Saarchem (Krugersdorp, South Africa). Citric acid, disodium hydrogen phosphate, and formaldehyde (99%) were from Merck (Darmstadt, Germany). Potassium dihydrogen phosphate, tryptone soy agar (constituents in g/L: 15.0 tryptone, 5.0 soy peptone, 5.0 sodium chloride, 13.0 agar, pH 7.3, +-0.1) and tryptone soy broth (constituents in g/L: 17.0 tryptone, 3.0 soy peptone, 5.0 sodium chloride, 2.5 dipotassium hydrogen phosphate, 2.5 dextrose, pH 7.3, +-0.1) were from Merck (Midrand, South Africa). Potassium chloride was purchased from Trinity Scientific (Hillcrest, South Africa). Microtiter plates (Nunc-Imuno[™] Maxisorp) were from Nalge NUNC International (Roskilde, Denmark), Falcon[®] tubes from Becton Dickinson Labware (Lincoln Park, USA), and culture dishes from Quality Scientific Plastics (USA).

3.3 Methods

3.3.1 Preparation of erythrocytes

The haemolytic activity of melittin and magainin 2 was investigated using goat red blood cells². Blood was drawn and stored with equal amounts of Alsevers solution (2.05% glucose, 0.80% sodium citrate, 0.42% sodium chloride and 0.055% citric acid, m/v, pH 7.2) at 4°C for 5 days [37]. To ensure erythrocyte separation and stabilisation, the blood samples were decanted and washed with fresh Alsevers solution every 24 hours. Erythrocytes were separated directly before use by centrifugation (900g for 10 minutes) washed and diluted (2.5% erythrocyte solution) in PBS (8% NaCl, 0.2% KCl, 1.15% Na₂HPO₄ and 0.2% KH₂PO₄, m/v, pH 7.2) [37].

3.3.2 Haemolysis dose response assays

The prepared erythrocytes were incubated at room temperature (22±2°C) for 30 minutes using an optimised concentration range of melittin (doubling dilutions, 0.2nM-3.51µM) and magainin 2 (doubling dilutions, 0.39-202µM) diluted in PBS (0.15 M, pH 7.2). To determine the extent of haemolysis, the cells and cell debris were removed by centrifugation for five minutes on a small bench-top centrifuge (PicoFuge®) and the absorbance of the supernatants measured at 405 nm using a Multiscan Titertek microtitre plate reader. The minimum haemolytic concentration (MHC or HC₅₀) was defined as the peptide concentration leading to 50% haemolysis³. Zero haemolysis (blank) and 100%

² This project was initiated at a time when the newly built BIOPEP and AFM laboratories did not have the necessary human blood hazard protocols in place, therefore non-human blood was used instead. We chose goat blood over rabbit blood, because we were insured of a constant supply of samples from animals uncontaminated by any physiological treatments, which could change erythrocyte morphology or function.

³ Deduced from the following equation: $Y = 100 / (1 + 10^{(\log HC_{50} \times \text{Hill slope})})$ where:

log HC₅₀=X-value of response halfway between top and bottom; Hill Slope = Hill Coefficient

haemolysis were determined by measuring the absorbance of the supernatant of the erythrocytes suspended in PBS (0.15 M, pH 7.2) and melittin (1 mg/mL) respectively.

3.3.3 Preparation of erythrocytes for AFM

The erythrocytes⁴ were incubated at ambient temperature with the peptide solutions for three minutes at different concentrations, as determined from the dose response assays (Fig. 3.1). Formaldehyde control samples were incubated for an additional three minutes with a 2% formaldehyde solution, and all samples were washed twice⁵ in PBS (0.15 M, pH 7.2). 5 μ l of each sample was added onto a freshly cleaved mica surface. The residual solution was removed with a piece of filter paper and allowed to air-dry for approximately three minutes before imaging. Each sample was imaged for approximately 10 minutes. Drying-related changes to the erythrocyte surface morphology became evident after 20 minutes.

3.3.4 Preparation of bacterial cells

The anti-bacterial activity of melittin and magainin 2 was tested using *E. coli* (HB101). Bacterial cells were incubated at 37°C for 24 hours on a tryptone agar plate. Five colonies were selected and transferred to 6 mL tryptone soy broth (TSB) and grown overnight at 37°C. 200 μ L of the suspension was sub-cultured in 7 mL TSB and grown to an optical density (OD) of 0.6 at 620nm and further diluted to an OD of 0.285 [38].

⁴ The erythrocyte concentration used during the haemolysis assay was optimised to ensure that no bunching occurred on the mica surface during imaging. This became evident during our initial image optimisation test runs (before conducting the haemolysis assays), where extreme bunching and double cell layers made for ineffective data analysis. We found that a 2.5% erythrocyte solution provided an effective spread of cells over a 5 μ m² imaging area.

⁵ Alsevers solution affected our initial data analysis. Therefore the washing step was introduced during erythrocyte preparation and again used during image preparation to also clear away cell debris. This step did not affect the peptide image data generated.

3.3.5 Antibacterial activity dose response assays

The dose-responses of melittin (doubling dilutions, 0.43-17.57 μM) and magainin 2 (doubling dilutions, 0.57-36.83 μM) were determined by incubating 70 μL of the bacterial suspension and 30 μL of each peptide (dissolved in analytical quality water) on a microtitre plate. To determine the extent of growth inhibition, light dispersion was measured after 17 hours of incubation (37°C) at 620nm using a Multiscan Titertek microtitre plate reader⁶. 100% growth was determined using 70 μl bacterial suspension and 30 μl H₂O (analytical quality). 100% inhibition was determined using 1 mg/ml melittin.

3.3.6 Preparation of *E. coli* for AFM

To prepare the bacterial samples for imaging, 70 μl of the sub-cultured bacterial suspension was incubated for three minutes with 30 μl of each peptide. Melittin and magainin 2 samples were dissolved in analytical quality water using effective concentrations determined from the dose response assays (see 3.4.1.2). The *E. coli* samples were centrifuged at 1000g (Eppendorf Centrifuge 5417C) for ten minutes and the supernatant discarded. The pellet was then gently resuspended in a 1 mL NaCl solution (0.9 % m/v, pH 7.2) and 5 μL added onto a freshly cleaved mica surface. The residual solution was removed with a piece of filter paper and allowed to air-dry for approximately three minutes before imaging. Each sample was imaged for approximately 10 minutes. Drying-related changes to the *E. coli* surface morphology became evident after 20 minutes.

⁶ The equation used for the sigmoidal curve with variable slope was:
 $Y = \text{bottom} + \frac{(\text{top} - \text{bottom})}{(1 + 10^{\log_{10} \text{IC}_{50} \times \text{Hill slope}})}$ where the bottom is the Y-value at the bottom plateau and top is the Y-value at the top of the plateau; IC₅₀ is the X-value of the response halfway between top and bottom; Hill slope = Hill coefficient. IC₅₀ is 50% inhibitory concentration.

3.3.7 AFM Imaging

The TMX 2000 Explorer (Topometrix, Santa Barbara, CA) atomic force microscope was used for all imaging of erythrocytes and bacterial cells. The imaging parameters were optimised by varying the resonance frequency, force constant and set point until clear images were obtained without damaging the samples. We operated in contact mode using commercially available v-shaped cantilevers (200x18 μ m) from Topometrix, with a resonance frequency of 5-15kHz and a force constant of 0.032N/m. Si₃N₄ pyramidal light force tips were used and imaging forces were adjusted to a set point of -30nA. A 165nm step height standard Topometrix grid was used for calibration of the height (z) and lateral (x,y) measurements of the stage. Data analysis was performed using Topometrix SPM Lab version 3.06.06.

3.4 Results

3.4.1 Dose response parameters

3.4.1.1 Erythrocyte dose-response

Melittin and magainin 2 showed a MHC (minimum haemolytic concentration) of 0.36 μ M and 64 μ M (Fig. 3.1), and a Hill slope factor of 0.97 and 6.144 respectively. Peptide concentrations above and below the MHC were used during AFM imaging to record the structural changes induced by melittin and magainin 2 on erythrocytes.

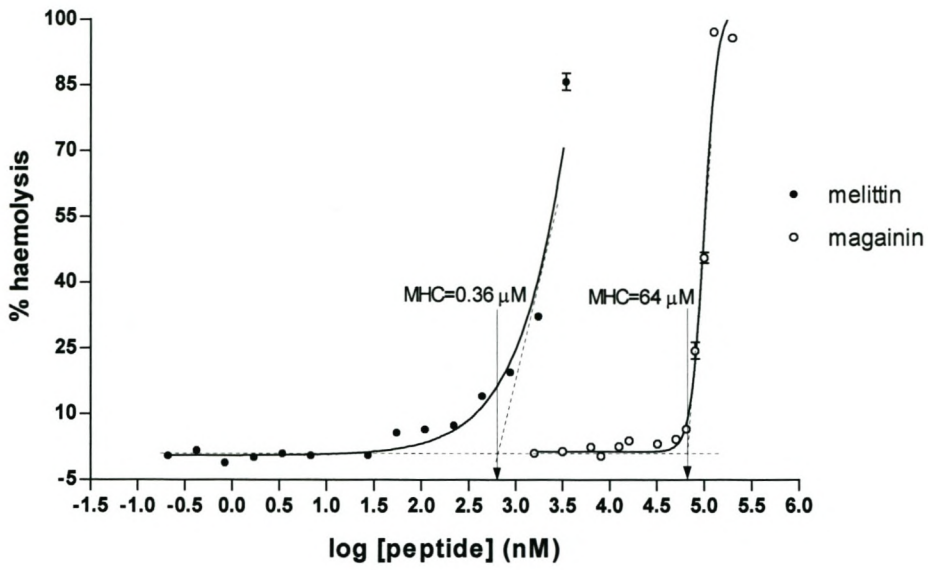


Figure 3.1 A graph illustrating melittin and magainin 2 dose-response parameters for erythrocytes.

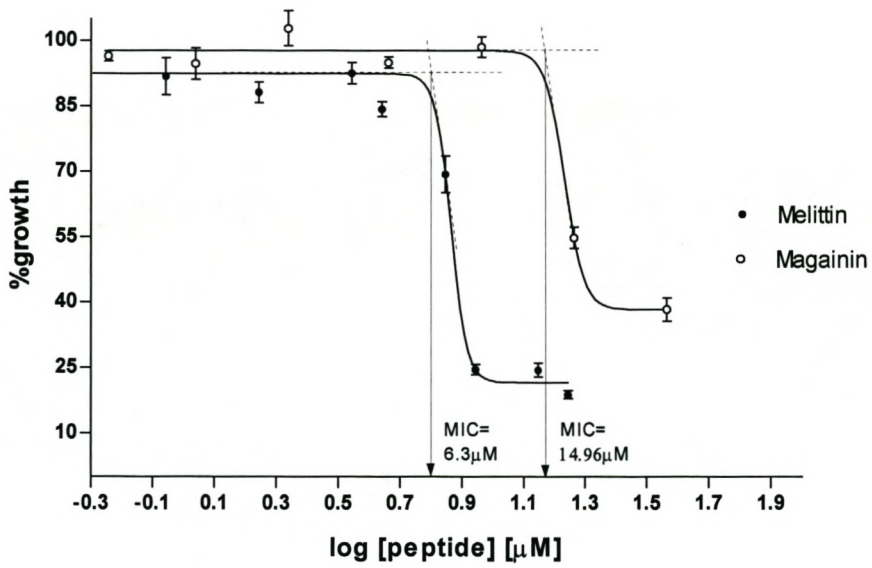


Figure 3.2 A graph illustrating melittin and magainin 2 dose-response parameters for *E. coli*.

3.4.1.2 *E. coli* dose-response

In contrast to the erythrocyte dose-response parameters, melittin and magainin 2 showed a similar MIC (minimum inhibitory concentration) of 6.3 μM and 14.96 μM , and a Hill slope factor of -17 and -13 respectively (Fig 3.2). During AFM imaging, peptide concentrations above and below the MIC were used to record the structural changes induced by melittin and magainin 2 on *E. coli*.

3.4.2 Atomic Force Microscopy

During the AFM studies we imaged over 100 blank controls at $5\mu\text{m}^2$ to capture all possible morphological variations on the target cells for comparison with the peptide data to ensure that the morphological changes were indeed induced by and unique to the peptide. Image collection on melittin and magainin 2 was also continued until representative data regarding all morphological cell variations had been captured.

3.4.2.1 Erythrocyte cell shape

Our major concern during the visualisation process was the influence our sample preparation would have on the images obtained, as it did not involve any form of fixation. Instead visualisation took place at ambient temperature and atmosphere, with slight drying of the samples as a result of the removal of residual water. It was noticed that the cells flattened out on the mica surface, most likely as a result of the combined effect of semi-drying and hydrophobic association with the mica. This change in cell shape did not influence the initial membrane interaction of melittin and magainin 2 because of two reasons: First, the interaction between the peptides and the erythrocytes took place under physiological conditions before the removal of any residual water. Second, the specific properties of the membrane skeleton impart the strength and deformability required for the cell to withstand the tremendous forces of circulation and to squeeze through microcapillaries [39]. This allows flattening or swelling of the cells to occur without initially compromising the membrane structure of the erythrocytes. This also allows semi-drying to occur without influencing the surface-structure changes imaged after peptide interaction (<20 min).

The average diameter of goat erythrocytes reported in literature is 2.4 - 3 μm [40]. Our wet images (no drying), displayed a typical doughnut shape (Fig. 3.3a) with a mean average diameter of $3.10 \pm 0.03 \mu\text{m}$. The discoidal erythrocyte shape corresponds to the minimum of its membrane elastic energy [41]. This consists of the bilayer-bending energies and the skeleton shear elastic energy, while the cell volume and the membrane area are kept constant [41]. Although it was possible to generate wet images, we could not produce consistent results due to interference with the cantilever, therefore semi-drying of the samples was necessary to limit this interference. The semi-dry erythrocyte controls (Fig. 3.3b) although slightly flattened, still retained the characteristic indentation and membrane morphology of the wet images with a mean average diameter of $3.70 \pm 0.07 \mu\text{m}$ (see Table 3.2). The addition of formaldehyde prevented cell flattening (Fig. 3.3c), but resulted in an increase in diameter to a mean average of $4.70 \pm 0.19 \mu\text{m}$. This occurs because formaldehyde induces changes in protein conformation, which in turn would effect peptide-lipid interactions [42]. Subsequently, this fixing agent was only used as a control.

The incubation with melittin (Fig. 3.4a) and magainin 2 (Fig. 3.4b) below their MHC caused the cells to swell to form a convex shape. The melittin and magainin 2 treated erythrocytes increased from a mean average diameter of $3.70 \pm 0.07 \mu\text{m}$ to $4.65 \pm 0.12 \mu\text{m}$ and $4.70 \pm 0.21 \mu\text{m}$ respectively (Table 3.2). The formaldehyde samples pre-treated with peptides showed no further increase in size. This result was as expected, because cross-linking of membrane proteins and phospholipid-headgroups limits the elasticity of the membrane and the swelling that occurs before lysis.

Table 3.2 Size parameters for semi-dry erythrocytes and *E. coli*.

Target cell	Blanks	Melittin	Magainin 2
Erythrocytes	3.70±0.07 μm (n=50)	4.65±0.12 μm (n=40)	4.70±0.21μm (n=40)
Erythrocytes and formaldehyde	4.70±0.18μm (n=10)	4.97±0.21μm (n=10)	4.61±0.17μm (n=10)

3.4.2.2 Erythrocyte surface morphology

Fine structural details of the erythrocyte lipid bilayer, such as proteins protruding from the lipid surface, were not visible. The addition of the peptides caused the formation of lesions, grooves or vesicles, depending on the peptide and concentration used.

The addition of melittin at 0.218μM (below MHC) resulted in the formation of distinct lesions on the surface of the erythrocytes (Fig. 3.5a). These lesions varied in size from 70-95nm in surface diameter, however the cell structure still remained intact. It must be emphasised that this is 10-fold larger than “pores” found in literature [64], indicating that we are observing an event consequent to melittin's mechanism of action. This is due to the resolution constraints of our atomic force microscope methodology⁷. The largest lesions generally appeared in the central region of the cell (biconcave area) connected by lines of smaller lesions clustered together. It is possible that the change in surface infrastructure and membrane tension make the central area more vulnerable to peptide attack. The close grouping or banding of lesions may be the consequence of lipid segregation causing same-type lipids to cluster together [19]. This in turn would cause lesions to occur around those lipid types, which are structurally more vulnerable to attack (detailed in discussion). Higher melittin concentrations (0.4μM, 10% higher than MHC) resulted in additional lesions, cell fusion and vesiculation (Fig. 3.5b).

⁷ This hold true for all images of erythrocytes and *E. coli*, in this AFM study.

A closer analysis of melittin samples below the MHC at 0.218 μM , show that the lesions are connected by lines or grooves (Fig. 3.6), in fact, these “lines/grooves” appear to periodically widen to form the lesions observed (70-95nm).

In contrast to the lesions observed in melittin-treated erythrocytes, the addition of magainin 2 (50.7 μM , below MHC) resulted in the formation of distinct grooves (consequent to magainin's mechanism of action) on the surface of the taught cell (Fig. 3.7a) with possible vesiculation damage (Fig. 3.7b). Higher concentrations (101 μM , >50% higher than MHC) resulted in irreversible haemolysis caused by cell surface collapse (Fig 3.7c). This resulted in more cell debris and minimal vesicle formation when compared to the structural changes induced by the melittin samples. Furthermore we observed that although the magainin 2 samples showed similar “lines/grooves” to melittin, they did not appear to widen to form large visible lesions (Fig. 3.8), although there was one rare exception where a small lesion (95nm in diameter) was visible (Fig. 3.9). The results correlated well with the dose response parameters, allowing us to assign specific mechanisms of action for melittin and magainin 2 based on previous model membrane studies (detailed in discussion).

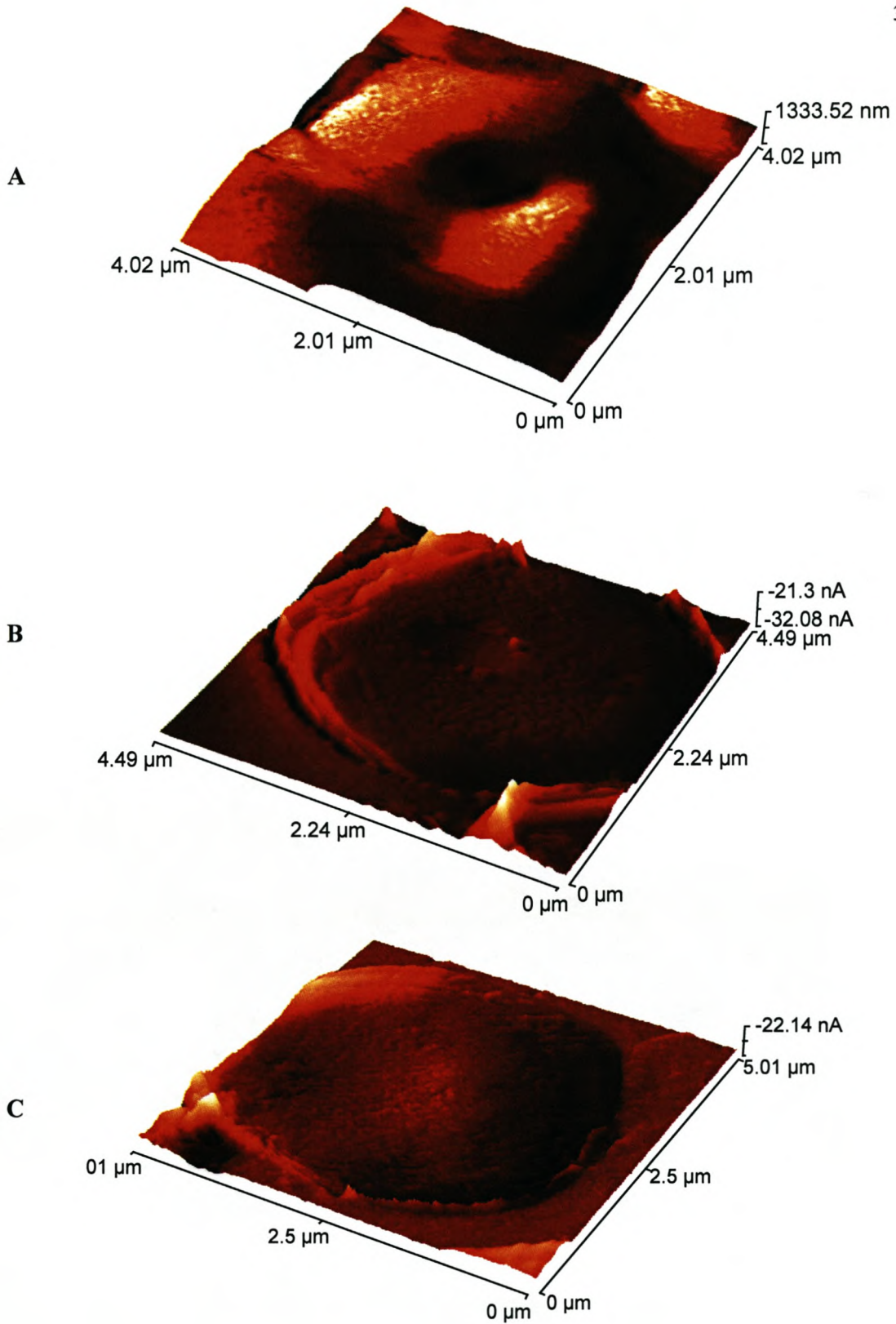


Figure 3.3 AFM images of erythrocyte controls **A**: wet image; **B**: semi-dry image; **C**: formaldehyde control image.

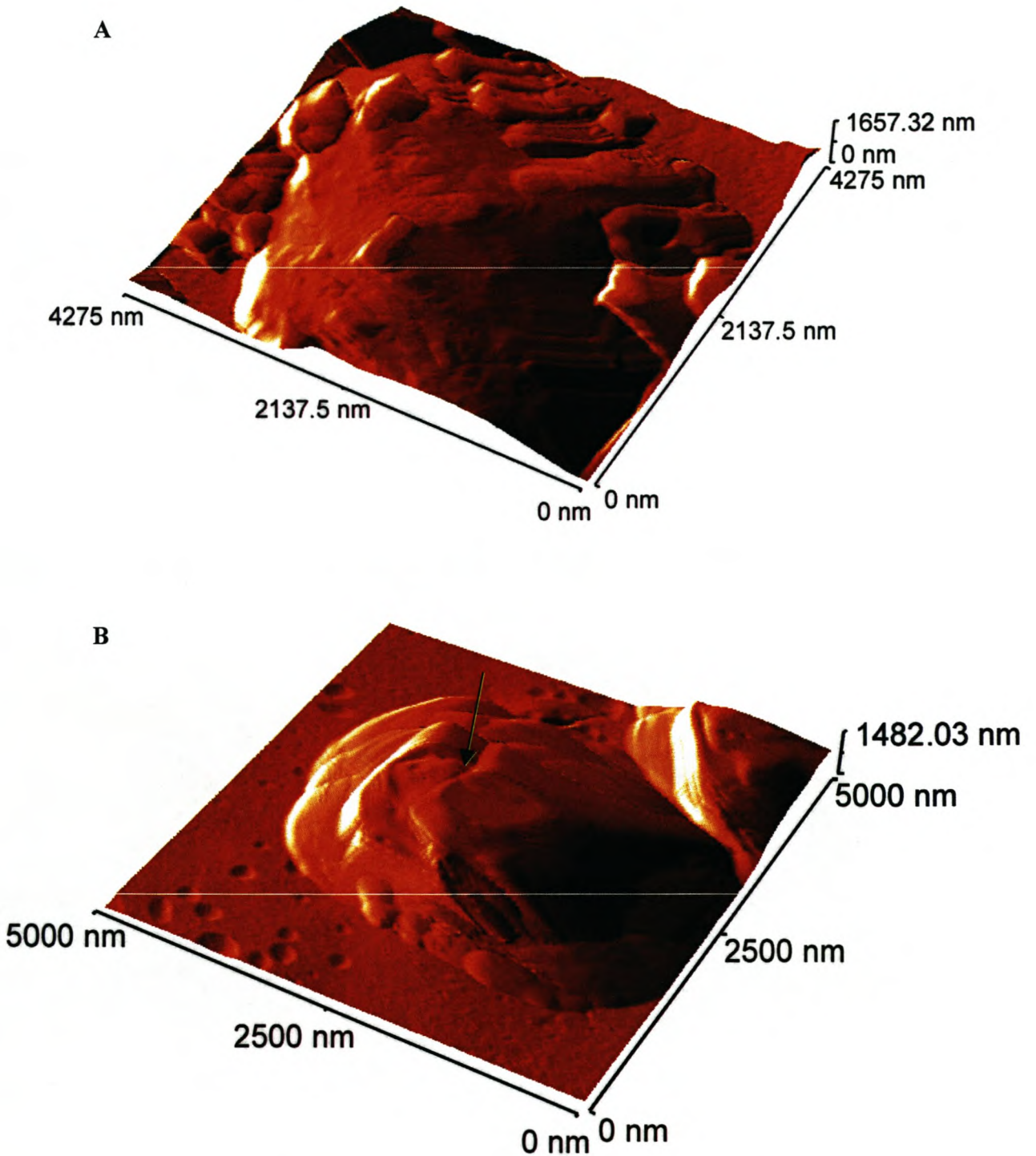


Figure 3.4 **A:** AFM image of melittin-induced erythrocyte swelling below MHC ($0.218\mu\text{M}$) and **B:** AFM image of magainin-induced erythrocyte swelling below MHC ($50.7\mu\text{M}$) with arrow indicating grooves forming on surface.

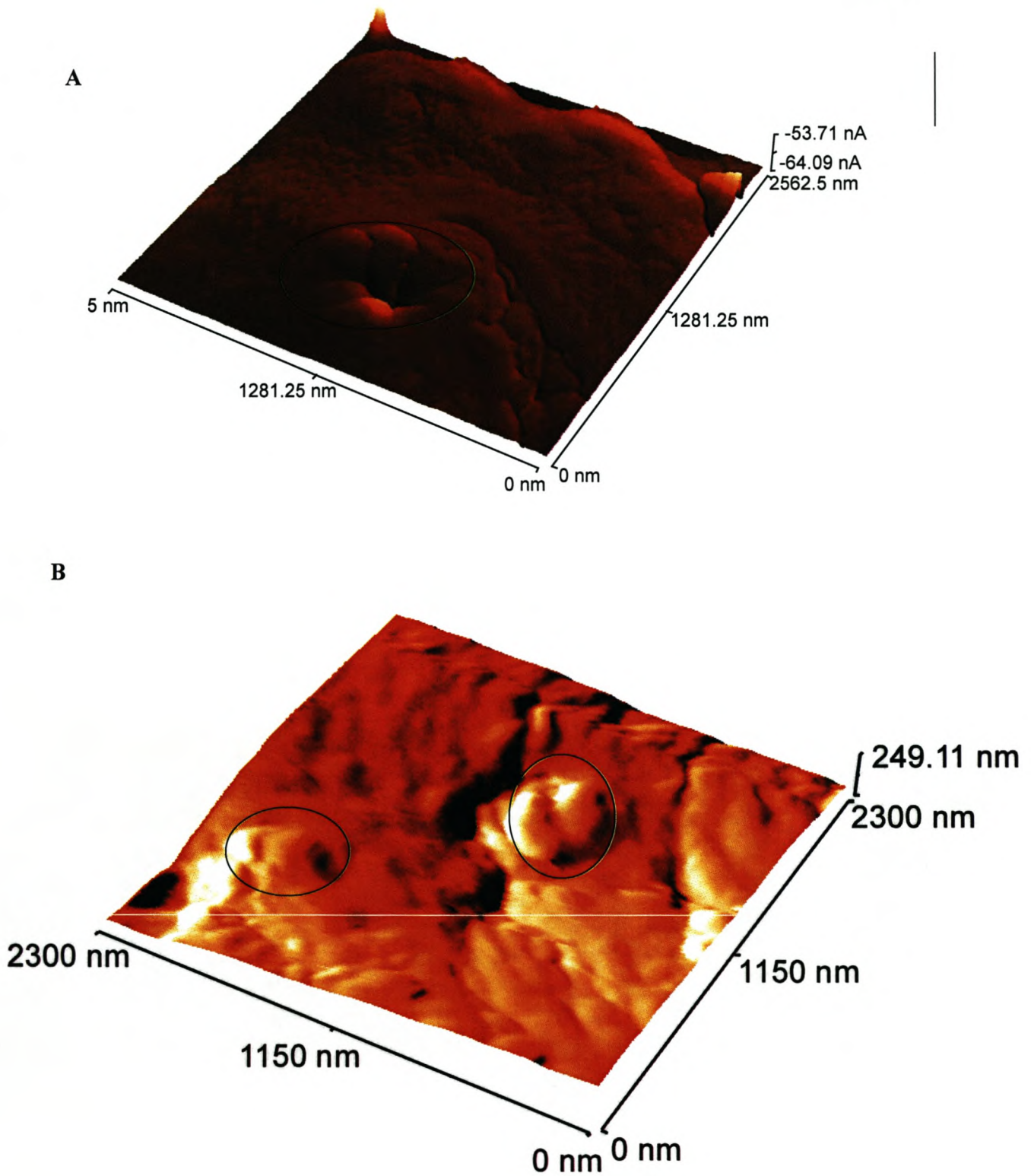


Figure 3.5 **A:** Melittin-induced lesion (circle) below MHC ($0.218\mu\text{M}$) and **B:** melittin-induced lesions above MHC ($0.40\mu\text{M}$), with forming vesicles (circles).

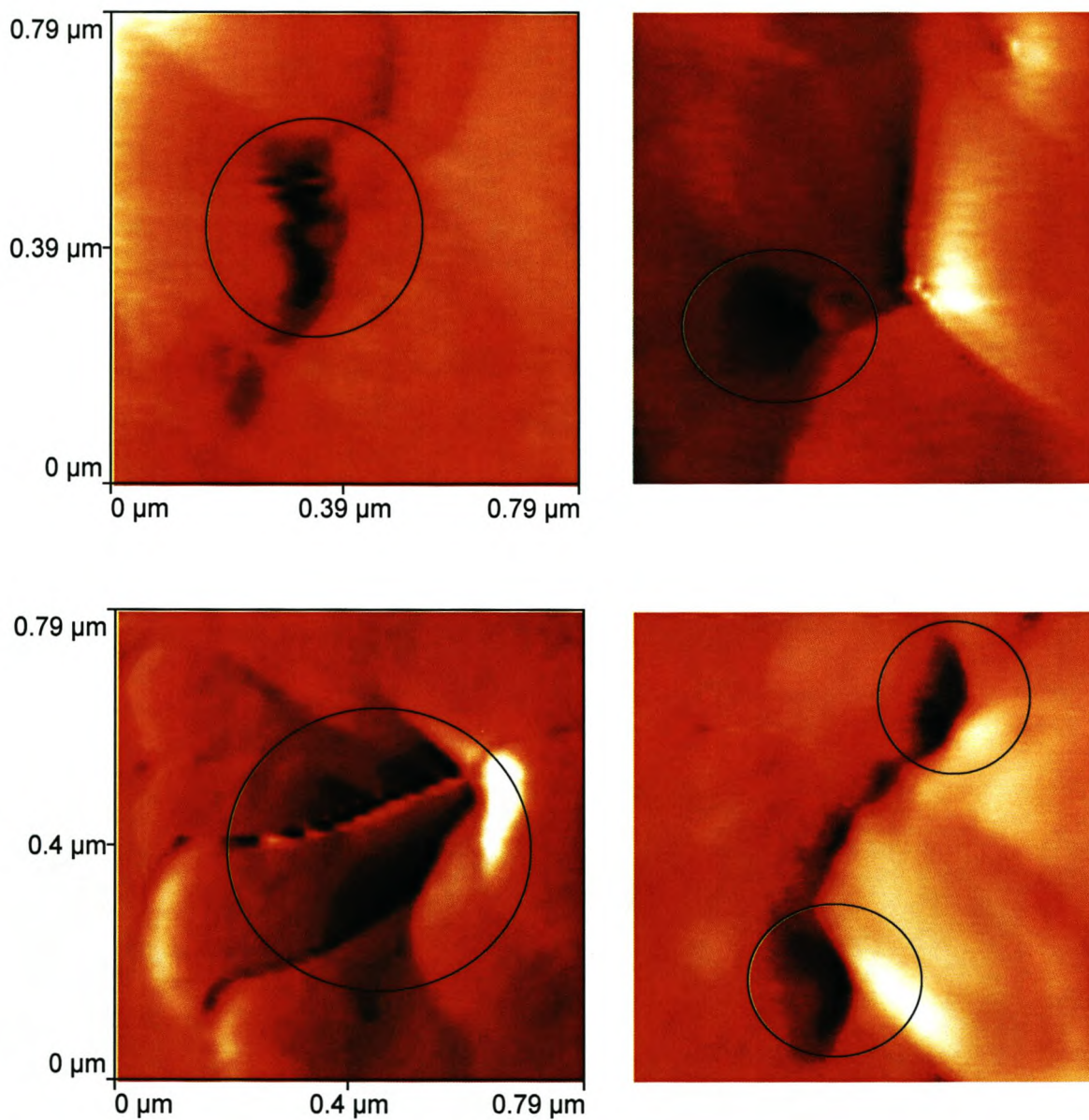
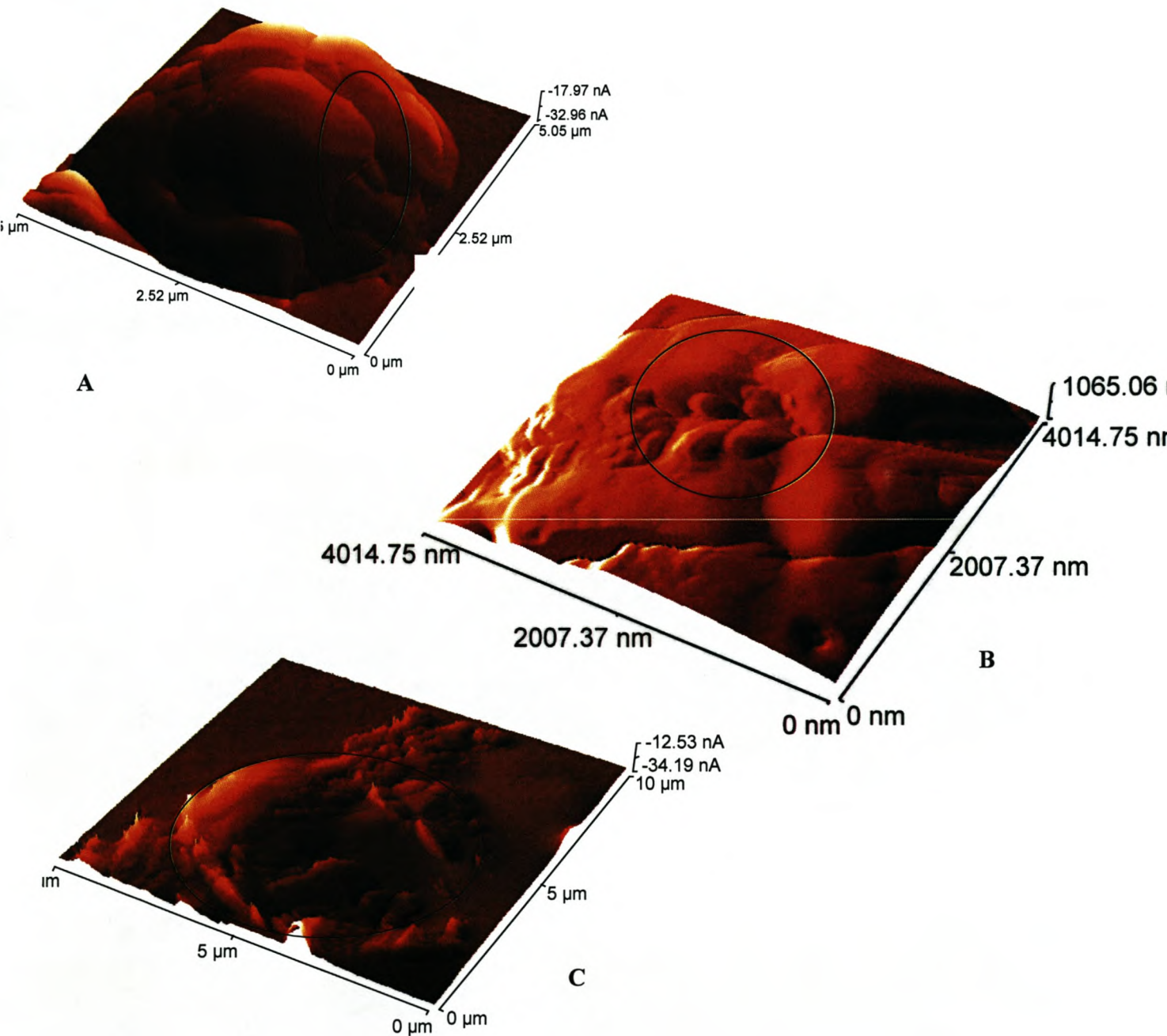


Figure 3.6 AFM images on the erythrocyte surface with circles indicating the variation in shape and size that occurs as a result of melittin-induced lesions (70-95nm) below MHC (0.218μM).

Figure 3.7 **A:** Magainin-induced groove (circle) and **B:** magainin-induced cytoplasm leakage on erythrocyte surface below the MHC ($50.7\mu\text{M}$). **C:** Magainin-induced haemolysis (cell outline indicated by circle), above MHC ($101\mu\text{M}$).



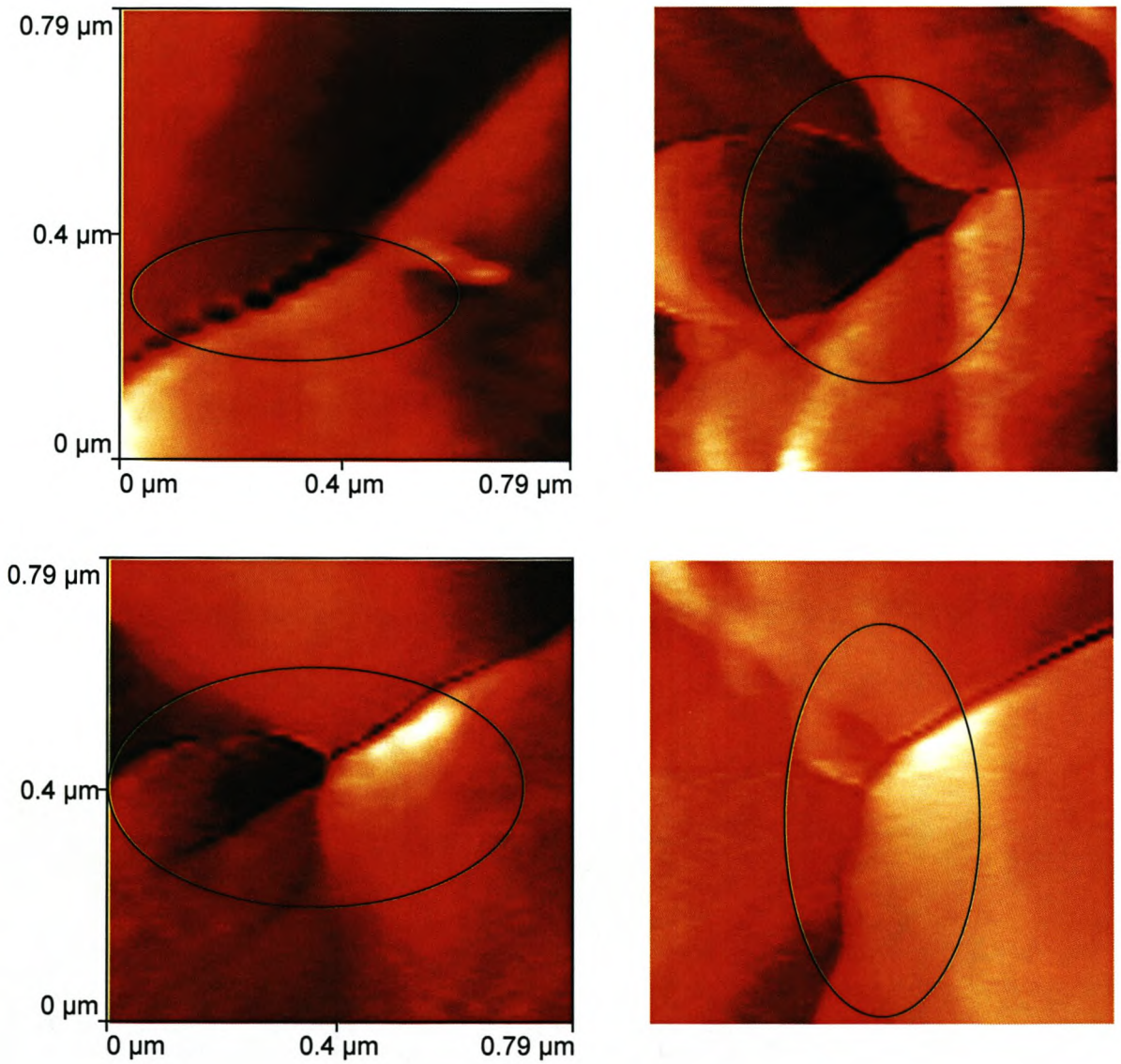


Figure 3.8 AFM images with circles indicating magainin-induced grooves below MHC (50.7 μ M) on the erythrocyte surface.

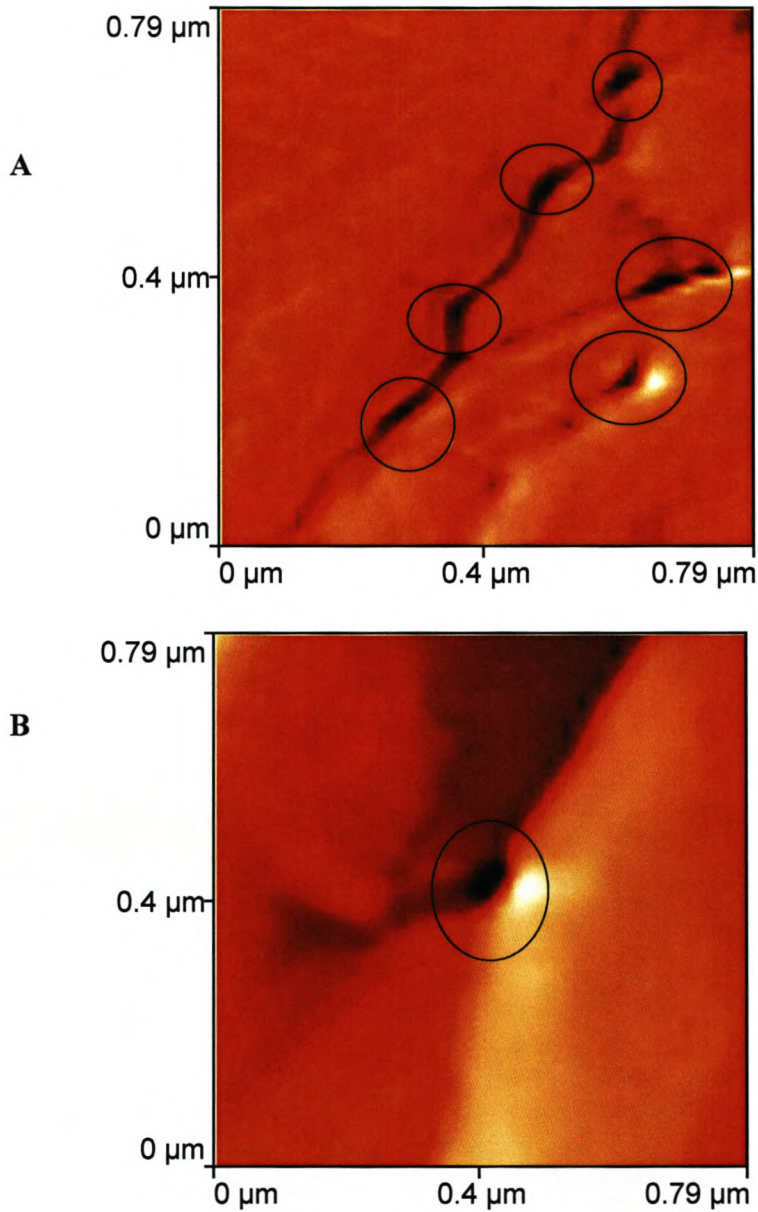


Figure 3.9 Comparison of AFM images indicating lesions (circles) on erythrocytes induced by **A**: melittin and **B**: magainin 2. It is interesting to note that the melittin sample appear to form grooves which widen into small lesions. Although a similar event occurred with the magainin 2 sample it should be mentioned that this lesion (95nm) was the only one captured for magainin 2.

3.4.2.3 Bacterial cell shape and morphology

The rigid cell wall of *E. coli* supports the cell structure during imaging, preventing the distortion observed with the erythrocyte cells. Figure 3.10 represents the typical structure recorded for *E. coli* with an average length of $3.32 \pm 0.14 \mu\text{m}$ and width of 1.91 ± 0.14 ($n=25$). This is in accordance with cell sizes reported in literature [43]. We did not observe the distinctive swelling found for the erythrocytes due to the structural stability provided by the bacterial cell wall.

Below melittin's MIC ($2.17 \mu\text{M}$), structural changes of the bacterial cell wall were induced, resulting in the formation of lesions (consequent to melittin's mechanism of action) and an outward bulging of the inner membrane (Fig. 3.11, top image). A further increase in concentration ($8.78 \mu\text{M}$, $\pm 40\%$ times higher than the MIC) resulted in lysis of the cell (Fig. 3.11, bottom image), with minimal vesiculation.

Below the MIC, at a concentration of $1.08 \mu\text{M}$, melittin appeared to form similar lesions (95-130nm) with connecting lines on *E. coli* (Fig. 3.12) as observed for the erythrocytes (70-95nm; Fig. 3.6). At a higher concentration of $2.18 \mu\text{M}$, still below the MIC, the lesions appeared to decrease in size (30-85nm) and appeared more randomly distributed, with only some minimal vesiculation (Fig. 3.13).

Below magainin's MIC ($4.1 \mu\text{M}$), we also observed lesions (consequent to magainin's mechanism of action) on the surface and an outward bulging of the inner membrane of *E. coli* (Fig. 3.14a). At approximately twice the concentration of melittin, magainin 2 ($20.3 \mu\text{M}$, $\pm 35\%$ higher than MIC) still showed lesions and the same outward leakage of the inner membrane as below the MIC, but also induced mass vesiculation (Fig. 3.14b), which was not observed for melittin-treated samples (Fig. 3.11, bottom). Electron microscopy studies have also shown magainin-induced lesions or blebs on the bacterial membrane [13].

Below the MIC, at a concentration of $2.02 \mu\text{M}$, the magainin 2 lesions (150-340nm; Fig. 3.15) with connecting lines appeared larger than the melittin lesions (95-130nm; Fig. 3.12). At a higher concentration of $4.06 \mu\text{M}$, still below the MIC, the magainin 2 lesions appeared to be of similar size to the lower concentration level (200-360nm; Fig. 3.16).

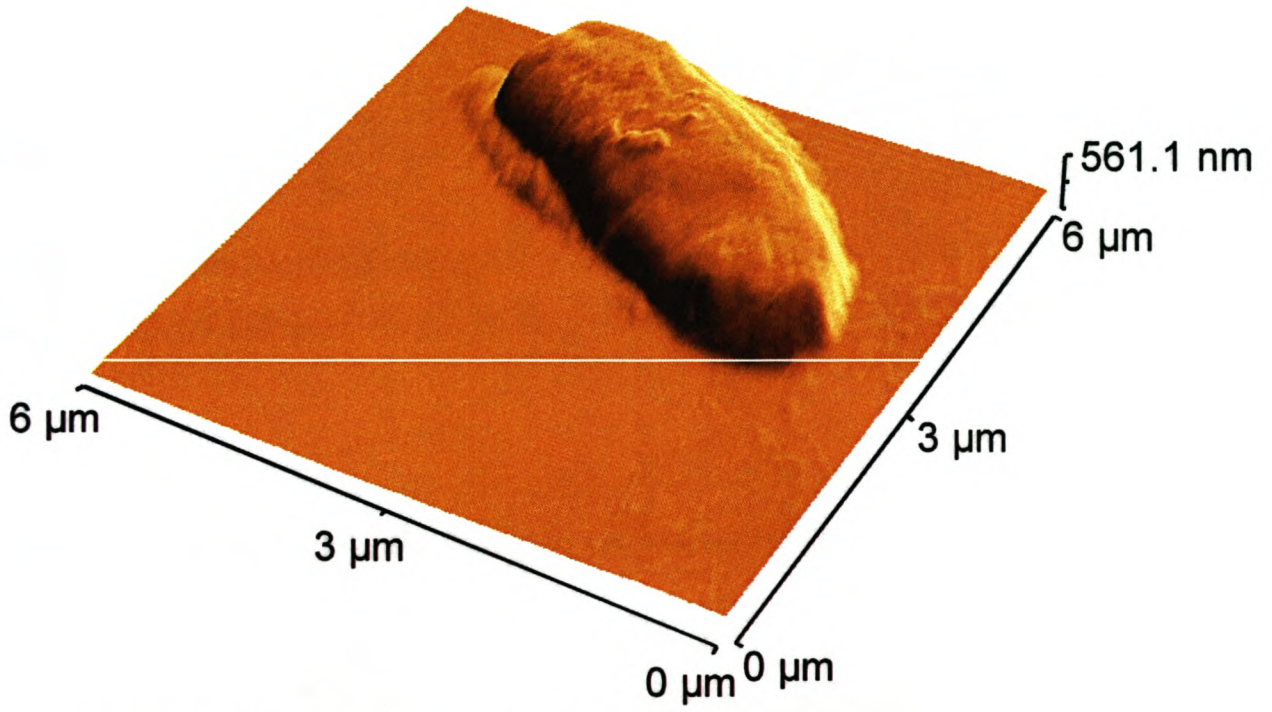


Figure 3.10 AFM control image of *E.coli*.

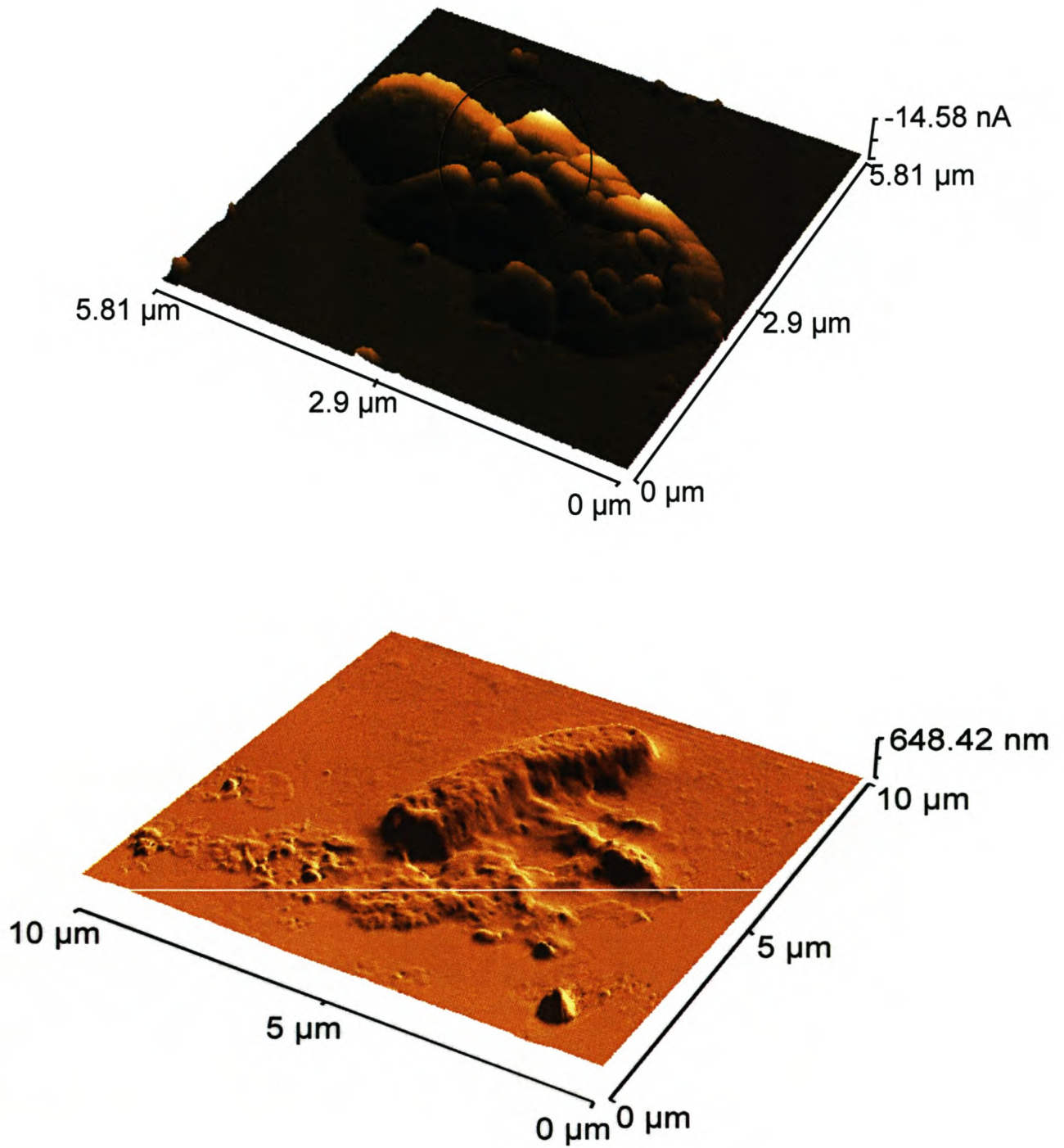


Figure 3.11 AFM images of *E. coli* with melittin-induced lesions (top image) below the MIC ($2.17\mu\text{M}$) resulting in an outward bulging of the inner membrane (circle). Melittin-induced lysis (bottom image) above the MIC ($8.78\mu\text{M}$).

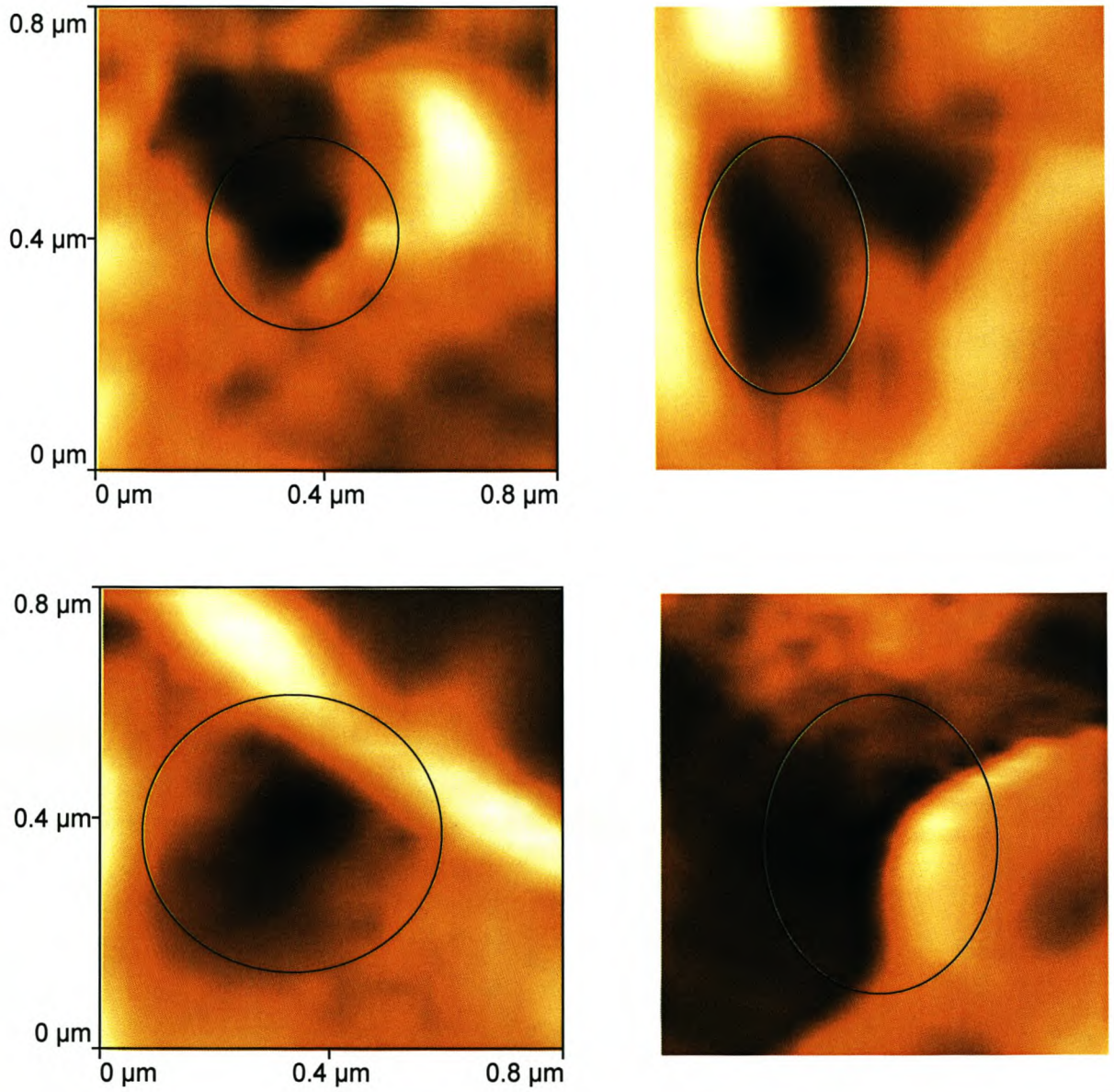


Figure 3.12 AFM images with circles indicating melittin-induced lesions (95-130nm) below MIC (1.08μM) on the *E. coli* surface.

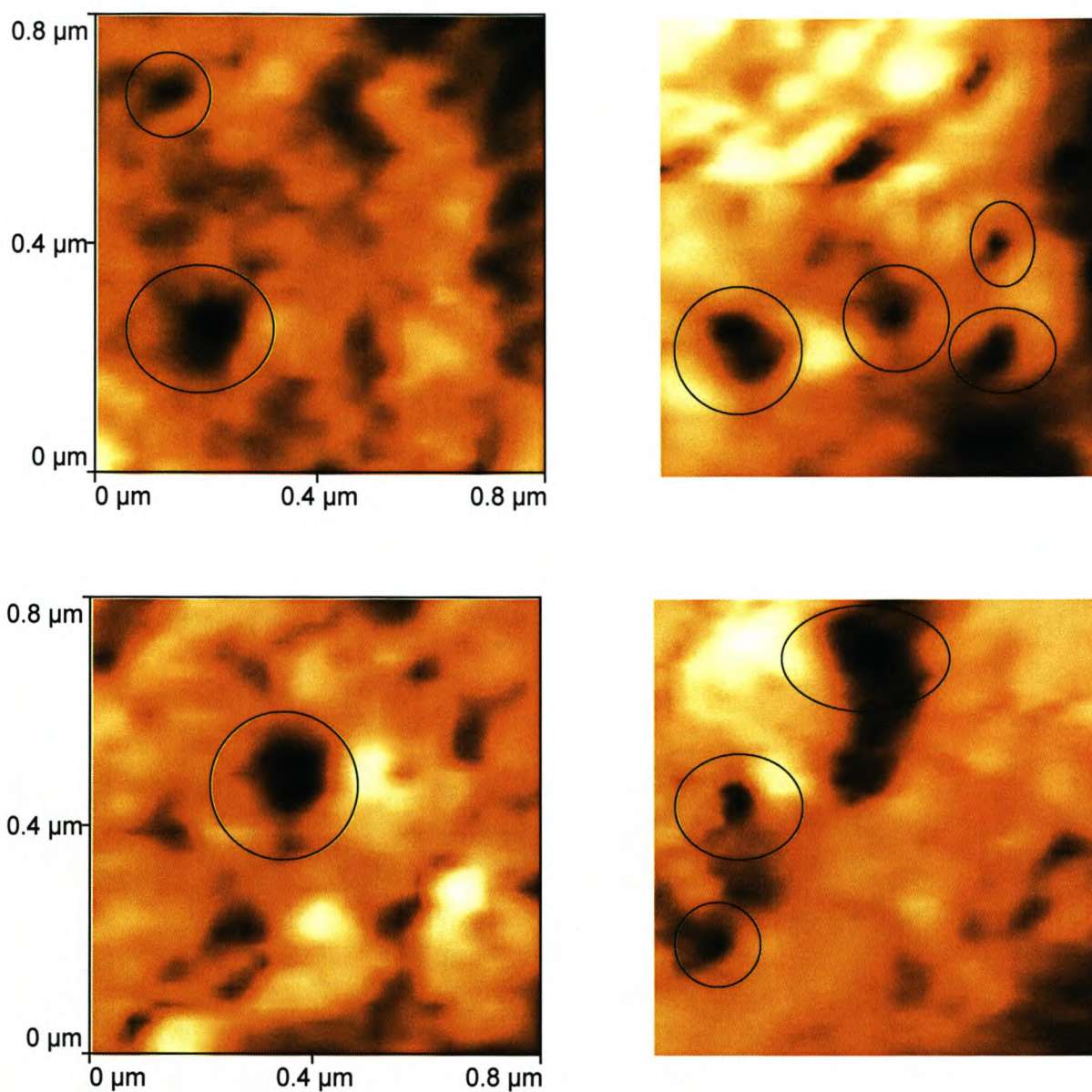
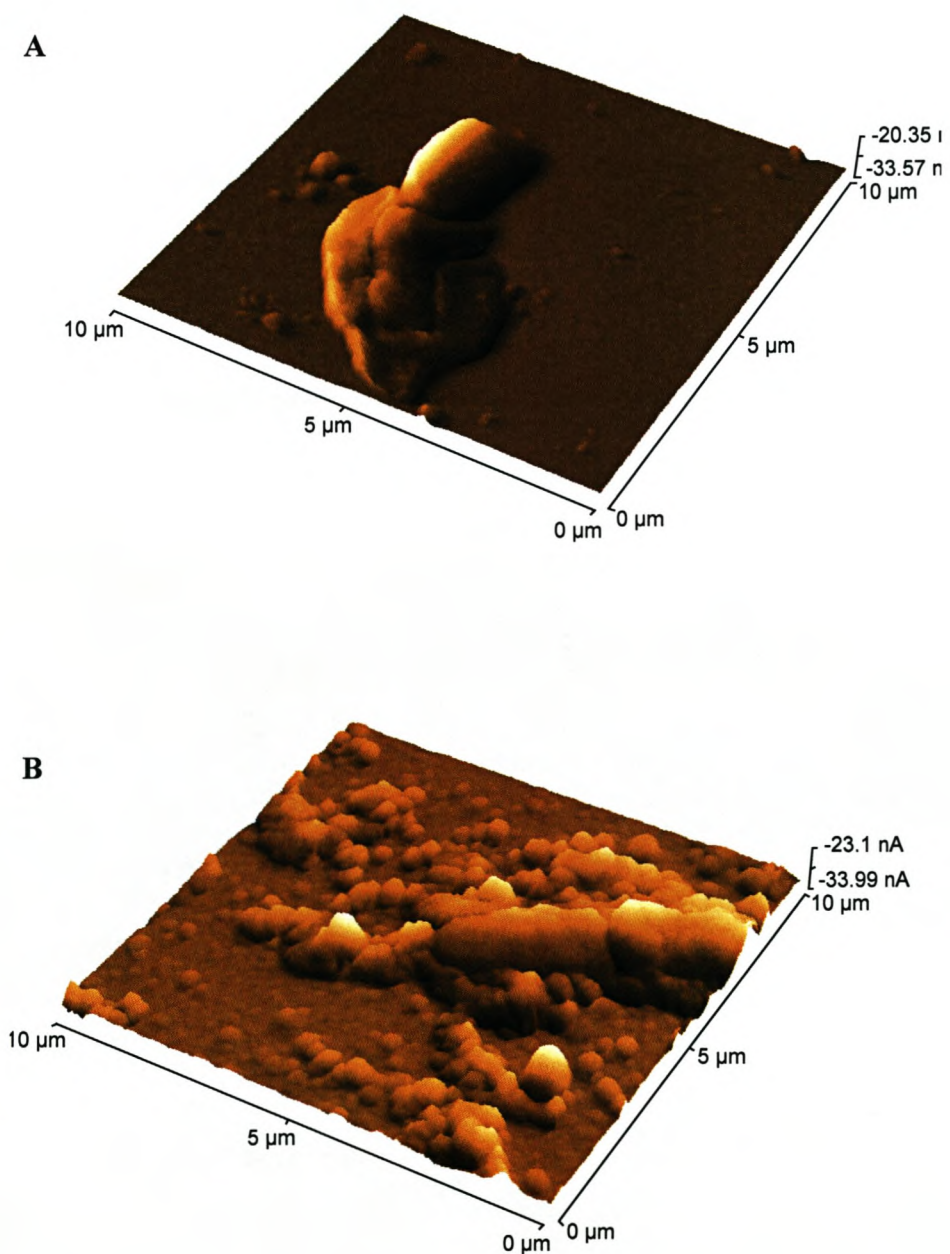


Figure 3.13 AFM images on the *E. coli* surface with circles indicating smaller melittin-induced lesions (30-85nm) at higher concentration, but still below MIC (2.18μM).

Figure 3.14 AFM images of *E. coli* with **A**: magainin-induced lesions resulting in an outward-bulging of the cells membrane below the MIC ($4.1\mu\text{M}$) and **B**: mass vesiculation above the MIC ($20.3\mu\text{M}$).



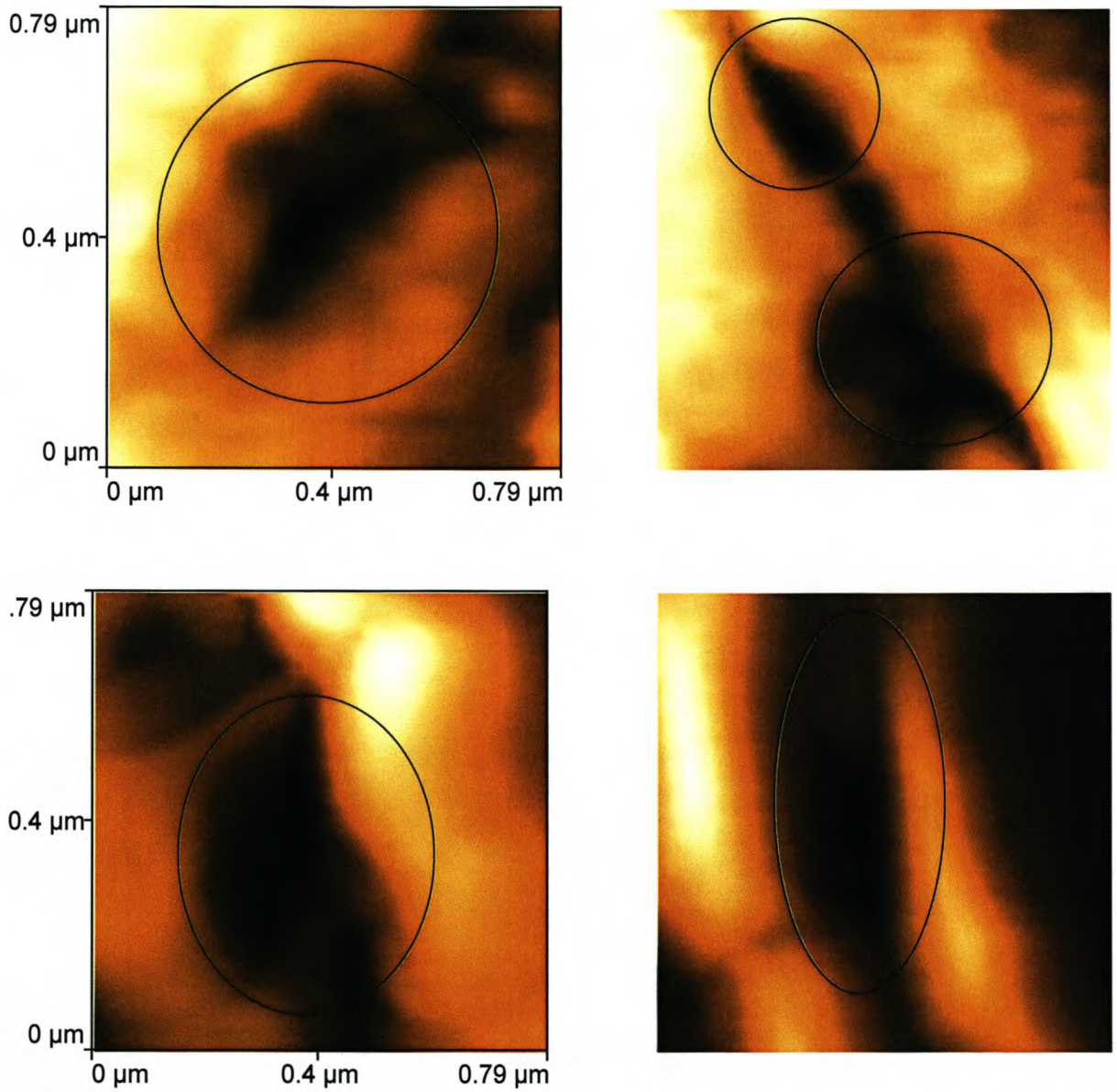


Figure 3.15 AFM images with circles indicating large magainin-induced lesions (150-340nm) below MIC (2.02μM) on the *E. coli* surface.

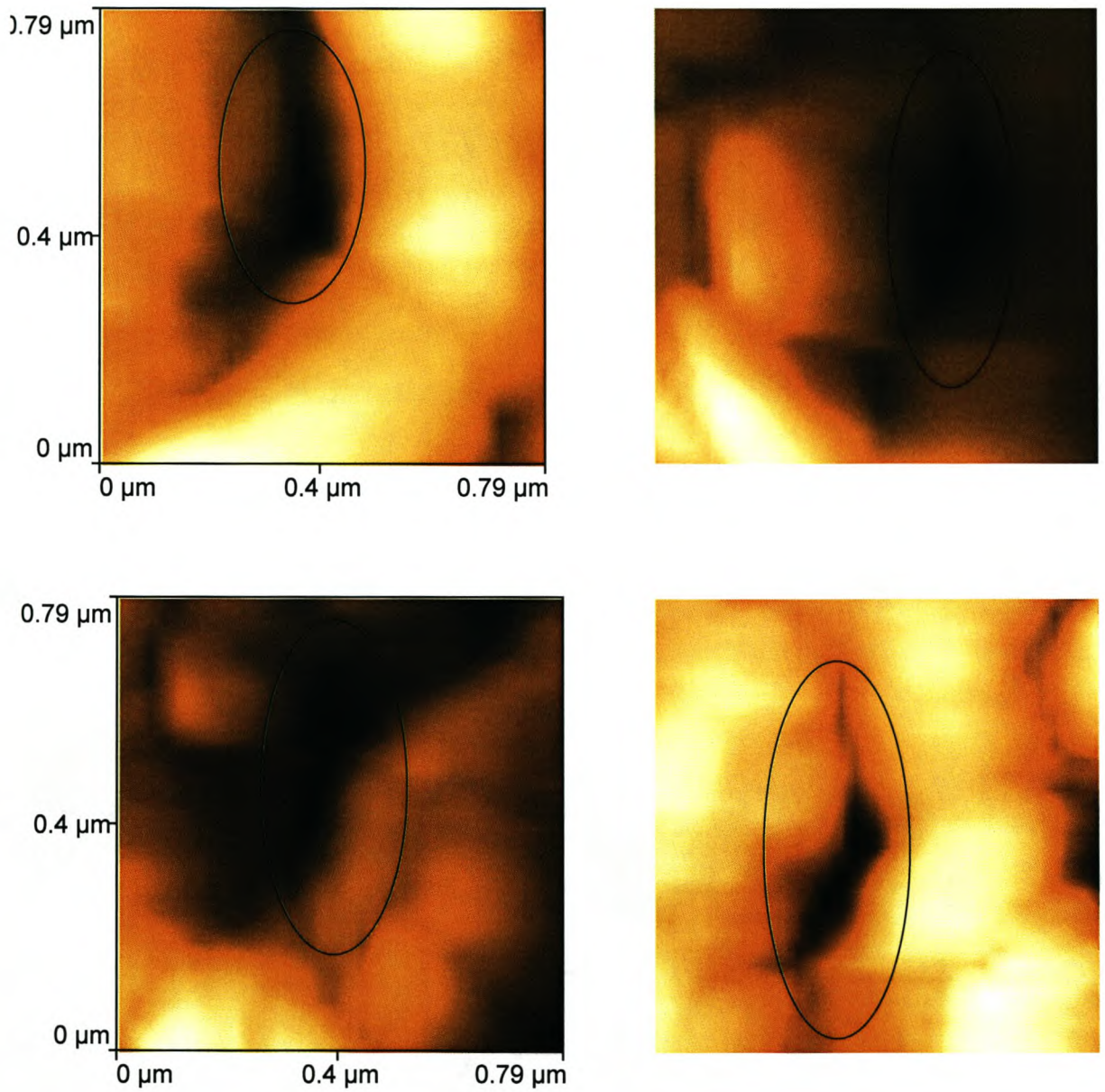


Figure 3.16 AFM images with circles indicating large magainin-induced lesions (200-360nm) still below MIC (4.06μM) on the *E. coli* surface.

3.5 Discussion

Peptide orientation in a target membrane has developed a firm foothold in the literature as a strong indicator of mechanism of action [64]. Horizontal orientation is indicative of membrane perturbation by means of the “carpeting” model, whereas perpendicular orientation points towards a pore-like mechanism, such as the “barrel-stave” model [64]. A change in orientation from parallel to perpendicular is indicative of pore-formation by means of the “toroidal” model [64].

Magainin’s steep dose-response gradient on erythrocytes (Fig. 3.1) appears similar to an on/off switch suggesting a mechanism of action similar to the “carpeting” model. This is a situation in which lytic peptides are in contact with the phospholipid head group throughout the entire process of membrane permeation [47,48]. According to this model, lytic peptides bind with a horizontal orientation onto the surface of the target membrane and cover it in a carpet-like manner. Compared to the controls (Fig 3.3b), we observed that magainin 2 induces swelling (Fig. 3.4b) and forms grooves below the MHC that in some samples span the erythrocyte membrane (Fig. 3.7a, Fig. 3.8) resulting in haemoglobin leakage (Fig. 3.7b). Above the MHC, we observed magainin-induced membrane collapse (Fig. 3.7c). Previous studies supporting the carpet mechanism indicate that magainin’s weaker hydrophobic interaction with the erythrocyte membrane results in the formation of a less-structured α -helix [49-51]. Consequently, magainin 2 orientates itself parallel to the membrane [50,52,53] allowing shallow penetration of its hydrophobic residues into the hydrophobic core [52,54]. The shallow penetration prevents the induction of positive curvature on the PC and SM components of the erythrocyte membrane, and the natural predominant effect of negative curvature strain remains, preventing the formation of pores [27]. If this is the case, then mass accumulation and shallow penetration of magainin 2 on the erythrocyte surface will cause the membrane to fold inwards forming shallow grooves as seen in Figure 3.7a. However, this does not explain why the grooves appear to form star or ladder like patterns (Fig. 3.8). Previous studies have indicated that biological membranes have specific lateral organisation and that lipid segregation occurs and has physiological relevance [19,46]. If same-type lipids were grouped together in bands it would make certain areas of

the target membrane more vulnerable to peptide attack, depending on the prominent curvature strain of that lipid-type. This could explain why magainin-induced grooves on erythrocyte membranes did not appear to be randomly distributed. Instead, they were always connected by lines or clustered in bands across the membrane (Fig. 3.8). Above the MHC, the grooves or lines would continue to expand due to the accumulation of peptide. This progressive destabilisation of the membrane surface eventually leads to membrane collapse, as seen in Figure 3.7c.

Our observations indicate that magainin 2 maintains a parallel orientation on erythrocyte membranes, which in turn supports a mechanism similar to the “carpeting” model, below and above the MHC [47,48].

In contrast, the “barrel-stave” mechanism [16] has featured strongly in the literature over the last few years as a possible mechanism of action for melittin [64], but is this really the case? This mechanism describes the formation of transmembrane channels/pores through vertical bundles of amphipathic α -helices. These bundles are arranged so that their hydrophobic surfaces insert into and interact with the lipid core of the membrane, while their hydrophilic surfaces face each other to form the interior wall of the aqueous pore, which is exposed to the hydrophilic exterior environment. This model fits into previous studies that have shown that melittin orientates itself perpendicular to the membrane normal [44,45], and can induce positive curvature strain [46] on PC and SM bilayers by deep insertion into the bilayer causing swelling of the cell to occur. However, recent contrasting studies indicate variations in melittin orientation and pore size making the “toroidal” model a more likely candidate [64]. The model describes changes in peptide orientation during insertion, from horizontal to vertical, while maintaining contact with the lipid head group. Consequently the lipid monolayer bends inwards with the peptide, from the top leaflet to the bottom leaflet, so that unlike the “barrel-stave” model, both the lipid head groups and the peptides line the pore. The gradual increase of the dose-response curve gradient for melittin (Fig. 3.1) supports the “toroidal” model. Compared to the controls (Fig 3.3b), we observed that there is swelling of the cell below the MHC (Fig. 3.4a) and lesions connected by grooves (Fig 3.5a, Fig. 3.6). Above the MHC more lesions form, which eventually

causes segments of the membrane to break away as smaller vesicles (Fig. 3.5b), ultimately resulting in the destruction of the erythrocyte.

If melittin undergoes an orientation change [64] it can be expected that a certain proportional part of bulk phase will be in a horizontal orientation and a certain proportion in a perpendicular orientation. The portion of melittin in the horizontal orientation will form grooves, based on the same argument presented for magainin 2 (shallow penetration prevents positive curvature of the erythrocyte membrane). The portion of melittin in the perpendicular orientation will undergo deep penetration and induce positive curvature on the erythrocyte membrane. Previous studies on melittin have shown that positive curvature strain can be associated with the formation of pores [46] and that the progressive recruitment of additional melittin monomers will induce excessive positive curvature strain on the membrane [46]. This would increase pore formation, swelling and membrane stress, ultimately rupturing the entire surface of the cell. This would explain the lesions we observed (Fig 3.5a, Fig. 3.6). As a greater proportion of the melittin bulk phase undergoes transition to a perpendicular orientation, it can be expected that the melittin-rich grooves will periodically widen to form more lesions (Fig. 3.6).

Our observations support the re-orientation of melittin on the erythrocyte surface, which in turn supports the “toroidal” model as a mechanism of melittin-induced pore formation on erythrocytes. Furthermore, the small lesion formed by magainin 2 shows (Fig. 3.9), but does not equivocally prove, that on rare occasions it can also change orientation from parallel to perpendicular (see Chapter 4: “Phase-Transition” model). Although studies indicate that magainin 2 has a parallel orientation [50,52,53], it must be taken into account that most studies make use of bulk phase averages, opening the possibility that a small percentage of magainin 2 could have an alternative orientation.

The interaction of peptides with *E. coli* (Fig. 3.10) differs from erythrocytes due to the presence of an outer cell wall containing lipopolysaccharides (LPS) and differences in inner membrane phospholipid composition (Table 3.1). The electronegative environment of the cell wall also increases the binding affinity of melittin and magainin 2. Studies have shown that magainin 2 does bind to the LPS, permeabilising the outer membrane [59], and that

some peptides translocate to the inner membrane and disrupt the infrastructure [23,24]. Our images confirm these studies as cell wall disruption and inner membrane bulging of magainin-treated *E. coli* was observed below the MIC (Fig. 3.14a). Furthermore, magainin-induced lesions on the inner membrane, below the MIC, at 2.02 μM (Fig. 3.15; 150-340nm) and 4.06 μM (Fig. 3.16; 200-360nm) were of similar diameter, but larger than those induced by melittin (Fig. 3.12), albeit at twice the concentration. At higher concentrations above the MIC, magainin-induced vesiculation occurred (Fig. 3.14b), similar to that observed for melittin on erythrocytes (Fig. 3.5b), which as previously indicated also appears to undergo membrane re-orientation.

Previous model membrane studies indicate that magainin 2 initially interacts in a parallel orientation and imposes positive curvature strain on PE model membranes [46,60], even though PE is naturally negative-curvature inducing. This results in membrane thinning which increases the membrane deformation energy, thereby destabilising the surface-lying state inducing a transmembrane orientation [61] and pore formation with the helices of magainin 2 intercalated between the lipid head groups [18]. The progressive recruitment of additional magainin 2 monomers will increase pore formation, swelling and membrane stress, ultimately rupturing the surface of the cell to form the grooves and lesions observed in Figure 3.15 and 3.16.

Our observations indicate that magainin 2 undergoes a similar re-orientation on the *E. coli* membrane surface as observed with melittin on erythrocyte membranes. Furthermore, this supports studies on magainin's mechanism [27] in which investigators proposed a "toroidal pore" mechanism of action on the inner membrane of *E. coli*.

Melittin induced the formation of lesions similar to magainin 2 on the surface of the *E. coli* cell wall, below the MIC, followed by an outward bulging of the inner membrane (Fig. 3.11, top image). The outward bulging is most likely facilitated by the translocation and binding of melittin to the inner membrane which disrupts the supporting infrastructure network. As the inner membrane bulges outwards additional melittin will also bind, increasing the rate of lysis. Furthermore, melittin-induced lesions on the inner membrane below the MIC, at a concentration of 1.08 μM (Figs. 3.12; 95-130nm), were of similar diameter to the melittin-induced lesions on erythrocyte membranes (Fig. 3.6; 70-95nm),

which as previously indicated also appears to undergo membrane re-orientation. At a higher concentration of $4.06\mu\text{M}$, still below the MIC (Fig. 3.13; 30-85nm), the lesions appeared smaller. At higher concentrations above the MIC, cell lysis occurred, however unlike magainin 2 very little vesiculation was evident (Fig. 3.11, bottom image).

Studies have shown that melittin induces positive curvature strain on PE and PG vesicles [55,56,57], which are the major components of the inner membrane (Table 3.1). Furthermore, the induction of positive curvature strain is associated with the formation of pores [27]. Melittin-induced lesions above the MIC (Figs. 3.12; 95-130nm; $1.08\mu\text{M}$), could therefore be the result of pore-formation [58], which is supported by the induction of positive curvature by melittin, again, as on erythrocyte membranes, indicating a re-orientation on the membrane surface and supporting a “toroidal” mechanism of action. However, the decrease in lesion size below the MIC (Fig. 3.13; 30-85nm; $4.06\mu\text{M}$) and decrease in vesiculation (Fig. 3.11, bottom image) promote the possibility that melittin may ultimately destroy the cell by attacking an intracellular target, at least at high concentrations. The lack of vesiculation could alternatively be the result of stable pore formation with melittin in a strong perpendicular orientation causing swift cell lysis without extensive surface damage. One might suggest a possible “barrel-stave” mechanism as an alternative, however this is unlikely, due to the electrostatic interaction between the cationic peptide and the negatively charged head groups of the bacterial membrane surface.

Our images also support previous studies indicating that biological membranes have specific lateral organisation and that lipid segregation occurs and has physiological relevance [19,46]. If same-type lipids were grouped together in bands it would make certain areas of the target membrane more vulnerable to peptide attack, depending on the prominent curvature strain of that lipid-type. This could explain why peptide-induced lesions on erythrocyte and bacterial membranes did not appear to be randomly distributed. Instead, they were always connected by lines or clustered in bands across the membrane.

In summary, our results indicate that magainin 2 maintains a parallel orientation on erythrocyte membranes, which in turn supports, a mechanism similar to the “carpeting” model. Furthermore, melittin on erythrocytes and both melittin and magainin 2 on *E. coli*

undergo membrane re-orientation. This in turn supports a “toroidal pore” mechanism of action.

3.6 Conclusions

AFM successfully allowed the visualization of antimicrobial peptides interacting with target membranes without the influence of fixing agents.

In comparison with model membrane studies, the AFM results show that a peptide can function by more than one mechanism of action depending on the structural composition of the membrane, which appears to have a specific segregated lateral organisation. Magainin 2 (non-toxic) selectively targets cell membranes using different mechanisms of action. In this way it can lyse bacterial membranes (anti-bacterial agent) using one mechanism, while using another mechanism to interact with mammalian cells at physiological concentrations, without destroying them. In contrast, melittin (toxic) is non-selective and possibly uses the same mechanism of interaction with bacterial and mammalian membranes. Furthermore, we propose the “Phase-transition” model as a new holistic model for the mechanism of action of antimicrobial peptides (Chapter 4).

Future studies imaging in solution will allow visualisation under true physiological conditions. The biological applications of AFM are still relatively new, but it is clear that AFM will open new insights into our understanding of the mechanism of action of antimicrobial peptides.

3.7 References

1. Rautenbach M. and Hastings J.W. (1999) *Chemica oggi* **11/12** 81-87
2. Oren Z. and Shai Y. (1998) *Biopolymers* **47** 451-463
3. Boman H.G, Faye I., Gudmundsson G.H., Lee J.Y. and Lidholm D.A. (1991) *Eur. J. Biochem.* **201** 23-31

4. Zasloff M. (1992) *Curr. Opin. Immunol.* **4** 3-7
5. Nicolas P. and Mor A. (1995) *Annu. Rev. Microbiol.* **49** 277-304
6. Boman H.G. (1995) *Annu. Rev. Immun.* **13** 61-92
7. Jack R.W. and Jung G. (1998) *Chimia* **52** 48-55
8. Zasloff M. (1987) *Proc. Natl. Acad. Sci. USA* **84** 5449-5453
9. Maloy W.L. and Kari U.P. (1995) *Biolpolymers* **37** 105-122
10. Zasloff M., Martin B. and Chen H.C. (1988) *Proc. Natl. Acad. Sci. USA* **85** 910-913
11. Chen H.C., Brown J.H., Morell J.L. and Huan. (1988) *FEBS Lett.* **236** 462-466
12. Bessalle R., Kapitkovsky A., Gorea A., Shalit I. and Fridkin M. (1990) *FEBS Lett.* **274** 151-155
13. Matsuzaki K., Sugishita K., Harada M., Fujii N. and Miyajima M. (1997) *Biochim. Biophys. Acta* **1327** 119-130
14. Matsuzaki K., Sugishita K., Fujii N. and Miyajima K. (1995) *Biochemistry* **34** 3423-3429
15. Dempsey C.E. (1990) *Biochim. Biophys. Acta* **1031** 143-161
16. Ehrestein G. and Lecar H. (1977) *Quart. Rev. Biophys* **10** 1-34
17. Gazit E., Boman A., Boman H.G. and Shai Y. (1995) *Biochemistry* **34** 11479-11488
18. Ludtke S.J., He K., Heller W.T., Harroun T.A., Yang L. and Huang H.W. (1996) *Biochemistry* **35** 13723-13728
19. Epand R.M. (1998) *Biochim. Biophys. Acta* **1376** 353-368
20. Lohner K., Hermetter A. and Paltauf F. (1984) *Chem. Phys. Lipids* **34** 163-170
21. Lohner K., Balgavy P., Hermetter A., Paltauf F. and Laggner P. (1991) *Biochim. Biophys. Acta* **1061** 132-140
22. Ferguson A.D., Hofmann E., Coulton J.W., Diederichs K. and Welte W. (1998) *Science* **282** 2215-2220

23. Guo L., Lim K.B., Podiye C.M., Daniel M., Gunn J.S., Hackett M. and Miller S.I. (1998) *Cell* **95** 189-198
24. Hancock R.W. (1997) *Trends Microbiol.* **37** 37-42
25. S.G. Wilkinson; Microbial Lipids, vol. 1, C. Ratledge, S.G. Wilkinson Eds.; Academic Press, London, 1988, pp. 299-488
26. W.M. O'Leary and S.G. Wilkinson; Microbial Lipids, vol. 1, C. Ratledge, S.G. Wilkinson Eds.; Academic Press, London, 1988, pp. 117-201
27. Matsuzaki K. (1999) *Biochim. Biophys. Acta* **1462** 1-10
28. Blondelle S.E., Lohner K. and Aguilar M-I. (1999) *Biochim. Biophys. Acta* **1462** 89-108
29. Bechinger B. (1999) *Biochim. Biophys. Acta* **1462** 157-183
30. Bechinger B. (1997) *J. Membr. Biol* **156** 197-211
31. Hwang P.M. and Vogel H.J. (1998) *Biochem. Cell Biol.* **76** 235-246
32. Park C.B., Kim H.S. and Kim S.C. (1998) *Biochem. Biophys. Res. Commun.* **244** 253-257
33. Engel A., Lyubchenko Y. and Müller D. (1999) *Trends Cell Biol.* **9** 77-80
34. Feng H. (2000) *Nature Struct. Biol.* **7** 354-355
35. Engel A., Gaub H.E. and Müller D. (1999) *Curr. Biol.* **9** 133-136
36. E. Atherton and R.C. Sheppard; "Solid phase synthesis: A practical approach", in: The practical approach series, D Rickwood, B.D. Hames Eds.; IRL Press, Oxford University Press, Oxford 1989
37. B. Mishel and S. Shiigi; Selected Methods in Cellular Immunology, W. H. Freeman and Company, San Francisco 1980
38. du Toit E.A. and Rautenbach M. (2000) *J. Microbiol. Methods* **42** 159-165
39. Svetina S., Iglic A. and Zeks B. (1994) *Ann. N. Y. Acad. Sci.* **710** 179-191
40. <http://www.carolsweb.net/ccf/blood.htm>

41. Iglic A., Kralj-Iglic V. and Hagerstrand H. (1998) *Eur. Biophys. J.* **27** 335-339
42. Zhang P.C., Bai C.L., Huang Y.M., Zhao H., Fang Y., Wang N.X. and Li. Q. (1995) *Scanning Microsc.* **9** 981-988
43. B. Alberts, D. Bray, J. Lewis, M. Raff, K. Roberts and J.D. Watson; Molecular Biology of the cell, 3rd edition; Garland Publishing Inc., New York 1994, p12
44. Vogel H. and Jähnig F. (1986) *Biophys. J.* **50** 573-582
45. Vogel H. (1987) *Biochemistry* **26** 4562-4572
46. Matsuzaki K., Sugishita K., Ishibe N., Ueha M., Nakata S., Miyajima K. and Epanand R.M. (1998) *Biochemistry* **37** 11856-11863
47. Pouny Y., Rapaport D., Mor A., Nicholas P. and Shai Y. (1992) *Biochemistry* **31** 12416-12423
48. Oren Z., Lerman J.C., Gudmundsson G.H., Agerberth B. and Shai Y. (1999) *Biochem. J.* **341** 501-513
49. Matsuzaki K., Mitani Y., Akada K., Murase O., Yoneyama S., Zasloff M., Miyajima K. (1998) *Biochemistry* **37** 15144-15153
50. Williams R.W., Starman R., Taylor K.M.P., Gable K., Beeler T. and Zasloff M. (1990) *Biochemistry* **29** 4490-4496
51. Hirsh D.J., Hammer J., Maloy W.L., Blazyk J. and Schaefer J. (1996) *Biochemistry* **35** 12733-12741
52. Matsuzaki K., Harada M., Funakoshi S., Fujii N. and Miyajima K. (1991) *Biochim. Biophys. Acta* **1063** 162-170
53. Matsuzaki K., Murase O., Tokuda H., Funakoshi S., Fujii N. and Miyajima K. (1994) *Biochemistry* **33** 3342-3349
54. K. Matsuzaki and J. Seelig; Peptide Chemistry, M. Ohno Ed.; Protein Research Foundation, Osaka, 1995, pp. 129-132
55. Batenburg A.M., van Esch J.H. and de Kruijff B. (1988) *Biochemistry* **27** 2324-2331

56. Batenburg A.M., Hibbeln J.C.L., Verkleij A.J. and de Kruijff B. (1987) *Biochim. Biophys. Acta* **903** 142-154
57. Batenburg A.M., van Esch J.H., Leunissen-Bijvelt J., Verkleij A.J. and de Kruijff B. (1987) *FEBS Lett.* **223** 148-154
58. Matsuzaki K., Yoneyama S. and Miyajima K. (1997) *Biophys. J.* **73** 831-838
59. Matsuzaki K., Sugishita K. and Miyajima K. (1999) *FEBS Lett.* **449** 221-224
60. Wieprecht t., Dathe M., Epand R.M., Beyermann M., Krause E., Maloy W.L., MacDonald D.L. and Bienert M. (1997) *Biochemistry* **36** 12869-12880
61. Huang H.W. (1995) *J. Phys. II (France)* **5** 1427-1431
62. He K., Ludtke S.J., Worcester D.L. and Huang H.W. (1996) *Biophys. J.* **70** 2659-2666
63. Uragami M., Dewa T., Inagaki M., Hendel R.A. and Regen S.L. (1997) *J. Am. Chem. Soc.* **119** 3797-3801
64. Yang L., Harroun T.A., Weiss T.M., Ding L. and Huang H.W. (2001) *Biophys. J.* **81** 1475-1485

Chapter 4

General Discussion

The aim of this study was to first successfully synthesise magainin 2, second develop and optimise a new microscopy method using atomic force microscopy (AFM), and third investigate the mechanism of action of antimicrobial peptides on target membranes using this visualisation technique.

4.1 Peptide Synthesis

Although automation will undoubtedly pave the way for fast effective peptide synthesis, the Fmoc-polyamide shake flask procedure used in the BIOPEP peptide laboratory is very effective in developing not merely an understanding of peptide synthesis, but instilling a solid foundation for chemical problem-solving in the future. One of the more important lessons learnt was the necessity for quality control checks on all derivatives, even newly acquired ones, prior to synthesis. This was partially the reason for the first unsuccessful synthesis, where a suspected aspartimide reaction [1] on A22 resulted in the loss of side-chain deprotection of S23, causing additional unwanted analogues and a decrease in peptide yield. The aspartimide reaction can be partially suppressed by the inclusion of 1-hydroxybenzotriazol in the cleavage/deprotection mixture [2]. In the second synthesis this problem was prevented by rigorously testing all derivatives and activating agents, however, attachment of the first C-terminal amino acid to the resin linker is also particularly important. The extent of this first reaction will determine the yield of final peptide. Sites on the resin not reacted in this initial process, can potentially become acylated in subsequent cycles, which can lead to the formation of related C-terminally truncated by-products. That is why particular care was taken during the coupling of the C-terminal Fmoc-Ser(tBu) and blocking of the remaining hydroxyl-groups with tBoc-Gly. These safety measures were effective in preventing the initial problems experienced in the first synthesis. Caution was also taken to prevent incomplete couplings by increasing the excess of amino acid derivative during coupling. Although mass action is a major driving force during the coupling reaction of

peptide synthesis, the influence of extremely high reactant and product concentrations in a solid phase system with limited soluble reactant access was underestimated. The high amino acid derivative concentrations did not influence the success of the coupling reactions during the first two-thirds of the synthesis, but caused coupling and deblocking problems over the last third. This typically occurs with growing peptide chains because of steric crowding and intersite side reactions [2]. Furthermore, this may lead to incomplete solvation of the peptide-resin complex, sudden shrinkage of the gel matrix, and reduced reagent penetration ultimately resulting in failure of the acylation reaction [2]. This resulted in deletion and insertion analogues that could not be purified from the main product. So although the initial synthesis problem was solved in the second synthesis, a new problem was inadvertently created, which compromised the synthesis. Coupling concentrations were decreased to the recommended three-fold excess [3] during a third synthesis, while still maintaining rigorous testing on all the derivatives and activating agents. This prevented subsequent steric-crowding and the formation of any truncated or insertion by-products. The fundamental lesson learnt is that effective peptide synthesis optimisation depends on exhaustive critical analysis of failed syntheses before undertaking new syntheses. This analysis and quality control measures allowed the synthesis and purification of magainin 2, from a 19-residue precursor on solid phase, of very high purity (>96%) for use in biological and AFM experiments.

4.2 AFM Visualisation

AFM is a powerful visualisation technique, however, the sensitive nature of the biological samples made optimisation critical to success, especially as it was hypothesised that a more authentic result may be obtained if no fixing agent was used. During the development of our AFM technique it was observed that the greatest problems were cantilever sensitivity towards the buffered solutions and the elasticity of the target cell surface. Typically, the buffered solutions used to suspend our biological samples would interact with the tip. Consequently, most of the method development was focused on optimising the suspension solutions of target cells. This decreased interference with the cantilever tip and limited target cell damage and stress. It is therefore essential to critically analyse the solution criteria for all biological experiments before starting your AFM image acquisition. The softness/elasticity of the biological samples also had to be addressed. If the cantilever force was set too high, it would push the sample surface inwards, which would result in distorted images. This problem was addressed with each cell type by systematically changing the force parameters until consistent

imaging was obtained. Another important aspect is the time consuming nature of image capturing. It takes 90-120 seconds to capture an image; so building a sufficient database can become a time-consuming procedure due to the large variation in morphology that occurs. It was important to capture repeatable high quality controls to ensure that the experimental results were authentic. Our technique successfully allowed the visualization of antimicrobial peptides interacting with target membranes without the influence of fixing agents.

The AFM results were discussed in Chapter 3, and indicate that magainin 2 maintains a parallel orientation on erythrocyte membranes and mass accumulation on the surface results in the formation of grooves. In relation to previous model membrane studies the mechanism can be associated with the “carpeting” model [4]. Furthermore, melittin on erythrocytes and both melittin and magainin 2 on *E. coli* undergo membrane re-orientation. Mass accumulation results in the formation of grooves because of parallel orientation and lesions due to perpendicular orientation. In relation to previous model membrane studies the mechanism can be associated with the “toroidal pore” model [5, 6].

In relation to results and hypothesis generated through previous model membrane studies, our AFM results can be interpreted to show that a peptide can function by more than one mechanism of action depending on the structural composition of the membrane, which appears to have a specific segregated lateral organisation. Magainin 2 (non-toxic) selectively targets cell membranes using different mechanisms of action. In contrast, melittin (toxic) is non-selective and uses the same mechanism of interaction with bacterial and mammalian membranes. However, these models relate to model membranes, and not necessarily biological membranes. Model membrane studies tend to compartmentalise the mechanism of action of a peptide to a specific lipid type providing only a snapshot of what the mechanism would look like under those specific conditions, and not if all the components of a cell membrane were present to influence the mechanism. We therefore believe that if all these compartmentalised “snapshots” were combined then it cannot be excluded that the "carpet" and the "toroidal" mechanism are subsets of one mechanism and that the structural parameters of the peptide and the lipid membrane could determine which subset of the mechanism and peptide orientation will be most prominent under a specific set of physiological conditions. We know that the orientation of a peptide strongly influences the interaction with the membrane and the mechanism of action. Yet model membrane studies still lead to contradicting results (see 1.1.4 and Table 1.3) because of the experimental differences and

constraints of the analysis procedures. Most analytical procedures used to determine the orientation of a peptide, such as nuclear magnetic resonance and circular dichroism, work on statistical averages. This means that the structure or orientation of the bulk-phase of the molecules is determined. It is possible that the bulk-phase structure/orientation is not the structure/orientation of the active species (see Table 1.3). Consequently, the mechanism of action still remains in doubt.

Therefore we would like to propose a new model based on previous model membrane studies and on our AFM results. It must be emphasised that this model is speculative, as no such comparisons have previously been undertaken; therefore the objective is to initiate a synergism between model membrane studies and future AFM studies on biological membranes. With this model we hope to offer an explanation for 1) the confusion regarding orientation using model membrane studies and 2) the variation in pore size.

4.3 The “Phase-Transition” model:

The model entails that all antimicrobial peptides function by means of one universal mechanism, which involves a time dependent change in peptide orientation from parallel to vertical. (Fig. 4.1).

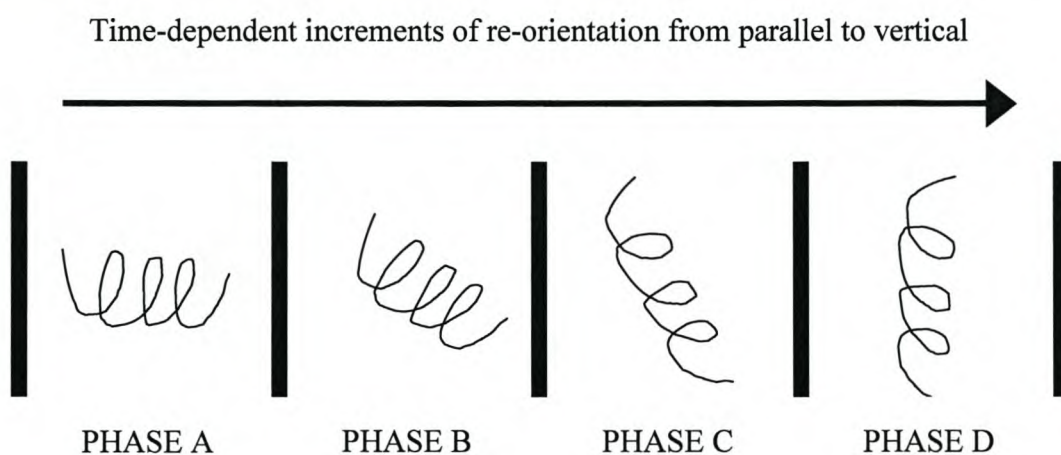


Figure 4.1 A diagram illustrating the “phase-transition” (PT) model.

The change in orientation from parallel to vertical is not instantaneous, but takes place in incremental time-dependent steps. Its structural parameters and those of the lipid membrane determine the speed at which a peptide can move through each increment. If the two complement each other the peptide will move through the orientational increments rapidly, forming stable pores leading up to cell lysis. Intracellular targets can also possibly be reached with the formation of stable pores. If, however, the peptide and lipid membranes are not complementary, the peptide will move slower through each increment of orientation. An equilibrium could possibly be found in an orientation somewhere between parallel and vertical, which may lead to local membrane curvature changes and membrane thinning (Fig 4.2). The orientation where the peptide finds equilibrium, will determine which part of the “phase transition” model is emphasised, and in turn the morphological damage that will lead up to cell lysis. The nearer the peptide is to a parallel orientation, the greater the morphological damage leading up to lysis. Therefore a peptide can still utilise the same mechanism on different lipid compositions and cause different morphological damage, depending on the final orientation of the peptide and therefore which part of the “phase-transition (PT)” model is emphasised (Fig 4.2). This could explain why we saw differently sized lesions, depending on the type of peptide and biological membrane.

If we compare our model with existing models we find that the “carpeting” model could possibly represent PHASE A of the PT model where no pore formation is possible (Fig 4.2), whereas the “toroidal” model could represent PHASE B-D (Fig. 4.2) where pore formation can occur.

In conclusion, to better understand how peptide structural parameters influence the mechanism of action, it is essential that studies move away from model membrane studies towards studies on real target membranes. Although AFM is not the ultimate solution, it is definitely a step in the right direction.

Future studies will focus on comparing the influence of melittin, magainin 2 and for example alamethicin, the only known peptide with a confirmed “barrel-stave” mechanism of action, on similar target cells that have different lipid compositions. Furthermore analysis of the influence of melittin and magainin 2 on model membranes using AFM could clarify some of the contradictory results found so far.

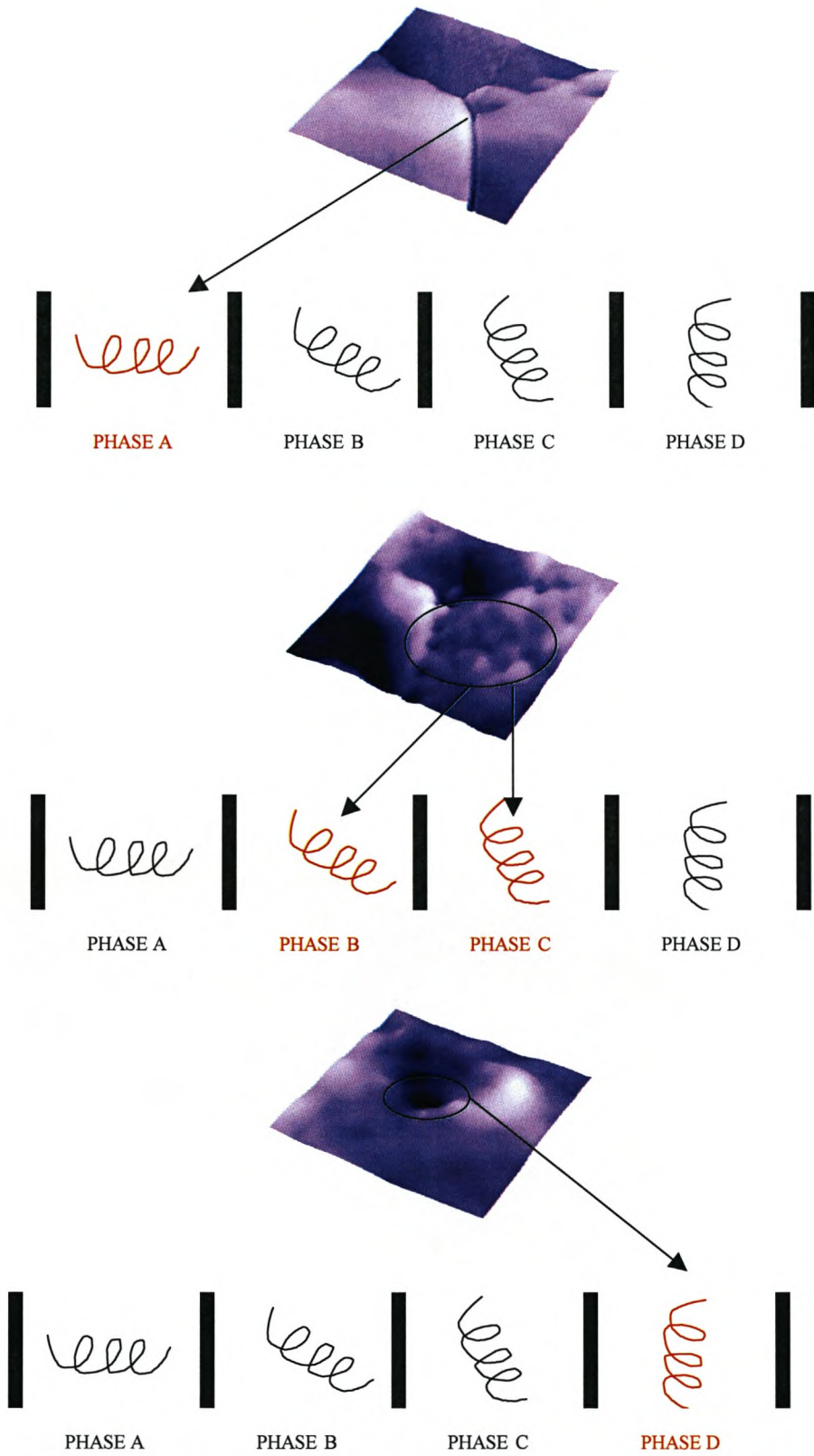


Figure 4.2 The PT model using hypothetical AFM images as a demonstration of possible morphological damage as a result of peptide phase transitions.

4.4 References

1. Atherton E., Sheppard R.C. (1989) Solid phase synthesis: A practical approach, In: The practical approach series (Series Eds., Rickwood D., and Hames B.D.), IRL Press, Oxford University Press, Oxford, pp.1-61
2. Chan W.C., White P.D. (2000) Fmoc Solid Phase Peptide Synthesis: A practical approach, In: The practical approach series (Series Ed., Hames B.D.), Oxford University Press, Oxford, pp.1-39
3. Rautenbach M. (1999) The synthesis and characterisation of analogues of the antimicrobial peptide iturin A₂, Ph.D. Thesis (Biochemistry), University of Stellenbosch, pp.1-31
4. Pouny Y., Rapaport D., Mor A., Nicolas P. and Shai Y. (1992) *Biochemistry* **31** 12416-12423
5. Ludtke S.J., He K., Heller W.T., Harroun T.A., Yang L. and Huang H.W. (1996) *Biochemistry* **35** 13723-13728
6. Matsuzaki K., Murase O., Fujii N. and Miyajima K. (1996) *Biochemistry* **35** 11361-11368